Title
Local and systemic responses to ectopic apoptosis in Drosophila melanogaster

Author
Gerhold, Abigail Rebecca

Publication Date
2012

Peer reviewed|Thesis/dissertation

Local and systemic responses to ectopic apoptosis in *Drosophila melanogaster*

By

Abigail Rebecca Gerhold

A dissertation submitted in partial satisfaction of the

requirements for the degree of

Doctor of Philosophy

in

Molecular and Cell Biology

in the

Graduate Division

of the

University of California, Berkeley

Committee in charge:

Professor Iswar Hariharan, Chair
Professor David Bilder
Professor Thomas Cline
Professor Nipam Patel
Professor David Schaffer

Spring 2012

Abstract

Local and systemic responses to ectopic apoptosis in *Drosophila melanogaster*

by

Abigail Rebecca Gerhold

Doctor of Philosophy in Molecular and Cell Biology

University of California, Berkeley

Professor Iswar Hariharan, Chair

During normal development, organ growth is tightly regulated such that a high degree of fidelity to both size and shape is maintained. Often this constancy is achieved by a robust arrest of growth once final size has been reached. In response to injury, however, some organs are able to engage in additional growth, thereby regenerating the lost or damaged tissue. Regenerative capacity varies widely across the animal kingdom. Some organisms can replace lost appendages, such as limbs or tails, restore damaged internal organs, such as the heart or liver, or even regenerate their entire body plan from a small fragment. Other animals, notably humans, exhibit markedly reduced regenerative capacity. Damaged tissue is replaced by a scar and organ function is accordingly lost or reduced. Why some organs and organisms possess impressive regenerative abilities, while others lack this seemingly beneficial trait remains largely unresolved. Improving our understanding of how regeneration occurs in the former may inform therapeutic efforts to improve regeneration and repair in damaged human tissues.

Tissue damage elicits local and systemic responses that determine the efficacy of the ensuing repair and regeneration. Locally, damaged or dying cells are removed and additional tissue growth or remodeling must be undertaken to restore tissue integrity. On the systemic level, injury can lead to the recruitment of immune cells and the activation of an inflammatory response. Long-range signaling from the wound site may also broadly impact animal physiology by affecting processes such as metabolism. Reciprocally, regeneration may be influenced by organismal factors, such as age and nutrient availability. Very little is known about the cellular and molecular mechanisms underpinning these various aspects of regeneration.

We have used the regenerative capacity of Drosophila larval imaginal discs to investigate the local proliferative and the systemic immune responses to tissue damage. Chapter 2 describes a system that we have developed to produce tissue damage and regenerative growth in imaginal discs. Using genetic mosaics we generate clones of cells that carry a temperature-sensitive cell-lethal mutation. We can thus selectively ablate these cells upon shifting to an elevated temperature and assess the regenerative capacity of the surviving sister clones. This system has allowed us to conduct a genetic screen for recessive

mutations that selectively impair regenerative growth. Using traditional methods and whole-genome re-sequencing we have identified several of the mutations isolated in our screen. We have found that regenerative growth occurs, in part, by an acceleration of tissue growth and thus appears to sensitize cells to the loss of factors generally required for more rapid growth. In this way, regenerative growth may share features with some types of overgrowth. Indeed, two of our mutations are common targets for anti-cancer drugs.

In Chapter 3, we investigate the innate cellular immune response to tissue damage in Drosophila. Using ionizing radiation to generate widespread apoptosis in proliferating larval tissues, we find that broad changes in the blood cell population ensue. These include macrophage activation and the differentiation of lamellocytes, an otherwise cryptic cell fate. Using the power of Drosophila genetics, we consider a model in which the engulfment of apoptotic cells by activated macrophages allows these cells to stimulate a broader, inflammatory-like immune response.

Table of Contents

List of Figures

List of Tables

Acknowledgements

Thank you to my mentor Iswar, who encouraged me to pursue my own ideas and always keep an open eye to the bigger scientific picture. His broad perspective on science, readiness to support "risky" projects and willingness to move the lab in new directions as his interest dictates have been a truly positive influence on my approach to science.

I owe my start in science to Sarah Hake, who took me into her lab despite my complete lack of training or experience and supported me whole heartedly both while I worked with her and afterwards. My experience doing science in her labs was likely the strongest driving force in my decision to pursue a PhD. Her enthusiasm for and success in science, while maintaining a beautiful work-life balance are truly inspiring. I would also like to thank Hector Candela, whose tireless mentorship during my first summer in lab, was invaluable.

I owe much to all the members, past and present, of the Hariharan lab: Adrian Halme, who got me started and with whom I continue to enjoy interesting and informative conversations about science and everything else; Tania Reis and Sarah Siegrist for their support, both personal and professional, and for constantly encouraging experimental rigor; Yassi Hafezi who was an excellent bay-mate and who led the way for all us "younger" graduate students; Melanie Worley, Linda Setiawan and Justin Bosch, for all their feedback, ideas and constant comradery; Albert Yu for his efforts at the bench and putting up with my long to-do lists. Thanks too to members of the Bilder lab for sharing ideas and reagents. Thank you especially to Sarah Wilder for moral support and many great conversations about science and the rest of life.

Thank you to my thesis committee for their guidance over the years: David Bilder, David Schaffer, Tom Cline and Nipam Patel. Many thanks in particular to Nipam for introducing me to Woods Hole.

Finally, I am overwhelming indebted to my family and friends who in innumerable ways make it all worthwhile.

Chapter 1

Introduction

During normal development, metazoans typically grow until they reach a characteristic size at which point growth slows or stops. While some tissues experience a certain degree of turnover, most organs undergo a fixed amount of growth and arrest at a defined size. In some cases however, damage to or loss of part of an organ or body part can trigger additional growth or re-modeling such that the lost tissue is restored. The restoration of a damaged organ or lost body part constitutes the broadest definition of regeneration. The extent to which different organisms and different organs can regenerate is widely variable. For example, the human liver displays a robust regenerative capacity, while little or no regeneration occurs within the human heart. Thus one of the great challenges facing regenerative medicine is to understand how regeneration occurs in organs and organisms that possess this ability. Such knowledge may allow for the development of therapies to enhance the regenerative capacity of poorly regenerating tissues.

Regeneration can occur at many levels of biological organization.

Certain organisms, most notably planaria, can regenerate their entire body plan from remarkably small fragments. Other organisms, such as axolotls and zebrafish, are able to regenerate complex structures, such as a limb, fin or tail. Regeneration also can occur at the level of individual organs, such as the mammalian liver. In addition, other tissues that normally exhibit a relatively high rate of turnover, for example the intestinal epithelium and the epidermis, can increase the production of new cells in response to damage. Finally, regeneration also occurs at the cellular level, as evidenced by the regeneration of axons in damaged nerve cells (reviewed in (BELY and NYBERG 2010)).

In all these cases, regeneration refers to the replacement of tissue following significant trauma. This type of regeneration has been referred to as injury-induced or facultative regeneration. However, regeneration can also describe the ongoing process of renewal and repair that maintain tissue homeostasis in response to normal levels of cell death and ageing (reviewed in (POSS 2010; STOICK-COOPER *et al.* 2007a)). Whether facultative and homeostatic regeneration define distinct phenomena or are rather gradations on a spectrum of mechanistically related events is unclear.

Regeneration in diverse organisms and at different levels of biological organization may share common attributes.

Given the broad range of phenomena considered regeneration, the question arises as to whether there are likely to exist any common principles. The ability to regenerate is relatively widespread and examples can be found in most animal phyla. This observation has lead to the hypothesis that regenerative capacity may be a homologous rather than an analogous trait (reviewed in (BELY and NYBERG 2010; SÁNCHEZ ALVARADO 2000)). As such, regeneration in diverse systems is likely to share some underlying properties.

Indeed, it is possible to find commonalities between remarkably different examples of regeneration. For example, in many cases apoptotic cells at the site of injury appear to play a key role in driving the regenerative process. Apoptotic cells have been implicated in the regeneration of a wide range of tissues in a variety of organisms, including *Hydra* (CHERA *et al.* 2009), *Xenopus* (TSENG *et al.* 2007), planaria (PELLETTIERI *et al.* 2010), mice (LI

et al. 2010), the mammalian liver (MAEDA *et al.* 2005) and *Drosophila* imaginal discs (HUH *et al.* 2004; PÉREZ-GARIJO *et al.* 2004; RYOO *et al.* 2004). However, the mechanism by which dying cells promote regeneration remains largely unknown.

Several signaling pathways have been identified as key for regeneration in a range of organisms. For example, Wnt signaling is associated with regeneration in many organisms, where it functions to re-establish patterning axes and/or to drive regenerative growth (CHERA *et al.* 2009; MCCLURE and SCHUBIGER 2008; NEJAK-BOWEN and MONGA 2011; PETERSEN and REDDIEN 2008; SMITH-BOLTON *et al.* 2009; STOICK-COOPER *et al.* 2007b). The Wnt pathway is evolutionarily conserved and functions extensively during normal development. Thus its frequent use during regeneration may reflect a link between regenerative competence and the ability to re-initiate a normal developmental program.

If regeneration is a basal trait, the question then arises as to why it has been maintained in some phyla and lost in others. Regenerative ability may be preserved because it provides a selective advantage for the organism or it simply has not been selected against and is maintained by default (reviewed in (BELY and NYBERG 2010)). It is easy to imagine that the ability to regenerate a lost limb would likely benefit the affected animal. However, it is also clear that for some organisms the ability to regenerate is tightly coupled to aspects of their life cycle. For example, in planaria, regeneration is driven largely by the same forces that operate during normal cellular turnover and asexual reproduction (reviewed in (SÁNCHEZ ALVARADO 2007; SÁNCHEZ ALVARADO and TSONIS 2006)).

Regenerative capacity has also disappeared in many phyla. The ability to regenerate could be lost because a structure rarely needs to be regenerated in the wild or if loss of the structure does not significantly impair survival (reviewed in (BELY and NYBERG 2010)). Regeneration could also be selected against if an aspect of maintaining regenerative competence impaired survival in some way. Regeneration often involves the dedifferentiation and proliferation of quiescent cells. Such plasticity, although enabling regeneration, may also make these cells more susceptible to growth disregulation, allowing for the development of disease states such as cancer. Indeed, while the human liver is capable of robust regeneration, dysfunctional regeneration following sustained liver injury is thought to contribute to hepatocellular cancer (reviewed in (NEJAK-BOWEN and MONGA 2011)).

The broad distribution of regenerative competence across animal phyla could be due to the presence of class of regeneration-specific genes or to the maintenance of a regeneration-specific function for phylogentically conserved genes (reviewed in (POSS 2010)). As our understanding of the molecular underpinnings of regeneration in diverse organisms increases, we may better be able to address the reasons for the variability in regenerative competence.

Regeneration is a multi-faceted process, involving both local and systemic responses.

In the broadest terms, regeneration involves three events: (1) the perception of injury and the translation of this information into a regenerative response; (2) regenerative growth to replace the lost mass; and (3) the re-patterning or specification of the regenerate.

The signals which initiate regeneration may originate from a local source such as damaged or dying cells within the wounded tissue or from neighboring cells. Wound

healing, whereby cellular debris or dying cells are cleared and tissue integrity is re-established, may impact the regenerative capacity of the damaged tissue. Indeed, in some cases, a specialized structure called the wound epithelium forms over the site of injury and is a critical event for subsequent regeneration events. In non-regenerating tissues, wound healing is often accomplished by scar formation which may prevent full regeneration of the lost tissue.

The decision to regenerate may also be impacted by systemic factors. Cells that are recruited to the site of injury, such as cells of the immune system, may participate in local signaling events. Humoral factors may influence regenerative capacity, such as growth factor availability. Regeneration may also be affected by broad parameters such as nutrient availability and organismal age.

In most cases, regeneration involves a local increase in proliferation to replace the lost tissue mass. Regenerative growth requires either post-mitotic or quiescent cells to re-enter the cell cycle or the activation of a stem or progenitor cell population. This additional growth must then be regulated to ensure that a regenerate of appropriate size and proportion is produced.

Finally, the regenerate must also be patterned such that all requisite tissue or cell types are produced and that the regenerated structure integrates appropriately into the existing body plan. This process may occur concomitantly with re-growth or subsequently once the lost tissue mass has been restored.

In all these areas we have only the most preliminary understanding of the underlying cellular and molecular mechanisms. Outstanding questions include: (1) What are the sources and nature of the signals that initiate regeneration? (2) What are the characteristics of regenerative growth and are there genetic pathways that specifically regulate this type of growth? (3) How do injury and regeneration impact the host organism and conversely, how is regenerative competence influenced by host factors such as age, nutrition state and the immune system? (4) How is regenerative growth regulated such that fidelity to organ size is maintained?

My thesis used Drosophila as a model to study several aspects of regeneration, first by conducting a genetic screen for genes specifically required for regenerative growth and second by characterizing the cellular immune response to damaged tissue. I will first provide background for the portion of my thesis investigating regenerative growth, followed by an introduction to cellular immunity and its role in regeneration.

Regenerative growth

Regenerative growth occurs by blastema formation or compensatory proliferation.

In most described cases, at all levels of biological organization, regeneration requires additional cell proliferation to replace the lost tissue. Even during axon regeneration, the associated Schwann cells dedifferentiate and proliferate to support the regenerating axon (reviewed in (STOLL and MÜLLER 1999)). Regeneration involving extra cell proliferation is called epimorphosis. Less common is morphollaxis, during which remodeling of the remaining tissue restores the lost structure in the absence of any substantial cell division.

Epimorphic regeneration can occur with or without the formation of a regeneration blastema. A blastema is a mass of proliferative cells, derived from fully or partially dedifferentiated cells or stem cells, which forms at the wound site and ultimately gives rise to the lost structure. Blastema formation is observed following limb, fin or tail amputation in regenerating vertebrates, in planarians after head or tail amputation and following surgical injury to Drosophila imaginal discs.

Epimorphic regeneration also occurs in the absence of a distinct blastema by non- or only loosely localized cell proliferation. The dividing cells may be stem cells, dedifferentiated cells or mature surviving cells within the damaged tissue. Regenerative growth in the absence of a blastema has been referred to as compensatory growth or proliferation. Compensatory proliferation is frequently used to describe regeneration of the liver and of *Drosophila* imaginal discs following apoptotic cell loss. However other tissues also exhibit non-blastemal epimorphic regeneration, such as the zebrafish heart and the newt lens.

Whether the regenerative growth that characterizes blastemal regeneration differs significantly from that occurring during compensatory proliferation is not known. Interestingly, apoptotic cells have been implicated in driving regeneration in both cases, suggesting that blastemal regeneration and compensatory proliferation have at least some features in common.

Regenerative and developmental growth may differ at some level.

During regeneration, damage and wound healing induce a population of cells to undergo additional proliferation. Regenerative growth may be driven directly by signals emanating from the site of damage. Alternatively, healing of the wound site may lead to the re-establishment of patterning cues which then drive growth in a partial re-iteration of normal development. These models need not be mutually exclusive and indeed there is evidence in support of both. In either case, this extra growth occurs within a very different context than developmental growth. Developmental growth often occurs concomitantly with patterning and is undertaken by a field of progenitor cells that are generally highly proliferative by nature. In addition, growth of a given organ proceeds concurrently with that of other organs and the surrounding or systemic environment is designed to be growth-permissive.

During regeneration, growth occurs in the context of a fully- or partially-patterned structure and requires responsive cells to undergo extra non-developmentally programmed proliferation. These cells must be competent to engage in additional proliferation, which depending on the contributing cell type, may require de-differentiation, re-entry into the cell cycle, or acceleration of basal proliferation rates. Regeneration also occurs within a fully- or partially-developed organism. Hence both the systemic environment and the time available for re-growth are likely to differ from that experienced by cells in the developing organ.

Thus, one might expect the following characteristics to differ between regenerative and developmental growth: (1) the initiating signals, if damaged-derived; (2) the signaling pathways driving cell growth and proliferation, if the presence or levels of morphogens or growth factors differ; (3) the activity or presence of regulators maintaining plasticity and proliferative competence; (4) the levels or activity of factors broadly required for cell

proliferation or growth, particularly if the rate of regenerative growth is accelerated relative to developmental growth.

Regenerative growth in Drosophila

In Drosophila two tissues have been shown to exhibit regeneration – the adult mid-gut and the larval imaginal discs. The adult mid-gut epithelium is constantly replenished by the division of a population of intestinal stem cells (ISCs). Apoptosis or infection of mature enterocytes stimulates an increase in the proliferation of ISCs such that gut homeostasis is maintained (JIANG *et al.* 2009). Imaginal discs are the larval precursors of adult structures such as the wing or eye. They develop from a 15-40 cell primordium and undergo a 1000-fold increase in cell number before differentiating during metamorphosis (reviewed in (BRYANT and SIMPSON 1984)). During the larval stages, these tissues show a remarkable regenerative capacity and are able to recover from extensive apoptotic cell loss or surgical injury. Adult mid-gut and imaginal disc regeneration provide models for the investigation of homeostatic and facultative regeneration, respectively. For the purposes of my thesis, I have focused on imaginal disc regeneration.

Blastemal regeneration in imaginal discs

Early experiments showed that surgically fragmented imaginal discs, cultured within the abdomen of an adult female host, were capable of regenerating the removed region (BRYANT 1975; HADORN and BUCK 1962; SCHUBIGER 1971). In addition, discs that were fragmented *in situ* were also able to regenerate (BRYANT 1971). In both cases, experimental discs were isolated late during larval development at a time when normal developmental growth is largely complete (BRYANT 1971; BRYANT 1975; FAIN and STEVENS 1982; MARTÍN *et al.* 2009). Even if afforded the opportunity to undergo additional growth by transplantation and culture, undamaged discs will maintain proliferative stasis (KIEHLE and SCHUBIGER 1985). Thus imaginal discs are capable of engaging in additional regenerative growth following injury.

While the final differentiation of imaginal disc cells does not occur until metamorphosis, cells are strictly determined to produce specific structures (SCHUBIGER 1971). However, following fragmentation, the missing structures are replaced by the regenerating tissue. On occasion regenerating disc cells can even switch fates from one disc to another, for example from leg to wing, in a process known as transdetermination (reviewed in (MAVES and SCHUBIGER 2003; MCCLURE and SCHUBIGER 2007)). Thus regenerating imaginal disc cells possess a certain degree of developmental plasticity and regeneration requires participating cells to access this trait.

Characterization of imaginal disc regeneration following surgical ablation revealed evidence of blastema formation at the wound site (ABBOTT *et al.* 1981; KIEHLE and SCHUBIGER 1985; O'BROCHTA and BRYANT 1987). A tightly localized increase in cell proliferation was observed adjacent to the cut site, the size of which was proportional to the amount of tissue removed (O'BROCHTA and BRYANT 1987). Clonal analysis has suggested that the blastema can be derived from as few as 5-10 founder cells (GIBSON and SCHUBIGER 1999) that are located within the wound edge (BOSCH *et al.* 2008).

Despite over 50 years of study, we know surprisingly little about the properties of blastemal cells and what genetic pathways promote and regulate blastemal growth. This lag is due largely to the techinical challenges posed by disc fragmentation and culture. Classically, it has been proposed that cells within the imaginal disc have specific positional values and that when normally non-adjacent positional values come into contact, as would occur during wound healing, intercalary growth ensues such that all intermediate values are replaced (FRENCH *et al.* 1976). A similar model has been suggested to explain re-growth during vertebrate limb regeneration (reviewed in (STOCUM and CAMERON 2011)). However the molecular nature of the proposed positional value and the mechanism by which cells compare values remains largely theoretical. Furthermore, in imaginal discs increased cell division appears to precede wound closure suggesting that a free wound edge or other stimuli may initiate regenerative growth (BOSCH *et al.* 2008; KARPEN and SCHUBIGER 1981; KIEHLE and SCHUBIGER 1985).

Several recent studies have undertaken to better describe the characteristics of blastemal regeneration in imaginal discs. Analyses of disc wound healing showed that Jun N-terminal Kinase (JNK) pathway activity was increased at the wound edge and that this activity was necessary for proper healing to occur (BERGANTIÑOS *et al.* 2010; BOSCH *et al.* 2005; MATTILA *et al.* 2005). The majority of blastemal cells were derived from cells that had experienced JNK signaling and while blastema formation occurred with roughly the same kinetics when JNK signaling was abrogated, both the size of the blastema and the number of dividing cells was reduced (BOSCH *et al.* 2008; MATTILA *et al.* 2005). Thus, either JNK signaling or complete wound healing is required to sustain blastema development.

JNK signaling has also been implicated in regulating cellular plasticity in regenerating discs. Members of the polycomb group (PcG) of chromatin regulators can influence the frequency of transdetermination during regeneration presumably by affecting the regulatory state of regenerating cells (KLEBES *et al.* 2005; LEE *et al.* 2005). JNK signaling downregulates PcG function in blastemal cells thereby increasing the likelihood of a transdtermination event (LEE *et al.* 2005).

In addition to the JNK pathway, Wingless (Wg) has been implicated in regulating blastemal growth. Our group has developed a genetic system that allows for the ablation and subsequent regeneration of the pouch region of the wing disc without the need for surgical manipulation and *in vivo* culture (SMITH-BOLTON *et al.* 2009). In both this system and in cultured fragmented leg discs, Wg levels were elevated in the presumptive blastema (GIBSON and SCHUBIGER 1999; MCCLURE *et al.* 2008; SMITH-BOLTON *et al.* 2009). Reducing Wg signaling may reduce the expression of cell cycle regulators within the blastema (SMITH-BOLTON *et al.* 2009) and overexpression of Wg can generate ectopic blastemas (JOHNSTON and SCHUBIGER 1996).

Several studies have attempted to identify regeneration-specific genes by expression analysis in regenerating discs. Two early attempts screened a series of P-*lacZ* enhancer-trap insertions for altered expresssion in regenerating discs (BROOK *et al.* 1993; RUSSELL *et al.* 1998). Interestingly, both reports identified a class of enhancer traps that were expressed only in regenerating discs, pointing to the existence of regeneration-specific genes. However, neither study pursued the functional significance nor validated the genetic identity of any of the insertions found. A later report further characterized a set of these enhancer traps and identified 4 genes that reduced or delayed blastema formation, *rpd3*, *combgap* (*cg*), *jing* and *Aly* (also known as *RNA and export factor binding protein 1*,

Ref1) (MCCLURE and SCHUBIGER 2008). Two genes, *jing*, a transcriptional repressor, and *rpd3*, a histone deacetylase, have been implicated in chromatin modification; however their specific role during regeneration has yet to be elucidated (MCCLURE and SCHUBIGER 2008).

In addition, two groups have used microarray analysis to identify genes with altered expression in regenerating discs. Both studies found that transcription factors and chromatin remodelers were prevalent among genes that were upregulated in regenerating discs (BLANCO *et al.* 2010; KLEBES *et al.* 2005). The JNK pathway was further implicated in promoting regeneration, as well as wound healing, and a role for Notch signaling was suggested (BLANCO *et al.* 2010). Two previously uncharacterized genes, *regeneration* (*rgn*) and *augmentor of liver regeneration* (*Alr*), each with a homolog implicated in vertebrate regeneration, were found to affect the initiation and size of the regeneration blastema, respectively. Preliminary evidence linked both to the Wg pathway (MCCLURE *et al.* 2008).

Thus a molceular picture of blastemal regeneration is just emerging. The JNK pathway is required for wound healing, promoting cellular plasticity in blastemal cells and potentially for blastemal growth. Whether the JNK pathway affects blastemal growth independently of its role in wound healing is uncertain. Wg signaling is sufficient for blastema formation and two novel interactors have been identified. However, the requirement for the Wg pathway during regeneration and both upstream and downstream effectors are unknown. Notch may also play a role in regeneration, as do multiple chromatin regulators. Specific questions pertaining to the role of these individual pathways in regenerative growth remain and, likely, many additional components have yet to be identified.

Compensatory proliferation in imaginal discs.

Compensatory proliferation in imaginal discs was first inferred from the observation that with increasing dose of X-ray irradiation (IR) larger clones of cells were recovered in the resulting adult wings (HAYNIE and BRYANT 1977). IR induces mitotic recombination thereby allowing for the generation of marked homozygous clones within an otherwise heterozygous tissue. The authors concluded that IR caused the death or mitotic arrest of many cells within the developing imaginal disc and that the surviving cells underwent additional divisions to compensate for this loss (HAYNIE and BRYANT 1977). An increase in disc cell proliferation following apoptotic cell loss was directly observed some 20 years later. The increased proliferation did not appear tightly localized in a regeneration blastema, but rather was scattered across the affected tissue (MILÁN *et al.* 1997).

A model for apoptosis-induced compensatory proliferation was recently proposed. It was suggested that apoptotic cells could actively trigger compensatory proliferation by producing mitogenic signals (HUH *et al.* 2004; PÉREZ-GARIJO *et al.* 2004; RYOO *et al.* 2004). Evidence for this model comes largely from studies using "undead" cells. Undead cells are created when dying cells are prevented from executing the final steps of apoptosis by expression of the baculovirus effector caspase inhibitor p35. The result is a population of cells that are trapped in a partially apoptotic state.

Undead cells induce over-proliferation in neighboring cells, suggesting that activation of the apoptotic machinery in dying cells is sufficient to produce compensatory proliferation (HUH *et al.* 2004; PÉREZ-GARIJO *et al.* 2004; RYOO *et al.* 2004). The ability of undead cells to produce ectopic proliferation is dependent upon the activity of the initiator

caspase Dronc (HUH *et al.* 2004; KONDO *et al.* 2006; WELLS *et al.* 2006) and may also require JNK signaling (PÉREZ-GARIJO *et al.* 2009; RYOO *et al.* 2004). Undead cells express elevated levels of Wg and Decapentaplegic (Dpp) and both mitogens appear to be required for undead cell-induced compensatory proliferation (HUH *et al.* 2004; PÉREZ-GARIJO *et al.* 2004; PÉREZ-GARIJO *et al.* 2005; PÉREZ-GARIJO *et al.* 2009; RYOO *et al.* 2004).

The persistence of undead cells is a highly aberrant condition and may not fully reflect a normal physiological response. Indeed, neither Wg nor Dpp were required for IR-induced compensatory proliferation in the wing disc when undead cells were not present (PÉREZ-GARIJO *et al.* 2009). Further, when cell death was induced in differentiating cells within the eye-antennal disc, the ensuing compensatory proliferation was dependent on Hedgehog (Hh) signaling and did not appear to involve Wg or Dpp (FAN and BERGMANN 2008).

Thus it is unclear whether the ectopic proliferation induced by undead cells is related to the compensatory proliferation that occurs when dying cells are cleared normally from the epithelium. In particular, whether dying cells actively promote compensatory proliferation remains uncertain. At a molecular level, only the Hh pathway has been implicated in mediating compensatory proliferation and many questions remain as to the mechanism of Hh activation and activity in this context. In addition, whether Hh signaling plays a role in compensatory proliferation in other discs and when apoptosis is induced by other means is not known.

Are blastemal regeneration and compensatory proliferation related?

A blastema is a tightly localized increase in cell proliferation, while compensatory proliferation may or may not be localized by proximity to apoptotic cells. Despite this difference, the extra regenerative growth that occurs under both conditions has been attributed to the same theoretical model. As mentioned above, it has been posited that during blastemal regeneration, wound healing generates a discontinuity in the positional values of the remaining cells, which then drives intercalary growth to replace all missing values (FRENCH *et al.* 1976). It has been suggested that scattered apoptotic cell loss also results in the juxtaposition of cells with different positional values and that intercalary growth then restores the damaged disc to an appropriate size (MILÁN *et al.* 1997). If the same model accurately describes both phenomema, then one might expect some degree of overlap in the underlying molecular mechanisms.

Indeed, two recent papers have proposed that the Hippo/Salavdor/Warts (HSW) pathway may regulate regenerative growth in a variety of contexts (SUN and IRVINE 2011), (GRUSCHE *et al.* 2011). Using a variety of insults, including genetic ablation, fragmentation, γ-irradiation and clonally induced apoptosis the authors show that HSW pathway activity is suppressed in cells adjacent to the damaged tissue, allowing for increased nuclear localization and activity of the pro-growth transciption factor Yorkie (Yki). The HSW pathway is broadly involved in regulating cell growth and proliferation. Interestingly, several of the upstream regulators of the pathway are transmembrane or membrane-affliated proteins, suggesting that the HSW pathway could provide a potential molecular mechanism for the integration of positional information with growth control (reviewed in (HALDER and JOHNSON 2011; PAN 2010)). As such, the HSW pathway would be optimally

situated to regulate regenerative growth. However, major questions remain regarding the requirements for and mechanism of HSW pathway signaling during regeneration.

Another potentially shared feature of blastemal regeneration and compensatory proliferation is the role of apoptotic cells. In general, a blastema results when a large contiguous region of a disc is physically removed and compensatory proliferation occurs when tissue is lost to scattered cell death. Apoptotic cells may actively participate in the generation of compensatory proliferation; whereas a recent report has suggested that blastema formation may be independent of apoptosis (BOSCH *et al.* 2008). However, apoptotic cell loss can be a sufficient for blastema formation (SMITH-BOLTON *et al.* 2009). Thus the role of apoptosis in both cases merits further investigation.

One open question is whether the growth that occurs during blastemal regeneration and compensatory proliferation has common charateristics. Towards the end of larval development, imaginal disc growth slows as discs approach their final size, which is largely attained by the onset of pupariation (FAIN and STEVENS 1982). Damage to imaginal discs necessitates additional, non-developmentally programmed growth. Presumably, if the rate of this regenerative growth, whether blastemal or compensatory, is not accelerated relative to developmental growth, then the duration of the growth period must be lengthened to compensate. This exended growth period could occur by increasing the duration of the larval period or by a continuation of growth into the pupal stage.

Our group and others have shown that damage to imaginal discs delays the larval to pupal transition. Delayed pupariation results when discs are damaged by a variety of insults known to induce both compensatory proliferation and blastemal regeneration, including IR (HALME *et al.* 2010; POODRY and WOODS 1999; TENNANT 1931), *in situ* fragmentation (BRYANT 1971) and genetic manipulation (SIMPSON *et al.* 1980; SMITH-BOLTON *et al.* 2009). The amount of delay correlates with the amount of damage and subsequent re-growth (HALME *et al.* 2010; POODRY and WOODS 1999; SIMPSON *et al.* 1980; TENNANT 1931). If a robust delay is not achieved, the resulting adult structure is negatively impacted, suggesting that complete regeneration could not occur (HALME *et al.* 2010).

As the larval period is extended following disc damage, regenerative growth need not be accelerated relative to developmental growth. However, very few studies have directly assessed the rate of regenerative growth. Anaylsis of proliferation dynamics within the blastema have shown that blastemal cells have a cell cycle profile and doubling time that is comparable to non-blastemal cells, suggesting that they do not assume a more rapid rate of proliferation during regeneration (SUSTAR and SCHUBIGER 2005). However, only one time point after fragmentation was considered. It has been reported that the rate of proliferation within the blastema declines as regeneration progresses (ABBOTT *et al.* 1981), leaving open the possibility that regenerative growth may at some points outpace developmental growth. Interestingly, cells within the blastema were found to be slightly larger than non-blastemal cells (SUSTAR and SCHUBIGER 2005), suggesting that cell growth and division may not be coupled in the same manner.

Qualitative assessments of regenerative growth in discs following IR have given conflicting results. At 24 hours post-IR, we and others have observed an increase in the number of mitotic cells in irradiated discs as compared to untreated controls (JAKLEVIC and SU 2004) A. Halme, unpublished). However, a recent study did not report a similar trend (WELLS and JOHNSTON 2012). The authors further show that irradiated discs do not increase in size at a greater rate than controls and that, in addition to proliferating for longer during

an extended larval phase, irradiated discs show more mitoses during the pupal stage. This discrepancy should be resolved by a quantitative evaluation of the rate of cell proliferation and growth in discs undergoing compensatory proliferation.

Thus both blastemal regeneration and compensatory proliferation occur, at least in part, during a delayed larval to pupal transition. Whether this delay is triggered by damage or the ensuing re-growth is unclear. The latter may indicate that both types of regeneration can exert a similar systemic impact on the developing larvae. In addition, the shared requirement for an extended larval phase to complete regeneration may indicate common underlying features, such as growth rate. However, a more thorough assessment of basic growth parameters in each case is required before a relevant comparison can be made.

Summary

Drosophila imaginal discs provide a valuable model system to investigate several aspects of regenerative growth. Imaginal discs are capable of both blastemal regeneration and compensatory proliferation and provide a genetically tractable system in which to examine both. Furthermore, imaginal discs have been used extensively to conduct unbiased genetic screens for genes involved in developmental growth. This feature of imaginal discs may allow for the identification of new, regeneration-specific genes. Although the field of regeneration biology encompasses a wide range of phenomena, there is evidence to suggest that at least some aspects of regeneration may be conserved across phlya and different levels of biological organization. Thus, information gleaned from studies in Drosophila may inform our view of regeneration in other organisms. Importantly, the discovery of genes required for regenerative growth may identify potential therapuetic targets for improving regenerative performance in poorly regenerating mammalian tissues.

Cellular immunity and regeneration

Cells of the innate immune system can both promote and inhibit regeneration

In mammals, tissue injury illicits a profound local inflammatory response which is mediated by cells of the innate immune system (reviewed in (KOH and DIPIETRO 2011; MARTIN and LEIBOVICH 2005)). The degranulation of platelets and mast cells as well as the activation of resident macrophages, results in the production and release of a barrage of signaling molecules, thus triggering a massive influx of additional innate immune cells including neutrophils and monocytes. Neutrophils are primarily responsible for preventing infection by phagocytosing pathogens and releasing toxic products, including free radicals. An inadvertent effect of neutrophil activity, however, is damage to healthy host cells, thus increasing injury and potentially exacerbating inflammation. Recruited monocytes differentiate into macrophages which then act at multiple points in the wound healing process. Activated macrophages release pro-inflammatory signals and chemo-attractants that recruit additional immune cells. They also release factors that promote angiogenesis and fibroblast proliferation, which drive healing via scar formation. In addition, macrophages dampen the inflammatory response and participate in the resolution of

wound healing by clearing cellular debris and apoptotic cells, including spent neutrophils, and releasing anti-inflammatory cytokines.

While inflammatory cells are key for preventing infection and supporting wound healing, in so doing they may inhibit regeneration. At epidermal wounds in adults, the inflammatory response is thought to promote scar formation and fibrosis, at the expense of more perfect healing and regeneration of damaged structures. In contrast, embryos, which have little or no inflammatory reaction, heal wounds with remarkable fidelity leaving no lasting imprint (reviewed in (REDD *et al.* 2004)). Indeed, several studies in immune-deficient mice have suggested that attentuating the innate immune response, particularly the inflammatory action of neutrophils and macrophages, may improve tissue healing and regeneration (reviewed in (KOH and DIPIETRO 2011; MARTIN and LEIBOVICH 2005)).

Inflammation also impacts regeneration and repair in other adult organs, such as the heart (reviewed in (FRANGOGIANNIS 2008)). Myocardial infarcts generally result from the ischemic death of cardiomyocytes. The damaged tissue is not regenerated, but is replaced by a scar. The innate immune response is critical for infarct healing via fibrosis and scar formation; however it may also increase cardiomyocyte injury and drive excessive scarring leading to expansion of the infarct, adverse ventricular remodeling and progressive heart failure. Thus, in addition to increasing cardiomyocyte proliferation, improving heart regeneration may require modulation of the inflammatory response surrounding cardiac injury.

While cells of the innate immune system may reduce the regenerative capacity of tissues such as the heart and epidermis, in other organs they may promote regeneration. Most notably in the liver, which exhibits a robust regenerative ability, resident macrophages produce key cytokines that prime surviving hepatocytes for cell cycle re-entry (reviewed in (FAUSTO *et al.* 2006; TAUB 2004)). During skeletal muscle regeneration, macrophage-derived factors stimulate myogenic proliferation, thus actively enhancing muscle regeneration (reviewed in (CICILIOT and SCHIAFFINO 2010)).

The relationship between innate immune cells, in particular macrophages, and regeneration is complex and poorly understood at the molecular level. Whether macrophages are absolutely required for wound healing remains controversial. The comparative success of embryonic wound healing suggests that the positive influence of macrophages may be expendable when inflammatory reactions are largely absent. Experiments in Xenopus tail regeneration have similarly suggested that immune cells have a predominantly negative impact on regenerative capacity (FUKAZAWA *et al.* 2009). Conversely, during zebrafish fin regeneration, inflammatory cells appear to be innocuous bystanders, present at the wound site but not required for regeneration (MATHEW *et al.* 2007).

The mechanisms underlying macrophage recruitment to the wound site and participation in wound healing and regeneration are largely unknown. Moreover, the genes required for the development and function of mononuclear macrophages are mostly uncharacterized (reviewed in (CHOW *et al.* 2011; GEISSMANN *et al.* 2010)). In particular, it is thought that macrophages undergo a phenotypic switch between pro- and anti-inflammatory states. It is not known whether cells already present at the wound site change state in response to environmental cues or if monocyte precursors predetermined for each phenotype are selectively recruited at different points in the process of wound healing (reviewed in (KOH and DIPIETRO 2011)). In addition, the role of tissue-resident

macrophages, as opposed to macrophages derived from infiltrating monocytes, is often overlooked and poorly understood (reviewed in (CHOW *et al.* 2011)).

Finally, aside from local interactions, tissue damage and regeneration can also influence and are influenced by the rest of the host organism. It is possible that immune cells present at the site of injury may mediate some of this long-range signaling (reviewed in (EMING *et al.* 2009)). A more thorough understanding of the signaling pathways underlying macrophage recruitment and function during regeneration is key to being able to manipulate macrophage responses for therapeutic intervention.

Drosophila has proven a valuable tool for the study of innate immunity with respect to hematopoiesis (reviewed in (EVANS *et al.* 2003)), pathogen defense (e.g. Toll signaling) (reviewed in (DIONNE and SCHNEIDER 2008)) and macrophage-mediated phagocytosis (reviewed in (FRANC 2002)). However, the immune response to tissue damage is not well characterized. The absence of an adaptive immune system in *Drosophila* as well as the availability genetic resources, make it an valuable model in which to investigate several aspects of the innate cellular immune response to tissue damage.

The immune system in Drosophila is composed of two parts: humoral and cellular

The *Drosophila* innate immune system consists of a humoral or systemic response and a cellular response. The humoral response has been best studied in terms of the secretion of potent anti-microbial immune effectors by the fat body (AMPs), the functional equivalent of the mammalian liver (reviewed in (LEMAITRE and HOFFMANN 2007)). However, other humoral factors produced following infection do not have an obvious role in pathogen defense and may function as part of a broader stress response (AGAISSE *et al.* 2003; EKENGREN *et al.* 2001). In addition, some of the same signaling pathways that regulate the humoral response to infection can also modulate non-immune functions such as metabolism, thereby linking infection to broader systemic changes in animal physiology (DIANGELO *et al.* 2009).

Comparatively, the cellular arm of the immune system is less well characterized. The cellular immune system is comprised of three cell types broadly referred to as hemocytes: plasmatocytes, crystal cells and lamellocytes. These three categories are based on gross morphology and a selection of molecular markers; however, both morphological characterization and the increasing number of available markers suggest that the hemocyte population, particularly the broad classification of plasmatocytes, may be more complex and heterogeneous (reviewed in (CROZATIER and MEISTER 2007; JUNG *et al.* 2005). These cells are functionally related to those of the myeloid/monocyte lineage of vertebrates (reviewed in (EVANS *et al.* 2003; LANOT *et al.* 2001).(EVANS *et al.* 2003; LANOT *et al.* 2001) A poorly defined population of precursor cells known as prohemocytes give rise to all three cell types, although the hematopoietic lineage is not well established.

Plasmatocytes make up ~95% of the immune cells in embryos and larvae and are the only type of hemocyte present in the adult. Plasmatocytes differentiate into macrophages to engulf both pathogens and apoptotic cells. They also produce extracellular matrix proteins and AMPs. Crystal cells are found in the embryo and larva and produce the enzymes involved in melanization reactions. A third cell type, lamellocytes, are never seen in embryos or adults and rarely found in healthy larvae. They differentiate in larvae upon infestation by parasitoid wasps where they encapsulate the invading wasp egg. They may

also serve the more general function of encapsulating objects that are too large to be phagocytosed (LANOT *et al.* 2001; MEISTER 2004)).

Hematopoiesis in Drosophila

In Drosophila, hematopoiesis occurs in two waves, embryonic and larval. Embryonic hematopoiesis produces a population of plasmatocytes and crystal cells that persist through the larval stages and into the adult (HOLZ *et al.* 2003). Larval hematopoiesis occurs in the larval lymph gland and can give rise to all three types of plasmatocytes. Under normal conditions, cells within the lymph gland remain there until metamorphosis when the lymph gland ruptures (GRIGORIAN *et al.* 2011; LANOT *et al.* 2001). However, immune challenge by parasitoid wasps elicits precursor proliferation, lamellocyte differentiation and premature lysis of the lymph gland (LANOT *et al.* 2001; SORRENTINO *et al.* 2002). Interestingly, while no adult hematopoiesis has been described, when the lymph gland lyses both differentiated cells and undifferentiated precursors are released. The fate of these potential progenitor cells and their role in the adult has not been investigated (KRZEMIEN *et al.* 2010a).

Embryonic hematopoiesis

Embryonic hemocytes originate from a subpopulation of the head mesoderm, defined by both expression of the GATA transcription factor Serpent (Srp) and position within the embryo. These small round mesoderm cells are considered pro-hemocytes and give rise to both plasmatocytes and crystal cells (LEBESTKY *et al.* 2000; TEPASS *et al.* 1994). Crystal cells are specified by the activity of the Runx factor Lozenge (Lz), which is expressed in the first row of pro-hemocytes in the hematopoietic anlagen (BATAILLÉ *et al.* 2005; LEBESTKY *et al.* 2000). Not all cells that express *lz* go on to become crystal cells; a subset turn *lz* expression off and revert to a plasmatocyte fate (BATAILLÉ *et al.* 2005; LEBESTKY *et al.* 2000). Two closely related zinc finger transcription factors, Glial cells missing (Gcm) and Gcm2, limit crystal cell differentiation. The relative levels of Lz and Gcm/Gcm2 are thought to determine cell fate. Gcm is initially expressed in all pro-hemocytes and is subsequently repressed in cells that become crystal cells. Gcm/Gcm2 also promote plasmatocyte fate; however, additional factors must specify plasmatocyte identity as double *gcm*, *gcm2* mutants still make some plasmatocytes (ALFONSO and JONES 2002; BATAILLÉ *et al.* 2005; BERNARDONI *et al.* 1997). In addition, the FOG homolog U-shaped (Ush) is expressed in all plasmatocytes and its downregulation in crystal cells is required for their differentiation (FOSSETT *et al.* 2001).

At the beginning of germ band retraction, plasmatocytes start to migrate throughout the embryo, becoming phagocytically active macrophages and engulfing cell corpses created by programmed cell death (TEPASS *et al.* 1994). The PDGF/VEGF receptor tyrosine kinase Pvr and its ligands Pvf1-3 are required for both full maturation and survival of plasmatocytes and their proper migration (BRÜCKNER *et al.* 2004; CHO *et al.* 2002). Embryonic crystal cells remain localized near the proventriculus and their function in the embryo is not known (LEBESTKY *et al.* 2000).

By the end of embryogenesis there are 700 plasmatocytes, the vast majority of which have become phagocytically active macrophages (TEPASS *et al.* 1994) and roughly 30

crystal cells (LEBESTKY *et al.* 2000). In newly hatched first instar larvae, there are between 200-400 hemocytes (LANOT *et al.* 2001; MAKHIJANI *et al.* 2011). It is not known whether the remainder of the embryonic hemocytes undergo apoptosis nor what defines the population that persists into the larval stages.

In larvae, embryonic hemocytes are present circulating freely in the hemolymph and in sessile populations below the cuticle and associated with certain larval tissues (LANOT *et al.* 2001). Embryonic hemocytes proliferate to expand the circulating and sessile population from fewer than 400 cells at hatching to more than 5000 cells by the wandering stage (HOLZ *et al.* 2003; LANOT *et al.* 2001; MAKHIJANI *et al.* 2011; QIU *et al.* 1998). There are discrepancies in the literature as to the existence of prohemocytes in the circulating and sessile populations in larvae. Prohemocytes have been identified morphologically and dividing cells in each population are less phagocytically active, suggesting a less differentiated state (LANOT *et al.* 2001). Both the plasmatocyte and crystal cell population expands over larval development, yet crystal cells do not themselves divide, indicating the presence of a progenitor class (KRZEMIEN *et al.* 2010b; LANOT *et al.* 2001). In addition, it has been proposed that the sessile population can act as a hematopoietic compartment, at least vis-à-vis the production of lamellocytes, which would also suggest the presence of undifferentiated precursors (MÁRKUS *et al.* 2009). However, the identity of lamellocyte precursors is disputed and may include both prohemocytes and differentiated plasmatocytes (AVET-ROCHEX *et al.* 2010; CROZATIER *et al.* 2004; HONTI *et al.* 2010; LANOT *et al.* 2001; MAKKI *et al.* 2010; RIZKI 1962; SORRENTINO *et al.* 2002; STOFANKO *et al.* 2010).

Conversely, it has been reported that all embryonic hemocytes have assumed either a plasmatocyte or crystal cell fate by the end of embryogenesis and that no prohemocytes remain (TEPASS *et al.* 1994). Additionally, a recent report has shown that phagocytically active cells that express a marker of plasmatocyte fate, rather than undifferentiated prohemocytes, may drive expansion of larval hemocyte numbers (MAKHIJANI *et al.* 2011). Without definitive prohemocyte markers the presence of these cells and their contribution to circulating and sessile hemocyte numbers cannot be excluded. However, the proliferation of differentiated embryonic plasmatocytes constitutes an interesting alternative (MAKHIJANI *et al.* 2011). Whether all embryonic plasmatocytes are equally competent to become mitotically active during the larval stages or whether a only subset of the population displays this ability is not known.

Larval hematopoiesis

The lymph gland develops from precursors in the cardiogenic mesoderm and is first visible as 3 clusters of cells expressing the transcription factors Collier (Col), the orthologue of vertebrate Early B Cell Factor, and Odd-skipped, just prior to germ band retraction (CROZATIER *et al.* 2004; HOLZ *et al.* 2003; MANDAL *et al.* 2007). By the end of embryogenesis, these clusters have coalesced to form a pair of primary lobes of roughly 20 cells each that flank the anterior dorsal vessel and have begun to express Srp (JUNG *et al.* 2005). Unlike embryonic hemocytes, cells in the lymph gland do not differentiate during embryogenesis.

In second instar (L2) larvae, the primary lobes of the lymph gland have grown to ~200 cells each and 2-3 additional posterior lobes have emerged along the dorsal vessel. In late L2/early third instar (L3) larvae, cells on the periphery of the primary lobes begin to

express maturation markers, whereas cells in the posterior lobes generally remain undifferentiated throughout larval development. By late L3, the primary lobes of the lymph gland contain between 3000 - 5000 cells each and 2 distinct regions are evident. The peripheral or cortical zone (CZ) consists of loosely packed, differentiating cells. The medullary zone (MZ) is a region of densely arranged undifferentiated prohemocytes adjacent to the dorsal vessel (JUNG *et al.* 2005). A cluster of cells at the posterior tip of each primary lobe constitutes the posterior signaling center (PSC), which functions as a hematopoietic niche to maintain the population of undifferentiated prohemocytes in the MZ (CROZATIER *et al.* 2004; KRZEMIEŃ *et al.* 2007; LEBESTKY *et al.* 2003; MANDAL *et al.* 2007). Lineage tracing revealed that differentiating cells in the CZ originate as MZ prohemocytes and that cells within the PSC do not contribute to either the MZ or the CZ (JUNG *et al.* 2005).

Recent reports have added complexity to this model of the lymph gland. In L3 larvae, cells within the MZ become largely quiescent and were thought to be maintained as a reservoir of pluripotent progenitors (JUNG *et al.* 2005; MONDAL *et al.* 2011). However, a cessation of cell division in the MZ has not been universally observed (KRZEMIEN *et al.* 2010b). While the contribution of MZ cells to lymph gland expansion during L3 development is controversial, proliferation of CZ cells has been consistently documented (JUNG *et al.* 2005; KRZEMIEN *et al.* 2010b). These cells appear to constitute a pool of intermediate progenitors that undergo additional mitoses before differentiating (KRZEMIEN *et al.* 2010b). In addition, clonal analysis has suggested that prohemocytes become lineage-restricted early in development, prior to the formation of a distinct MZ and CZ (KRZEMIEN *et al.* 2010b). However, some plasticity must remain to allow for the differentiation of lamellocytes, an otherwise cryptic cell fate, following wasp parasitization. Interestingly, several reports have linked dysfunction in chromatin regulation with lamellocyte production (BADENHORST *et al.* 2002; REMILLIEUX-LESCHELLE *et al.* 2002) raising the possibility that lamellocyte fate may involve precursor reprogramming.

While the PSC has been proposed to be the functional equivalent of the vertebrate hematopoietic stem cell niche (KRZEMIEŃ *et al.* 2007; MANDAL *et al.* 2007), there is little evidence to suggest the existence of stem cells with the lymph gland. Analysis of clones generated in the embryonic lymph gland primordium demonstrated that all cells do not have a similar lineage potential, as a wide range of clone sizes was recovered in mature lymph glands (KRZEMIEN *et al.* 2010b; MINAKHINA and STEWARD 2010). However, proliferating cells appear evenly dispersed throughout the lymph gland until at least early L3 (JUNG *et al.* 2005; KRZEMIEN *et al.* 2010b; MONDAL *et al.* 2011) and no evidence has been found for a sub-population of cells with the characteristics of stem cells (KRZEMIEN *et al.* 2010b). Thus larval prohemocytes likely behave as a population of proliferative cells, similar to other tissues such as imaginal discs (KRZEMIEN *et al.* 2010b), The heterogeneity observed in the proliferative potential of embryonic lymph gland cells suggests a previously unappreciated level of complexity in the lymph gland primordium, which merits further investigation.

All three zones of the mature lymph gland exhibit distinct patterns of gene expression and the signaling pathways that govern lymph gland development and function are starting to be worked out. The PSC is specified during embryogenesis by the expression of Antennapedia (Antp) which maintains Col expression in a cluster of 5-6 cells at the posterior end of the developing lymph gland (MANDAL *et al.* 2007). The PSC also expresses high levels of the Notch (N) ligand Serrate (Ser) (LEBESTKY *et al.* 2003). Reducing Ser

activity in the PSC leads to decreased levels of Col and concomitantly a reduction in the MZ population of prohemocytes (KRZEMIEŃ *et al.* 2007). While it has been proposed that Ser could mediate signaling between the PSC and MZ (KRZEMIEŃ *et al.* 2007; LEBESTKY *et al.* 2003), it is not known whether N signaling is also required for prohemocyte maintenance independently of its role in promoting Col expression and thus PSC identity.

Cells in the PSC also express Hedgehog (Hh), Wingless (Wg), Unpaired3 (Upd3) and Pvf1 (MANDAL *et al.* 2007; MONDAL *et al.* 2011; SINENKO *et al.* 2009). Hh is not necessary for the specification of the PSC but is required for the PSC to maintain MZ prohemocytes in an undifferentiated state (MANDAL *et al.* 2007). Wg controls PSC size autonomously and functions non-autonomously to prevent migration and premature differentiation of MZ prohemocytes, potentially by regulating levels of Drosophila E-Cadherin (*Shotgun*) (SINENKO *et al.* 2009). Upd3 expression in the PSC is dispensable; however it is also expressed by MZ cells where it functions autonomously to sustain Janus kinase/Signal-transducer and activator of transcription (JAK/STAT) signaling (MAKKI *et al.* 2010). Interestingly, Pvf1 does not signal to prohemocytes in the MZ directly, but to cells in the CZ, which, in response, regulate levels of extracellular adenosine thereby preventing the differentiation of MZ prohemocytes (MONDAL *et al.* 2011). In addition to the production of secreted factors, the PSC also extends numerous cytoplasmic processes which contact MZ cells and may mediate the long-range influence of the PSC (KRZEMIEŃ *et al.* 2007).

MZ cells express downstream components of the Hh, Wg and JAK/STAT pathways, consistent with their role in maintaining prohemocyte identity (KRZEMIEŃ *et al.* 2007; MANDAL *et al.* 2007; SINENKO *et al.* 2009). However, the function of the JAK/STAT pathway in prohemocytes is contentious. JAK/STAT activity is dependent on signaling from the PSC, and loss of pathway activity correlates with premature prohemocyte differentiation (KRZEMIEŃ *et al.* 2007). However, recent reports suggest that while down-regulation of JAK/STAT signaling in the MZ is critical for lamellocyte differentiation following wasp parasitization, sustained JAK/STAT signaling is not required under normal conditions to keep MZ prohemocytes in an undifferentiated state (MAKKI *et al.* 2010; MINAKHINA *et al.* 2011; MONDAL *et al.* 2011). Rather, STAT is required downstream of PVR in cells in the CZ to mediate the retrograde signaling that maintains prohemocytes (MONDAL *et al.* 2011). In addition, STAT may be required cell autonomously for plasmatocyte differentiation in the CZ (MINAKHINA *et al.* 2011). Somewhat paradoxically, however, known reporters of the JAK/STAT pathway show only minimal or scattered activity in the CZ (KRZEMIEŃ *et al.* 2007; MONDAL *et al.* 2011).

MZ cells also exhibit tightly regulated levels of reactive oxygen species (ROS). Levels of ROS in MZ prohemocytes are a key determinant of differentiation: decreasing ROS levels reduces differentiation, while increasing ROS levels induces premature differentiation. ROS-induced prohemocyte differentiation is mediated by JNK signaling potentially via activation of FoxO and derepression of polycomb targets (OWUSU-ANSAH and BANERJEE 2009).

The CZ is defined by the expression of various hemocyte maturation markers (JUNG *et al.* 2005). Under normal conditions, both plasmatocytes and crystal cells begin to differentiate in the CZ of late L2/early L3 animals. Both plasmatocytes and crystal cells express Peroxidasin (Pxn) (NELSON *et al.* 1994), collagens (ASHA *et al.* 2003) and Hemolectin (GOTO *et al.* 2003). Plasmatocytes express the putative phagocytosis receptors Nimrod1 (Nim1C) (KURUCZ *et al.* 2007), Eater (KOCKS *et al.* 2005; SORRENTINO *et al.* 2007) and

Croquemort (Crq) (FRANC *et al.* 1996; IRVING *et al.* 2005), while crystal cells express Lz and the phenoloxidases ProPO (DUVIC *et al.* 2002) and DoxA3 (WALTZER *et al.* 2003). *Cut*, a homeodomain transcription factor, is one of the few potentially regulatory genes that is differentially expressed in the CZ; however, its function in hemocyte maturation is not known (JUNG *et al.* 2005).

Interestingly, the specification of cell fate in the lymph gland does not fully recapitulate embryonic development of the same cell types (KRZEMIEN *et al.* 2010a). Crystal cell differentiation is still dependent on Lz (LEBESTKY *et al.* 2000); however Ser signaling through N specifies crystal cells in the lymph gland (DUVIC *et al.* 2002; LEBESTKY *et al.* 2003) but may not be required in the embryo (BATAILLÉ *et al.* 2005). Gcm and Gcm2, which are required for plasmatocyte fate in the embryo, are not expressed in the lymph gland (BATAILLÉ *et al.* 2005). In addition, Pvr is not required for plasmatocyte maturation in the lymph gland (MONDAL *et al.* 2011) as it is in the embryo (BRÜCKNER *et al.* 2004; CHO *et al.* 2002). Ush, the down regulation of which is required for crystal cell fate (FOSSETT *et al.* 2001), inhibits the maturation of all three cell types in the lymph gland (GAO *et al.* 2009; SORRENTINO *et al.* 2007).

Parasitic wasp infestation induces prohemocyte proliferation and the differentiation of lamellocytes, which then encapsulate the invading egg (LANOT *et al.* 2001; SORRENTINO *et al.* 2002). Lamellocytes can be marked using antibodies directed against PS4 integrin α chain (PS4α) (KRZEMIEŃ *et al.* 2007), Filamin-240 (RUS *et al.* 2006) and the lamellocyte-specific antigen L1 (KURUCZ *et al.* 2003). Lamellocytes also express lacZ enhancer traps inserted in the JNK kinase kinase kinase, misshapen (msn) (BRAUN *et al.* 1997) and the JNK phosphatase and reporter for JNK pathway activity, puckered (puc) (IRVING *et al.* 2005). The role of the JNK pathway in mature lamellocytes is not well understood; however there is some evidence to suggest that JNK activity is required for a proper encapsulation response to wasp parasitization rather than for lamellocyte specification (WILLIAMS *et al.* 2006).

Despite the large number of genetic perturbations, both overexpression and loss-of-function, that lead to lamellocyte production (AVET-ROCHEX *et al.* 2010; MINAKHINA and STEWARD 2006; ZETTERVALL *et al.* 2004), very little is known about the mechanisms governing lamellocyte differentiation. One notable exception is the role of the JAK/STAT pathway. Analysis of mutants has shown that pathway components are both necessary and sufficient for lamellocyte formation (HARRISON *et al.* 1995; LUO *et al.* 1995; SORRENTINO *et al.* 2004; ZETTERVALL *et al.* 2004). Conversely, it has recently been shown that downregulation of the JAK/STAT pathway in lymph gland prohemocytes is a prerequisite for parasite-induced lamellocytes (MAKKI *et al.* 2010). It is unclear which cells require active JAK/STAT signaling for lamellocyte differentiation and at what point in the production process the pathway functions.

Finally, the lineage relationship between all 3 mature hemocyte classes is not well understood. It has been proposed that prohemocytes are pluripotent and that a single progenitor class gives rise to all cell types (LANOT *et al.* 2001). However, it has also been suggested that prohemocytes are lineage-restricted from an early developmental stage (KRZEMIEN *et al.* 2010b). Whether a hierarchy of more or less committed progenitors exists is not clear. Further, several studies have suggested that lamellocytes and crystal cells may share a common progenitor (KRZEMIEN *et al.* 2010b; SINENKO *et al.* 2004) and that plasmatocytes can transition to a lamellocyte fate (AVET-ROCHEX *et al.* 2010; HONTI *et al.*

2010; RIZKI 1962; STOFANKO *et al.* 2010). In general, very little is known about how plasmatocyte fate is specified and what factors govern their transformation into mature macrophages.

It is not known whether the two independently-derived populations of hemocytes in the larva, those in the lymph gland and those in sessile bands or in circulation, are similarly specified. As sessile and circulating hemocytes are derived from embryonic hemocytes it would be interesting to determine how/if they are regulated differently in the larva. A complete picture of Drosophila hematopoiesis will require additional definitive markers for all hemocyte types and clonal assays that allow for unambiguous lineage assignments.

The cellular immune response to wounding in Drosophila

Embryonic macrophages are known to clear cells that are removed by programmed cell death during development and can respond to ectopic apoptosis by increasing phagocytic activity (TEPASS *et al.* 1994). Indeed, the activity of macrophages is required for normal development of certain tissues, most notably the central nervous system (SEARS *et al.* 2003). Recently, elegant live-imaging studies have been used to document an inflammatory-like response of embryonic macrophages to laser-wounding of embryonic epithelia (STRAMER *et al.* 2005). Embryonic macrophages migrate to the wound site where they engulf cellular debris (STRAMER *et al.* 2005). This tendency has been used to identify many factors controlling the cytoskeletal rearrangements necessary for directed cell migration *in vivo* and has informed studies of leukocytes in mammals (reviewed in (FAUVARQUE and WILLIAMS 2011; PERI 2010)).

While developmental migration relies on the Pvr-Pvf pathway (BRÜCKNER *et al.* 2004; CHO *et al.* 2002), macrophage chemotaxis towards wound sites requires phosphoinositide 3-kinase (PI3K) (WOOD *et al.* 2006), thus suggesting a mechanism by which embryonic macrophages are able to distinguish between developmental cues and wound-induced signals. Further studies have identified H_2O_2 as a likely chemoattractant that can guide hemocyte migration to the wound site (MOREIRA *et al.* 2010). Interestingly, H_2O_2 has also been shown to mediate wound detection in zebrafish (NIETHAMMER *et al.* 2009). These studies have also demonstrated that embryonic macrophages are able prioritize competing chemotactic signals. Prior to stage 15, embryonic macrophages are refractile to wound cues and do not deviate from normal developmental migratory routes; however, a single apoptotic cell corpse can redirect migration during this refractory period (MOREIRA *et al.* 2010). How immune cells across species integrate and prioritize multiple competing guidance cues is not well understood.

Expression analysis of wounded wild-type and macrophageless embryos has suggested that the presence macrophages may also play a role in the induction of genes in the wounded epithelium (STRAMER *et al.* 2008). How this communication would occur is unknown. Another interesting parallel to vertebrate inflammatory reactions was revealed by the observation that embryonic macrophages are recruited back to developmentally specified migratory routes following the resolution of wound healing (MATHIAS *et al.* 2006; MOREIRA *et al.* 2010). Proper cessation of the inflammatory response is key and poorly characterized aspect of wound healing.

In larvae, hemocytes also accumulate at wound sites; however the means of recruitment is quite different. While macrophages actively migrate to embryonic wounds,

hemocytes amass at larval wounds by the adhesive capture of circulating cells from the hemolymph (BABCOCK *et al.* 2008). How larval hemocytes recognize and bind to damaged "self" tissue is not known. One clue has come from the observation that plasmatocytes adhere to imaginal disc and salivary gland tissue when the basement membrane is disrupted (PASTOR-PAREJA *et al.* 2008). In addition, transplanted fat body or imaginal discs that have been mechanically injured or treated with collagenase trigger lamellocyte encapsulation, while intact tissues do not (RIZKI and RIZKI 1980). Tissues targeted for encapsulation are first recognized by plasmatocytes, which then recruit lamellocytes by an unknown mechanism (HOWELL *et al.* 2011; RUSSO *et al.* 1996; WILLIAMS *et al.* 2005).

There is growing evidence that larval hemocytes can directly impact damaged imaginal discs. Tumorous imaginal discs attract plasmatocytes and it has been suggested that these tumor associated hemocytes (TAHs) influence tumor growth and progression (CORDERO *et al.* 2010; PASTOR-PAREJA *et al.* 2008). In homozygous *scribble* mutant larvae, which are characterized by neoplastic imaginal discs, ablation of the hemocyte population resulted in increased tumor growth (PASTOR-PAREJA *et al.* 2008). In this context, it was hypothesized that TAHs may reduce tumor growth by their ability to secrete basement membrane components (PASTOR-PAREJA *et al.* 2008). However, TAHs have been shown to enhance expression of matrix metalloproteases (MMPs) in tumorous imaginal discs by producing the JNK pathway ligand and tumor necrosis factor (TNF) orthologue Eiger (CORDERO *et al.* 2010). TAHs would therefore be expected to enhance tumor progression. Thus while larval hemocytes are likely to participate in paracrine signaling with damaged imaginal discs, the repercussions of this communication have yet to be resolved.

Hemocytes have also recently been shown to react to targeted ultraviolet (UV) irradiation induced damage of both the larval epidermis and the pupal retina. In response to UV damage, cells of the pupal retina produce Pvf-1, which prompts a Pvr-dependent macrophage-like morphology in associated hemocytes. This signaling is required to limit tissue loss through an unknown mechanism (KELSEY *et al.* 2012). Localized damage to the larval epidermis leads to an expansion in circulating hemocyte numbers, activation of the JAK/STAT pathway in hemocytes and the formation of melanotic masses, suggesting a broad innate immune response. In addition, a systemic repression of insulin signaling was observed, which was found to be hemocyte-dependent and required for survival (KARPAC *et al.* 2011).

Thus, hemocytes may coordinate local and systemic responses to damage, although how they may do so is poorly understood. Indeed, hemocytes have also been shown to relay the need for a humoral immune response from the site of infection to the fat body following both septic injury and oral infection (AGAISSE *et al.* 2003; DIJKERS and O'FARRELL 2007). Our lab has shown that damage to discs delays pupariation by impacting the neuroendocrine system of the host animal (HALME *et al.* 2010). However, the mechanism by which damage and/or regeneration is communicated from discs to the brain is unknown. One interesting possibility is that hemocytes at the site of injury could be partially responsible.

Summary

Cells of the innate immune system, in particular macrophages, are known to interact with damaged and regenerating tissues in a wide range of organisms; however, how these

cells impact the regenerative process remains largely unknown. In addition, the molecular mechanisms underlying macrophage recruitment, identity and function in this context are poorly understood. Drosophila have innate cellular immune system that is the functional equivalent of the vetrebrate monocyte/myeloid lineage. Many of the genes that regulate hematopoeisis and monocyte/macrophage function in mammals play a conserved role in Drosophila. Thus Drosophila may serve as a valuable model within which the genetics of macrophage specification and function may be dissected.

Recent evidence suggests that immune cells in Drosophila are recruited to sites of damage and may participate in the healing process. These cells may also mediate some of the systemic signaling that links injury and repair with broader aspects of animal physiology such as metabolism, humoral immunity and developmental timing. A comprehensive view of the mechanisms underlying these phenomena may inform our understanding of the role of the analogous cells in mammals.

Finally, while recent progress has begun to unravel hematopoeisis in Drosophila, substaintial gaps remain. In particular, how plasmatocyte fate is specified, how these cells transform into macrophages and how they are related in lineage to other hemocyte types are unknown. Several reports have hinted at a previously unappreciated level of heterogenieity in the hemocyte population. The existence of functional subtypes, particularly in the macrophage/plasmatocyte line, would open an exciting new field for study.

Portions of the following chapter were originally published as an article in *Genetics* 2011 Dec;189(4):1309-26.

Chapter 2

Identification and Characterization of Genes Required for Compensatory Growth in Drosophila

Abstract

To maintain tissue homeostasis, some organs are able to replace dying cells with additional proliferation of surviving cells. Such proliferation can be localized (e.g. a regeneration blastema) or diffuse (compensatory growth). The relationship between such growth and the growth that occurs during development has not been characterized in detail. *Drosophila melanogaster* larval imaginal discs can recover from extensive damage, producing normally sized adult organs. Here we describe a system using genetic mosaics to screen for recessive mutations that impair compensatory growth. By generating clones of cells that carry a temperature-sensitive cell-lethal mutation, we conditionally ablate patches of tissue in the imaginal disc and assess the ability of the surviving sister clones to replace the lost tissue. We have used this system together with a modified whole-genome re-sequencing (WGS) strategy to identify several mutations that selectively compromise compensatory growth. We find specific alleles of *bunched* (*bun*) and *Ribonucloside diphosphate reductase large subunit* (*RnrL*) reduce compensatory growth in the imaginal disc. Other genes identified in the screen, including two alleles of *Topoisomerase 3-alpha* (*Top3α*), while also required for developmental growth, appear to have an enhanced requirement during compensatory growth. Compensatory growth occurs at a higher rate than normal growth and may therefore have features in common with some types of overgrowth. Indeed, the *RnrL* allele identified compromises both these types of altered growth and mammalian ribonucleotide reductase and topoisomerases are targets of anti-cancer drugs. Finally, the approach we describe is applicable to the study of compensatory growth in diverse tissues in Drosophila.

Introduction

The organs of multicellular eukaryotes typically reach a characteristic size and shape at the end of their developmental growth. Most organs derive from a small number of progenitor cells and the amount of growth undertaken by these cells is in accordance with an organ-intrinsic size sensing mechanism (reviewed in (BRYANT and SIMPSON 1984; CONLON and RAFF 1999)). However, in response to tissue damage, surviving cells are often required to undergo extra divisions to replace tissue that has been lost. When a large and contiguous portion of an organ has been removed, this extra growth is referred to as regeneration, which typically involves the formation of a blastema, a zone of progenitor and/or stem cells that proliferate extensively to replace the lost tissue mass (reviewed in (BROCKES and KUMAR 2008; STOICK-COOPER *et al.* 2007a)). In contrast, compensatory proliferation (reviewed in (BERGMANN and STELLER 2010; FAN and BERGMANN 2008)) has been used to describe a phenomenon where the death of individual cells scattered through a tissue elicits additional proliferation in the surviving cells without the formation of a distinct blastema.

The characteristics of regenerative and compensatory growth are likely to differ, at some level, from the growth that occurs during normal development. During development, growth and patterning often proceed concurrently. In contrast, regeneration and compensatory proliferation often occur in the context of a fully- or partially-patterned structure and are stimulated by local injury. In both cases, cells that have activated the apoptotic pathway appear necessary for the extra proliferation (CHERA *et al.* 2009; HUH *et al.* 2004; PELLETTIERI *et al.* 2010; PÉREZ-GARIJO *et al.* 2004; RYOO *et al.* 2004; TSENG *et al.* 2007). Thus, an important and unresolved question is whether there are genetic pathways that specifically regulate regeneration and compensatory proliferation. Alternatively, pathways that are required for growth under normal conditions may function in different ways or at different levels during regeneration or compensatory proliferation.

Drosophila imaginal discs, the precursors of adult structures such as the eye and the wing offer an excellent opportunity to study regenerative or compensatory growth. They develop from primordia composed of 15-40 cells and typically experience a 1000-fold increase in cell number over larval development (reviewed in (BRYANT and SIMPSON 1984)). Larval imaginal discs show remarkable regenerative capacity. Damage from irradiation, surgical injury or genetic ablation, elicits additional cell proliferation producing normally sized and patterned adult organs (HADORN and BUCK 1962; HAYNIE and BRYANT 1977; MILÁN *et al.* 1997; SMITH-BOLTON *et al.* 2009).

Surgical injury to imaginal discs results in the formation of a blastema (ABBOTT *et al.* 1981; KIEHLE and SCHUBIGER 1985; O'BROCHTA and BRYANT 1987) as does the ablation of a large portion of the wing imaginal disc *in situ* using a genetic method (SMITH-BOLTON *et al.* 2009). Less localized damage to imaginal discs, as occurs upon treatment with X-ray irradiation, stimulates compensatory proliferation in the surviving cells (HALME *et al.* 2010; HAYNIE and BRYANT 1977; JAKLEVIC and SU 2004). In order to understand whether dying cells directly stimulate the proliferation of surrounding cells, several investigators have blocked the death of apoptotic cells by expressing the baculovirus p35 protein, an inhibitor of effector caspases. These “undead” cells appear to stimulate cell proliferation non-autonomously by expressing secreted proteins such as Wingless (Wg) and Decapentaplegic (Dpp) (HUH *et al.* 2004; PÉREZ-GARIJO *et al.* 2004; RYOO *et al.* 2004). The presence of undead

cells, however, may not fully reflect a normal physiological response to tissue damage. Indeed, a recent study has suggested that neither *dpp* nor *wg* are required for irradiation-induced compensatory growth when dying cells complete apoptosis and are cleared normally from the epithelium (PÉREZ-GARIJO *et al.* 2009). Thus the mechanisms that stimulate compensatory proliferation are still poorly understood.

It is therefore necessary to examine compensatory proliferation in a context that does not depend upon the generation of undead cells. Moreover, current systems to study regeneration in imaginal discs, both surgical and genetic, have not yet been adapted to allow for the discovery of loss-of-function mutations that alter regeneration. Finally, mosaic screens for recessive mutations have proven a powerful tool in the identification of genes that function during normal imaginal disc growth (reviewed in (ST JOHNSTON 2002)). Yet these types of screens have not been applied to study regenerative or compensatory growth.

Here we describe a system that uses genetic mosaics to conditionally ablate patches of cells within the developing imaginal disc and thereby induce regenerative or compensatory growth. We have used this method to characterize the properties of this additional growth and to conduct a screen for recessive mutations that impair it. Using an approach based on whole genome re-sequencing (WGS) we have identified several of the affected genes from our screen. Our results show that ablating patches of cells induces compensatory growth rather than a regeneration blastema. This compensatory growth is in part an acceleration of developmental growth and thus sensitizes cells to reduced levels of factors required for more rapid growth. Interestingly, two of the genes that we have identified are also common chemotherapeutic targets. Additional characterization of a set of our mutants suggests that these mutations may interfere with compensatory growth in different ways and that at least one also disrupts tissue overgrowth.

Results

A mosaic system to study compensatory growth in Drosophila imaginal discs.

To develop a system that would allow us to study regenerative or compensatory growth in imaginal discs, we took advantage of FLP/FRT-catalyzed mitotic recombination and a temperature-sensitive recessive cell-lethal mutation. This allowed us to generate patches of tissue that could be ablated upon shifting to the restrictive temperature (30°C). Thus, to achieve a disc of the appropriate final size, the surviving cells must undergo additional proliferation.

We used a temperature-sensitive recessive cell-lethal mutation in the *sec5* gene (*sec5^{ts1}*, hereafter *sec5^{ts}*) on an FRT chromosome (LANGEVIN *et al.* 2005; MURTHY *et al.* 2010). We generated several versions of the *sec5^{ts}* tester line in combination with either *eyeless-FLP* (*ey-FLP*) to generate clones in the eye antennal disc or *engrailed-GAL4* (*en-GAL4*) driving expression of a *UAS-FLP* transgene (*en>FLP*) or *Ultrabithorax-FLP* (*Ubx-FLP*) to make clones in the wing disc. A schematic representing ablation in the wing disc using *en>FLP* is shown in Figure 2.1, A and B. Here we produced clones by crossing to a line with a wild-type FRT chromosome that also carried a copy of GFP.

In the wing disc, *en* is expressed early and continuously in the posterior compartment, with an additional stripe of expression just anterior to the anterior-posterior (A-P) compartment boundary late in larval development (BLAIR 1992). This allowed us to generate discs in which the posterior compartment was composed almost entirely of two populations of cells: mutant *sec5^{ts1}* clones, marked by the absence of GFP expression, and the wild-type sister clones composed of cells that have two copies of GFP (Figure 2.1, B). *Ey-FLP* also produces discs that are largely homozygous for these two types of clones. The efficiency of mitotic recombination using *en>FLP* and *ey-FLP* is shown in Figure 2.1, C. *Ubx-FLP* was not similarly evaluated. In this case, *sec5^{ts}* clones are marked by the presence of GFP. We will hereafter refer to mosaic discs with *sec5^{ts1}* mutant clones as "ablated" discs and mosaic discs with non-ablating control clones as "control" discs. Unless otherwise specified, we used *en>FLP* to analyze wing discs in which ablation had been induced specifically in the posterior compartment.

To assess the effect of *sec5^{ts}* clones on imaginal disc development, animals were reared at 18°C until early third larval instar (L3), 7.5 days after egg lay (dAEL), when they were shifted to 30°C for 48 hours to ablate the homozygous *sec5^{ts}* tissue (Figure 2.1, B). Upon shift to 30°C, mutant *sec5^{ts}* cells stained positive for both cleaved caspase and TUNEL and were removed from the epithelium by a combination of basal extrusion and engulfment (Figure 2.1, D-E). Despite sustaining significant apoptosis, the resulting adult structures were normally sized (Figure 2.1, F-G) indicating that the surviving wild-type cells had compensated for the loss of their neighbors.

Unlike other methods for inducing imaginal disc damage that cause a delay in the larval to pupal transition presumably to allow adequate time for regeneration (HALME *et al.* 2010; SIMPSON *et al.* 1980; STIEPER *et al.* 2008), *sec5^{ts}*-induced ablation did not significantly delay development (Figure 2.2, A). The absence of a developmental delay indicates that, in this system, the necessary additional growth can occur during a larval stage of normal duration. However, similar to previous reports, we found that if we induced ablation later

in larval development (HALME *et al.* 2010; SMITH-BOLTON *et al.* 2009), the size and morphology of the resulting adult organs were adversely affected (Figure 2.2, B). The onset of pupariation may limit the amount of time available for regenerative growth; thus discs damaged closer to this transition cannot complete the regenerative process. Alternatively, older discs may be inherently less capable of engaging in regenerative growth.

Ablated discs replace the loss of sec5^{ts} clones by accelerating the rate of tissue

The surviving GFP-positive tissue in ablated discs must compensate both for the *sec5^{ts}* cells that have been eliminated and for the portion of the posterior compartment that would normally be generated by the proliferation of those cells. Although from the time of up-shift until 6 hours after up-shift (AUS), ablated and control discs were of comparable size, by 12 hours AUS, ablated discs were significantly smaller than their non-ablating counterparts (Figure 2.3, A and B). Interestingly, this difference was observed for both the posterior and the anterior compartment (Figure 2.3, B) suggesting that, similar to previous reports, damage to the posterior compartment may have a non-autonomous effect on the growth of the rest of the disc (MESQUITA *et al.* 2010; MILÁN *et al.* 1997).

Despite being significantly smaller than control discs at 12 hours AUS, ablated discs had largely recovered in size by 36 hours AUS (Figure 2.3, A and B), suggesting that the surviving GFP-positive tissue in ablated discs must grow more rapidly during this time than the GFP-positive tissue in control discs. Indeed, although both ablated and control discs started with a GFP-positive precursor population of comparable size, this population gave rise to more tissue over the same time period in ablated discs than in controls (Figure 2.3, A and C). The majority of this extra growth occurred between 12 and 36 hours AUS. During this time, the predicted rate of growth of the GFP-positive tissue in ablated discs was at least 1.5 times greater than the rate of growth in control discs (Figure 2.3, C).

Thus, the elimination of patches of *sec5^{ts}* cells from imaginal discs results in the efficient replacement of the lost tissue and the recovery of normally sized adult structures. This recovery is achieved without requiring a developmental delay and occurs by an increase in the rate of growth of the surviving tissue.

sec5^{ts} ablation produces compensatory proliferation throughout the affected tissue.

The extra growth induced by *sec5^{ts}* ablation could occur by a localized increase in proliferation adjacent to patches of dying cells, similar to the blastema formed in regenerating discs (ABBOTT *et al.* 1981; KIEHLE and SCHUBIGER 1985; O'BROCHTA and BRYANT 1987; SMITH-BOLTON *et al.* 2009) or to the non-autonomous proliferation stimulated by undead cells (HUH *et al.* 2004; PÉREZ-GARIJO *et al.* 2004; RYOO *et al.* 2004). Alternatively, it could occur in an apparently asynchronous and diffuse manner throughout the compartment as occurs during normal development (ADLER and MACQUEEN 1984). The latter could be achieved either by an increase in the rate of proliferation of individual cells or by an increase in the proportion of cells actively dividing or by a combination of both mechanisms.

As early as 6 hours AUS, ablated discs showed significant levels of apoptosis (Figure 2.4, A and E). The amount of apoptosis peaked after 12 hours at 30°C and by 36 hours AUS

the majority of TUNEL-positive puncta marked cellular debris basal to the disc epithelium (Figure 2.4, B-D: data not shown). At all time points, neither EdU labeling of S-phase cells nor phospho-histone H3 (PHH3) labeling of mitotic cells provided consistent evidence for a localized proliferative response to apoptosis (Figure 2.4, A-F). However, without a decrease in background levels of proliferation, a small localized increase in proliferation might be difficult to detect, particularly if the additional cell cycles were asynchronous.

To determine whether *sec5^{ts}* discs had quantitatively more mitotic cells than control discs, we calculated the density of PHH3-positive nuclei (PHH3+ nuclei/1000 pixels area) in the posterior compartment of discs from each population. At 12 hours AUS, ablated discs had a greater density of mitotic cells than controls (Figure 2.4, G), suggesting that a greater proportion of cells were actively dividing. This response occurred shortly after the onset of ablation when levels of apoptosis were the highest. The increase in mitotic cell density may account for the significant recovery in the size of the ablated compartment that we observed between 12 and 24 hours AUS (Figure 2.3, C). Unfortunately we were unable to directly measure proliferation rates, as available methods also rely on clones generated by FLP/FRT mitotic recombination.

At 24 hours AUS, ablated and control discs showed roughly the same density of mitotic cells (Figure 2.4, G). However, in discs dissected from wandering larvae (36-40 hours AUS), the density of mitotic cells declined in control discs while remaining constant in ablated discs (Figure 2.4, G). During normal wing disc development, cell doubling times increase significantly in late discs with most cells eventually arresting in G2 by the end of larval development (CHERA *et al.* 2009; FAIN and STEVENS 1982). Our observations suggest that at least some portion of compensatory growth was accomplished by a delay in this transition to G2 arrest.

Thus we can observe compensatory proliferation at two points during the ablation period. Early compensatory proliferation is coincident with high amounts of apoptosis, although not clearly localized to sites of damage, and occurs concomitantly with the majority of disc size recovery. Late compensatory proliferation occurs after most apoptosis is complete, by an extension of an earlier more rapid growth phase of disc development and may allow ablated discs to fully "catch up" to the size of control discs.

Analysis of candidate signaling pathways in discs undergoing compensatory growth.

Several reports have indicated that Jun N-terminal Kinase (JNK) signaling is required in undead cells for the production of non-autonomous proliferation (PÉREZ-GARIJO *et al.* 2009; RYOO *et al.* 2004). Dying *sec5^{ts}* cells showed increased expression of the JNK pathway reporter *puckered-lacZ* (*puc-lacZ*) (GLISE *et al.* 1995; GLISE and NOSELLI 1997; RIESGO-ESCOVAR *et al.* 1996) (Figure 2.5, A), suggesting that JNK may play a role in *sec5^{ts}* – induced compensatory proliferation. Indeed, ablation of *sec5^{ts}* clones that lacked Drosophila JNK, *basket* (*bsk*), resulted in adult eyes and wings that were strongly reduced in size (Figure 2.5, B and C, and data not shown). However, further analysis of double mutant *sec5^{ts}, bsk* clones in the eye disc revealed that these cells did not undergo apoptosis following shift to 30°C (Figure 2.5, D and E). While viable at the restrictive temperature, these cells were unable to properly differentiate (Figure 2.5, F and G) and were consequently absent from the resulting adult structure. We do not know at what point

during pupal development these cells were eliminated such that the overall size of the adult organ was adversely effected. Thus we cannot distinguish between a putative role for JNK in driving non-autonomous compensatory proliferation and its role in ensuring the ablation of *sec5^{ts}* tissue.

Undead cells promote ectopic proliferation by producing the mitogens Wg and Dpp (HUH *et al.* 2004; PÉREZ-GARIJO *et al.* 2004; PÉREZ-GARIJO *et al.* 2005; PÉREZ-GARIJO *et al.* 2009; RYOO *et al.* 2004) and the expression patterns of Wg and Dpp are altered in regenerating wing discs (SMITH-BOLTON *et al.* 2009). However, neither Dpp nor Wg are necessary for irradiation-induced compensatory proliferation (PÉREZ-GARIJO *et al.* 2009) and the functional significance of their modified expression in regenerating discs has not been established. Using *ey-FLP* and *Ubx-FLP* to induce clones in the eye and wing disc, respectively, we assessed the possible involvement of Wg and Dpp in *sec5^{ts}*-induced compensatory proliferation. Levels of phosphorylated Mad appeared unchanged in ablated discs, indicating that Dpp signaling was likely unaltered (TANIMOTO *et al.* 2000) {Figure 2.6 A and B, G and H).

In both ablated eye and wing discs, we did not observe ectopic Wg protein in *sec5^{ts}* clones located away from the endogenous zone of Wg expression (Figure 2.6, E and F, K and L). In ablated wing discs, we noted occassional patches of *sec5^{ts}* cells located within the normal Wg expression domain that showed elevated levels of Wg protein (Figure 2.6, F). This change is unlikely to be required for *sec5^{ts}*-induced compensatory proliferation, as removal of *wg* from *sec5^{ts}* clones did not impair disc recovery following ablation (data not shown). More frequently, we observed that *sec5^{ts}* clones disrupted Wg expression, and that protein levels were altered directly adjacent to these patches (Figure 2.6, F and N). These changes may occur as the normal Wg pattern is re-established around dying *sec5^{ts}* cells that are being cleared from the epithelium.

The Janus kinase/Signal-transducer and activator of transcription (JAK/STAT) pathway promotes intestinal regeneration in Drosophila {Jiang at al 2005} and is a potent stimulator of imaginal disc growth (reviewed in (ARBOUZOVA and ZEIDLER 2006)). We used the transcriptional reporter for the JAK/STAT pathway, *STAT-GFP* (BACH *et al.* 2007), to assay whether discs undergoing compensatory proliferation showed altered pathway activity. *STAT-GFP* expression was largely normal in eye and wing discs ablated using *ey-FLP* and *Ubx-FLP*, respectively. However, we observed scattered cells that expressed elevated levels of *STAT-GFP*, giving ablated discs a speckled appearance (Figure 2.6, C and D, I and J). These cells were located within or adjacent to the normal expression domain for *STAT-GFP* and were both ablating *sec5^{ts}* cells and neighboring wild-type cells (Figure 2.6, M). Thus, local increases in JAK/STAT pathway activity could drive the replacement of ablated cells in regions of the disc where the pathway is already active. However, it does not appear that ectopic pathway activation is universally responsible for promoting compensatory proliferation.

A genetic screen to identify recessive mutations that impair compensatory growth.

One strength of the *sec5^{ts}* system is that it allows for unbiased screens using genetic mosaics to find recessive mutations that potentially block compensatory growth. In order to conduct such a screen, we chose to use the developing eye instead of the wing, since in the adult eye, the proportion of wild-type and mutant tissue can be scored easily. This

feature is of particular importance when seeking to rule out mutations that merely impair normal growth (see below). To conduct our screen we generated *sec5^{ts}* clones that lacked a copy of the white gene and were consequently unpigmented in the adult eye. The reciprocal clones were pigmented. Thus when animals are shifted to 30°C in the L3 stage of larval development, the resulting adult eyes are normally sized and patterned, but composed largely of red (wild-type) tissue (Figure 2.1, F and Figure 2.7, A and B).

If instead, these "red" cells were homozygous for a mutation in a gene required for compensatory growth, they would not be able to compensate for the loss of the "white" tissue at earlier stages of development and the resulting adult eye should be smaller (Figure 2.7, C and D). However, this assay would not distinguish between mutations that affect developmental growth and those specific to compensatory growth. To attempt to eliminate the former, we conducted a secondary screen in which we generated mosaic eyes, but did not induce ablation of the *sec5^{ts}* tissue. When larvae develop at 18°C, adult eyes are mosaic with both white and red tissue present (Figure 2.7, A' and B). If a mutation disrupted a gene required for developmental growth, we would expect this to result in the underrepresentation of the red tissue in the adult eye even in the absence of tissue ablation (Figure 2.7, C). If the effect on developmental growth were minimal, we would expect the amount of red tissue to resemble the non-mutagenized control (Figure 2.7, D).

We performed a screen of the left arm of chromosome 2 (2L), screening approximately 11,000 individuals each carrying a unique EMS-mutagenized chromosome. The screen was carried out in two parts, with slight modifications to the mutation selection process. A flow diagram for the entire screen is given in Figure 2.8. Of the 735 mutations initially selected, only 31 were retained after re-testing and secondary screening. These 31 mutations fell into four 2-3 member lethal complementation groups and 22 putative single hits. The phenotypes ranged from eyes that were less than half the size of control eyes to those that were only slightly reduced in size but rough across the eye (Figure 2.7, E; Figure 2.9, A-A'). In a few cases, we also observed some variability in the amount of red mutant tissue in animals raised at 18°C where tissue ablation does not occur (Figure 2.7, E, e.g. *A4A7*). Thus a subset of mutations identified in the screen may also subtly compromise developmental growth. However, most of the 31 mutations appeared to fit our initial criteria: a reduction in eye size following ablation and a relatively normal contribution of mutant cells to the adult eye in the absence of ablation (Table 2.1).

Secondary assays to classify mutations isolated from the sec5^{ts} screen.

Our *sec5^{ts}* system required that compensatory growth occur at 30°C, while our secondary screen assessed developmental growth at 18°C. Thus one important consideration was whether any of our mutations affected normal tissue development at more elevated temperatures. To identify this class of mutant, we generated mosaic eye imaginal discs using a wild-type, non-ablating (white) sister clone. We first assessed the amount of red mutant tissue present when animals were raised under standard conditions (25°C) as compared to the amount of tissue generated by the non-mutagenized parental chromosome (Figure 2.9, B). We found that 14 of the 31 mutations caused an inferred moderate to strong growth defect under these conditions while the remaining 17 did not (Figure 2.9, B'). We then compared the amount of red mutant tissue present at 25°C to the

amount present if the animals were shifted to 30°C during larval development (Figure 2.9, C). Mutants were given a "strong" (S) classification if the amount of red tissue was substantially less at 30°C than at 25°C (Figure 2.9, C', e.g. *A2E9*). If the amount of red tissue was the same at both temperatures, we gave these mutants a "no change" (NC) classification (Figure 2.9, C', e.g. *A4B5*). Of the 17 mutants with no obvious growth impairment at 25°C, 11 displayed a noticeable growth defect when animals were shifted to 30°C (Figure 2.9, C'). In total, when compared to their inferred growth ability at 18°C, 25 of the 31 mutations showed a temperature-sensitive phenotype, either at 25°C or at 30°C (Table 2.2).

To circumvent the issue of temperature-sensitivity and to assess the impact of these mutations on compensatory proliferation induced by a different type of damage, we used *ey-FLP* to generate mosaic eye imaginal discs and X-ray irradiation (IR) during larval development to stimulate compensatory proliferation. IR causes widespread apoptosis, primarily in actively dividing cells and has been shown to induce a robust compensatory growth response in imaginal discs (HALME *et al.* 2010; HAYNIE and BRYANT 1977; JAKLEVIC and SU 2004). We compared the amount of red mutant tissue present in unirradiated animals to that found in animals subjected to IR during the early L3 larval stage (Figure 2.9, D). Of the 17 mutations with approximately normal tissue representation in untreated animals, 11 showed a reduction in the amount of red tissue following IR (Figure 2.9, D' and Table 2.2). Additionally, another 5 mutants that had a moderate to strong underrepresentation of red tissue in untreated animals, showed a further reduction in the amount of red tissue following IR (Figure 2.9, D' and Table 2.2). Thus 16 of the 31 mutations identified in our screen may also impede IR-induced compensatory proliferation, suggesting a more general requirement for the affected genes in producing compensatory growth.

The temperature-sensitive growth defect of many of our mutants could be due to a gene product that is inherently unstable at higher temperatures. However, to our knowledge no one has directly assessed the rate of cell division in imaginal discs at different temperatures. As larval development is accelerated at 30°C, disc growth may also proceed more rapidly. Thus one reason for the apparent temperature-sensitive phenotype of these mutants could be that they disrupt genes that are limiting for the acceleration of growth. This explanation could also apply to those mutations that showed reduced growth at 25°C while appearing normal at 18°C, as development proceeds roughly two times faster at 25°C than at 18°C. We noted that there was substantial overlap between mutations with a temperature-sensitive phenotype and an IR-sensitive one (10 of 15). If indeed both increased temperature and IR-induced damage provoke accelerated growth, these mutations may affect genes that are generally limiting for more rapid growth.

As a final assay, we tested a subset of mutations for the ability to dominantly modify regeneration of the wing disc using a genetic system developed by our lab that ablates the entire wing pouch (SMITH-BOLTON *et al.* 2009). Re-growth under these circumstances occurs by blastema formation, thus allowing us to assess the impact of our mutations on a different type of regenerative growth. We found that of the 7 mutations tested, 2 (*A4B5* and *A4A7*) dominantly reduced wing disc regeneration (Figure 2.10).

Our phenotypic characterization of all mutations recovered from the screen allowed us to set priorities for further study. Of the original 31 mutations, 17 had a minimal effect

on growth at 25°C. Of these 17, only 6 showed no temperature sensitivity at 30°C (*A4B5*, *A5G3*, *B12-3*, *B3-1*, *A2I3* and *A2B3*). Of these 6, 1 dominantly modified blastemal regeneration (*A4B5*), 3 were X-ray sensitive (*A5G3*, *B3-1* and *A2I3*) and 2 (*B12-3* and *A2I3*) fell into 2 different lethal complementation groups. (Figure 2.9). We initially gave highest priority to these 6 mutations with an increased interest in the 3 X-ray sensitive alleles, as all phenotypic evidence suggested that they might represent a class of genes required specifically for compensatory growth.

However, we also recovered a significant number of mutations that appeared to also be involved in developmental growth. Indeed, although *B12-3* and *A2I3* did not disrupt normal growth, the second alleles in each complementation group showed a moderate growth defect in the absence of ablation (*A4A7* and *B9-2*, respectively). In addition, *A4A7* dominantly reduced blastema-driven wing disc regeneration. In this case, *B12-3* and *A2I3* could be hypomorphic alleles capable of providing sufficient gene function for developmental growth but not for more rapid compensatory growth. In a third complementation group (*A1C5*/*A3G1*), both alleles showed a similar phenotype: a moderate growth defect following *sec5*^{ts} ablation, IR treatment, or shift to 30°C and a very mild growth defect at 25°C (Figure 2.9). Although these mutations were unlikely to specifically impact compensatory growth, the possibility that they might represent a class of genes that are required more when growth is accelerated, led us to also pursue their characterization further. We therefore sought to identify the affected genes in our complementation groups by traditional methods and adopted a new approach based on whole genome re-sequencing to identify the mutated genes in our top candidates, all of which appeared to be single-hit lethal, mutations.

Molecular characterization of three lethal complementation groups identified in the screen.

Using deficiency mapping and candidate gene sequencing we were able to find mutations in the *A2I3*/*B9-2* and *B12-3*/*A4A7* lethal complementation groups (Figure 2.11, A). In the group composed of *A4A7* and *B12-3* we identified mutations in *mitochondrial RNA polymerase* (*mtRNApol*). *A4A7*, which showed a stronger phenotype both following *sec5*^{ts} ablation and with respect to growth defects in the absence of ablation, results from a mutation that truncates the protein upstream of the catalytic domain, likely representing a null allele (Figure 2.11, B). *B12-3*, which showed no growth defect in the absence of ablation and weak phenotype following *sec5*^{ts} ablation, causes a glycine to glutamic acid substitution in a region of the protein containing no predicted functional domains and is likely to be a weak hypomorph (Figure 2.11, B). Mitochondrial RNA polymerases are required both for transcription of the mitochondrial genome as well as its replication and/or stability. While mutations in *mtRNApol* have not been described previously in Drosophila, mutations in the yeast orthologue lead to mitochondrial dysfunction and mutant cells grow more slowly than wild type (WANG and SHADEL 1999).

In the group consisting of *B9-2* and *A2I3*, we found mutations in *Topoisomerase3α* (*Top3α*). *Top3α* is a type IA topoisomerase that is involved in decatenating replicating chromosomes. In Drosophila, *Top3α* mutant larvae lack imaginal discs consistent with a mitotic defect (PLANK *et al.* 2005). Recent evidence suggests that *Top3α* is also involved in mitochondrial DNA genome maintenance (WU *et al.* 2010). *A2I3* generates a premature

stop truncating the gene product N-terminal to the active site. *B9-2* results from a small deletion within the active site that leads to a frame-shift and a premature stop. (Figure 2.11, B). Based on the position and nature of our mutations, both are likely to be strong or null alleles. Both alleles showed a robust phenotype following either *sec5*^{ts}- or IR-induced ablation. However, while *B9-2* moderately disrupted developmental growth, *A2I3* had a minimal phenotype under these conditions. Thus *A2I3* may be a slighter weaker allele that more severely compromises compensatory growth, which requires either additional or more rapid cell divisions.

For the third complementation group composed of *A3G1* and *A1C5,* mutations in *CENP-meta* (*cmet*) were identified. *cmet* is a kinetochore kinesin that is required for maintenance of chromosomes at the metaphase plate and lack of a functional gene product leads to mitotic abnormalities and cell-cycle arrest (MAIA *et al.* 2007; YUCEL *et al.* 2000). Both alleles introduce premature stop codons, *A3G1* by a small insertion causing a frame shift within the kinesin motor domain and *A1C5* by a point mutation further toward the C-terminal of the protein (Figure 2.11, B).

We also began deficiency mapping of 4 additional single-hit, lethal alleles (*A2G1*, *A5D4*, *A2D1* and *B12-1*). While the lethal mutation in this case may not correspond to the mutation causing the compensatory growth defect, this possibility can be addressed by testing second alleles of any candidate genes. Preliminary mapping information is given in Figure 2.12.

Thus, all genes identified in our analysis of the lethal complementation groups appear to be involved in cell growth or cell cycle progression and are not specifically required for compensatory growth. The recovery of two likely hypomorphic alleles that do not compromise developmental growth, suggests that there may be an increased demand for these gene products during compensatory growth.

Characterization of single-hit mutations using whole-genome re-sequencing (WGS).

Three mutations, *A4B5*, *A5G3* and *B3-1,* had no detectable growth defect under normal conditions, but had a consistent and robust phenotype when compensatory growth was induced. Additionally, *B3-1* and *A5G3* showed mild to moderate defects following X-ray irradiation (Figure 2.13). However, molecular characterization of these mutations was complicated by the fact that these were apparent single hits. If the lethal mutation was not also causative for the defect in compensatory growth, we would have limited options to then identify the gene of interest. The advent of massively parallel sequencing technologies has made it feasible to re-sequence a fly genome rapidly and relatively inexpensively. WGS has been used to identify point mutations in bacteria (SRIVATSAN *et al.* 2008) and *C. elegans* (SARIN *et al.* 2010). Moreover, recently there has been one successful reported application of WGS to identify an EMS-induced mutation in Drosophila (BLUMENSTIEL *et al.* 2009). This encouraged us to identify mutations for each of these three alleles using WGS. Candidate genes could then be followed in recombinant chromosomes to allow for the identification of the mutation relevant to the defect in compensatory proliferation.

In the previous study characterizing an EMS-induced mutation by WGS, flies homozygous for the mutant chromosome were viable and sterile. Thus it was possible to generate sequencing libraries from individuals in which the mutation of interest was homozygous. This allowed the authors to set very stringent cutoffs for mutation discovery

and to use available software to predict a consensus sequence for both the mutant and parental genotypes. By directly comparing these two consensus assemblies, they were able to identify putative mutations. In contrast, analysis of the mutations identified in our screen was complicated by the fact that each of the mutant chromosomes is homozygous lethal. The necessity of sequencing heterozygous individuals, in combination with the relatively modest levels of genome coverage available with current technologies, required us to modify standard mutation detection software for our purposes. Thus, to identify heterozygous mutations required a different approach to library construction and data analysis than has been used previously.

To identify mutations from heterozygous individuals we took the following approach. To avoid sequencing non-mutant chromosomes, we crossed each allele to each of the two others to generate 3 trans-heterozygous stocks (Figure 2.14, A). Since each chromosome represented a unique EMS-mutagenized version of the original parental genotype, we reasoned that each trans-heterozygous combination would also carry a copy of the wild-type parental allele thus making sequencing of the parental strain unnecessary. This reduced our sequencing costs significantly. By comparing the mutations found in all the three libraries it should, in principle, be possible to assign each mutation to a specific mutant chromosome (Figure 2.14, A). We obtained 5 to 7-fold coverage of chromosome 2L for each library (Figure 2.14, C) and mapped all reads to the reference genome using the software MAQ (Li *et al.* 2008).

In order to analyze our sequencing data we developed a Perl script that would allow us to extract potential mutations without relying exclusively on MAQ's SNP-calling criteria. Essentially, we generated a list that contained every putative mutation found in our sequencing data as compared to the reference genome. We then used a second customized script to perform a series of pair-wise comparisons using the mutation lists for each of our three libraries. For example, we asked for a list of mutations that were present in "ab" and "ac" but not in "bc" to identify polymorphisms unique to "a" or *B3-1* (Figure 2.14, A). By excluding mutations found in "bc", we eliminated most polymorphisms between the starting parental chromosome and the reference genome, as these would be present in all libraries. By only including mutations present in both "ab" and "ac", we decreased the instance of mutations reported due to mapping or sequencing errors, assuming that the same errors would not be present in both libraries. Finally, we developed a third script that allowed us to search mutations for those occurring specifically in coding sequences. We then refined this list further to include only mutations causing an amino acid change (non-synonymous mutations) and again to include only non-synonymous changes that were likely to be deleterious (Figure 2.14, E).

While our comparison strategy using the individual libraries should provide complete mutation lists for each genotype, our low coverage prompted us to take a second complementary approach. If, for example, a position in "ab" had insufficient sequencing coverage such that the mutant allele was not represented, we would have excluded this position even if a mutation were found in "ac". To address this concern we performed a second analysis by combining all reads from all libraries (Figure 2.14, B). Our combined data gave us 21-fold coverage of chromosome 2L (Figure 2.14, C). Using the same programs mentioned above, we filtered all mutations based on their frequency, excluding very rare or very common mutations as likely to be sequencing errors or parental alleles respectively

(Figure 2.14, B), generating a list of non-synonymous mutations that was refined further to include only deleterious changes (Figure 2.14, E).

All putative non-synonymous mutations were examined using Sanger sequencing. We initially found a surprisingly high false positive rate, approaching 90% in some libraries. This appeared to result from an inflated number of mutations called in the first several bases of mapped reads. When we plotted the read position for all mutations with a relatively high sequencing quality, we found that 30% of all mutations were found within base 2-5 of our reads (Figure 2.14, D). This was not due to a corresponding peak in sequencing quality scores, as these remained relatively constant across reads (Figure 2.14, D). We also did not find a corresponding base composition bias at these early positions (Figure 2.14, D), suggesting that these may not be sequencing errors, but may in fact be changes introduced and then propagated at the end of reads during library construction. To address this issue, we modified our first script to eliminate all mutations found in the first 5 bases of a read. This lowered our false positive rate to less than 25%, which is reasonable given the absence of a known mutation database to use to train mutation-calling parameters, the low sequencing coverage and the heterozygous nature of our alleles.

Based on our data analysis, we found 1 candidate mutation in *A4B5*, 2 in *B3-1* and 6 in *A5G3*. *A4B5* had a mutation in *Ribonucleoside diphosphate reductase, large subunit* (*RnrL*) while *B3-1* had mutations in *GDP-mannose 4,6-dehydratase* (*Gmd*) and *CG13817*. We outcrossed *B3-1* and *A4B5* to the parental strain for 5 generations at the end of which lines were re-isolated based on the eye phenotype following $sec5^{ts}$-induced ablation. The *A4B5* and *B3-1* chromosomes retained the mutations in *RnrL* and *Gmd* respectively. In contrast, one line re-isolated for *B3-1* had lost the second mutation in *CG13817*. An independently derived allele of *Gmd* also showed the same phenotype following $sec5^{ts}$ ablation. An uncharacterized second allele of *RnrL* did not recapitulate the $RnrL^{A4B5}$ phenotype (Figure 2.15).

A5G3 had mutations in six genes including *bunched* (*bun*) and *shuttlecraft* (*stc*). The stock was outcrossed to the parental strain and recombinant lines were selected based on separation of *bun* and *stc* from the other 4 mutations. When re-tested with the $sec5^{ts}$ system, only the recombinant lines carrying *bun* and *stc* showed the mutant phenotype (data not shown). We did not generate any recombinants between *bun* and *stc* which are relatively closely linked. While we cannot exclude the possibility that *stc* contributed to the phenotype, independently-derived alleles of *bun* showed the same mutant phenotype as *A5G3* (Figure 2.15). Thus we conclude that the mutant phenotypes of *A4B5*, *B3-1* and *A5G3* were caused by mutations in *RnrL*, *Gmd* and *bun* respectively.

RnrL encodes the large subunit of the ribonucleoside reductase holoenzyme (RR). We found a transition mutation causing a valine to methionine substitution at a highly conserved residue within the domain that is predicted to bind the small subunit (*RnrS*) (Figure 2.14, F). RRs catalyze the synthesis of deoxyribonucleotides from their corresponding ribonucleotides and are required to provide dNTPs for DNA synthesis in S-phase (ELLEDGE *et al.* 1992). They are also required for recovery following genotoxic stress by maintaining dNTP levels necessary for DNA repair (TANAKA *et al.* 2000).

Gmd is required for the de novo synthesis of GDP-fucose, the donor in fucosyltransferease reactions (reviewed in (BECKER and LOWE 2003)). As there is no salvage pathway for GDP-fucose synthesis in Drosophila, loss of *Gmd* is presumed to block all fucosylation (ROOS *et al.* 2002). We identified a transversion mutation that changes a highly

conserved methionine to a lysine near the C-terminal end of the *Gmd* active site (Figure 2.14, F).

bun is the Drosophila homolog of the mammalian Transforming Growth Factor-β1 stimulated clone (TSC-22), a putative tumor suppressor that is down-regulated in several tumor types (DOBENS *et al.* 1997). In the wing disc, *bun* clones were slightly smaller than their wild-type controls suggesting that *bun* plays a minor role in normal growth (GLUDERER *et al.* 2008; WU *et al.* 2008). Interestingly, *bun* was identified by two independent studies as transcriptionally up-regulated in regenerating imaginal discs, suggesting that *bun* may be preferentially required by cells undergoing extra or regenerative growth (ADDISON *et al.* 1995; BLANCO *et al.* 2010). We found a nonsense mutation at glutamine 935, which would result in the premature truncation of the three putative long isoforms of *bun*, bunA, bunF and bunG and generate a protein lacking the putative DNA-binding domain (Figure 2.14, F).

The identified mutations represent 3 putative phenotypic classes.

To characterize the phenotypes of $Gmd^{B3\text{-}1}$, $RnrL^{A4B5}$ and bun^{A5G3} further we tested these alleles in the *en>FLP* wing disc $sec5^{ts}$ ablation system (Figure 2.1, B). All three alleles showed a reduced-wing phenotype (Figure 2.16, A-D), suggesting that, as in the eye, mutation of any of these genes reduces compensatory growth in the wing. These effects cannot be attributed to an acceleration of development, which would be predicted to impair compensatory growth since imaginal discs from older larvae are less capable of regeneration (Figure 2.16, P). At the end of the ablation period (48 hours AUS), we found that only discs in which the compensating cells were mutant for bun^{A5G3} was disc size strongly affected (Figure 2.16, O). This reduction in size was observed in both the posterior and anterior compartment. We did not observe elevated levels of apoptosis in the posterior compartment and mitoses were still evident (Figure 2.16, F and K), suggesting that bun^{A5G3} mutant cells were viable and still capable of proliferating. The disc and adult wing phenotype of bun^{A5G3} suggest that *bun* may be required to initiate and/or sustain compensatory growth.

Although both $Gmd^{B3\text{-}1}$and $RnrL^{A4B5}$ caused substantial defects in the resulting adult wings (Figure 2.16, C and D), at 48 hours AUS wing imaginal discs from these animals were not correspondingly reduced in size (Figure 2.16, O). Discs in which the compensating cells were $Gmd^{B3\text{-}1}$ showed no obvious abnormalities, suggesting that the loss of *Gmd* does not impact the ability of disc cells to undergo compensatory growth and that *Gmd* may be required later during pupal wing development (Figure 2.16, G and L). Indeed, the most common defect observed in the adult wings of these animals is blistering (Figure 2.16, C), which is often caused by faulty adhesion between the dorsal and ventral wing surface .

Discs in which the compensating cells were $RnrL^{A4B5}$ were similar in size to discs with wild-type cells (Figure 2.16, O). However, the posterior compartment showed very high levels of apoptotic cells (Figure 2.16, H and M). These dying cells were not residual $sec5^{ts}$ cells, but were largely GFP-positive and hence homozygous for $RnrL^{A4B5}$ (Figure 2.16, M). Despite high levels of apoptosis, mitotic cells are still evident in the posterior compartment (Figure 2.16, H"). Thus cells with reduced RnrL function may be initially capable of engaging in compensatory growth and generating a fairly normally sized posterior compartment, but these cells are sensitized to apoptosis. Lack of *RnrL* would

reduce the amount of dNTPs available for DNA replication (ELLEDGE *et al.* 1992). Increased proliferation when DNA replication is compromised can result in high levels of apoptosis (reviewed in (SAMPATH *et al.* 2003)). Loss of *Top3α* might impair disentanglement of replicated DNA (PLANK *et al.* 2005) and could therefore have a similar effect. Indeed when we examined discs containing clones of one of the *Top3α* alleles identified in the screen we found similarly high levels of apoptosis (Figure 2.16, I and N).

Loss of RnrL partially inhibits Yorkie-induced tissue overgrowth.

RnrL did not obviously impair growth in imaginal discs under normal conditions but did compromise both blastemal regeneration and compensatory growth. Given the reported function of RRs in dNTP and thus DNA synthesis it is surprising that a mutation in *RnrL* would not cause a general growth defect. A likely explanation is that $RnrL^{A4B5}$, and potentially other mutations like it, may provide a sufficient threshold of gene function for normal growth but that increased demand for gene activity in rapidly dividing cells would result in a preferential inhibition of compensatory growth. If true, we might expect loss of *RnrL* to also curtail tissue overgrowth that can be induced by a variety of genetic changes. To test this possibility, we used the MARCM method to examine the effect of mutation of *RnrL* on clones of cells that overexpress an activated form of *yorkie* (*yki*) (OH and IRVINE 2008). The Yorkie protein is a potent stimulator of tissue growth in imaginal discs and increased levels of the mammalian orthologue of Yki, YAP, are found in several human cancers (HUANG *et al.* 2005).

While MARCM clones that were solely mutant for $RnrL^{A4B5}$ were indistinguishable from control clones of the parental genotype (Figure 2.17, A and B), an obvious difference was observed when these clones were also overexpressing *yki*. $RnrL^{A4B5}$, *UAS-yki* clones were smaller than parental, *UAS-yki* clones (Figure 2.17, C and D). In addition, the nuclear density appeared to be decreased in some $RnrL^{A4B5}$, *UAS-yki* clones and cell size increased (Figure 2.17, E and F), suggesting that cell growth and cell-cycle progression may have become uncoupled. The ability of $RnrL^{A4B5}$ to partially block *yki*-induced overgrowth suggests that wild-type levels of *RnrL* function are especially necessary for more rapidly dividing cells. Thus a subset of mutations that compromise compensatory growth may also limit tissue overgrowth.

Discussion

Genetic screens in Drosophila, and mosaic screens in particular, are a proven means for dissecting biological processes of interest, identifying novel genes and uncovering new roles for known genes. We have developed system that allows us to apply the power of Drosophila genetics to address the question of how compensatory growth is generated and regulated. We were able to conditionally ablate patches of cells within the developing imaginal disc by generating mosaic tissues in which one population of cells carried a recessive temperature-sensitive cell lethal mutation. We could then assay the ability of the surviving reciprocal clones to compensate for the tissue loss both by looking at features of the disc itself and by assessing the size of resulting adult structure. By developing a mosaic system, we were able to screen for recessive mutations that would disrupt this process.

Characterization of our system revealed that *sec5^{ts}* ablation did not induce blastema formation. Rather imaginal disc recovery occurred by compensatory proliferation in two stages. At early stages when levels of apoptosis were highest, ablating discs had a greater proportion of mitotic cells than control discs, suggesting that damage may directly promote additional proliferation. If surviving cells were responding directly to dying cells, it would suggest the existence of a regulatory mechanism distinct from those that are employed during normal disc development. However, unlike the non-autonomous proliferation induced by undead cells, we found no clear evidence that the increased proliferation is localized adjacent to the deleted tissue. In addition, at late stages, when normal growth in control discs slowed, ablated discs continued to show levels of proliferation comparable to slightly younger discs. As the amount of apoptosis in ablated discs was relatively low at this time, this late growth is unlikely to occur in direct response to damaged tissue. Thus compensatory growth may be a broader tissue-wide response. As such, it may be regulated by the same patterning and size-sensing mechanisms that function during normal development (MESQUITA *et al.* 2010).

Our analysis of candidate signaling pathways did not reveal a role for Wg or Dpp in *sec5^{ts}*-induced compensatory proliferation, suggesting that, in agreement with a previous report (PÉREZ-GARIJO *et al.* 2009), the non-autonomous proliferation stimulated by undead cells may be fundamentally different from the compensatory proliferation that occurs when dying cells are cleared normally from a damaged tissue. We also failed to find significant evidence in support of a role for the JAK/STAT pathway. Small localized increases in JAK/STAT pathway activity were observed adjacent to ablated tissue, but only in regions of the disc with endogenous pathway activation. Whether the JAK/STAT pathway is required for compensatory proliferation remains to be seen. If compensatory growth is an acceleration of normal growth, it may be achieved by increased traffic through growth-promoting pathways that are already active. Thus different pathways may be utilized in different regions of the disc, following the underlying pattern of growth regulation.

To find recessive mutations that block compensatory growth we conducted a mosaic screen. Three of the mutations that we identified as being most likely to specifically affect compensatory growth were found to disrupt the genes *bun*, *Gmd* and *RnrL*. Our data indicate that *bun* is required to produce a normal amount of compensatory growth. The normal biological function of *bun* and its mammalian orthologue TSC-22 are still poorly understood. In Drosophila, overexpression of BunA alone has no effect on imaginal disc

growth (GLUDERER *et al.* 2008). However, co-expression with Madm, a protein with a catalytically inactive kinase-like domain that can bind to BunA, results in increased growth of imaginal discs (GLUDERER *et al.* 2010). Mutant forms of *bun* have been shown to have a subtle effect on growth under normal conditions. Clones of cells lacking the long isoform of *bun* (*bunA*) display, at best, mild growth defects in imaginal discs. However, similar analysis of our allele, which should also eliminate *bunA*, did not reveal a general growth defect (Figure 2.18). Thus the requirement for *bun* during developmental growth is unresolved.

Eye imaginal discs that are composed almost entirely of mutant *bun* cells, develop into adult eyes composed of both fewer and smaller cells (GLUDERER *et al.* 2008). These discs were generated by mitotic recombination with a chromosome bearing a cell-lethal mutation and therefore produce a situation not all that dissimilar to our $sec5^{ts}$ ablation system. Additionally, *bun* has been shown to be upregulated in imaginal discs undergoing regeneration after either surgical or genetic ablation of a portion of the disc (ADDISON *et al.* 1995; BLANCO *et al.* 2010). Taken together with our findings, these observations implicate *bun* in the regulation of both regenerative and compensatory growth.

The mechanisms by which *bun* regulates growth are not known. Since *bun* encodes a protein that has a leucine zipper as well as a TSC box that appears capable of binding DNA *in vitro*, it was initially assumed that it functions as a transcriptional regulator. More recent studies have shown that Bun and Madm co-localize to the Golgi in S2 cells (GLUDERER *et al.* 2010) and that knockdown of Madm by RNAi interferes with protein secretion (BARD *et al.* 2006). Since both the expression and requirement for Bun seems to be increased when regenerative or compensatory growth are required, future of studies of Bun in this biological context may provide more mechanistic insights into Bun function.

Imaginal discs in which the compensating cells were $Gmd^{B3\text{-}1}$ recovered in size following ablation but were still unable to produce a morphologically normal adult structure. This suggests that *Gmd* may be more important for tissue patterning or morphogenesis following ablation than for compensatory growth *per se*. In Drosophila, *Gmd* has been studied primarily in the context of Notch signaling, where loss of *Gmd* blocks expression of Notch target genes and results in reduced growth of the wing disc (OKAJIMA *et al.* 2005). However, when this observation was tested by clonal analysis, rather than in homozygous mutant animals, *Gmd* clones did not have an obvious phenotype. Only when very large *Gmd* clones were generated was loss of the Notch target Wingless observed and only at sites distant from any wild-type cells, suggesting that the requirement for *Gmd* may not be cell autonomous (OKAJIMA *et al.* 2008). We did not observe defects in the expression of the Notch target Wingless even when the majority of the posterior compartment was composed of $Gmd^{B3\text{-}1}$ mutant cells (data not shown), suggesting that the defects that we observed in ablated adult structures were not a consequence of reduced Notch activity in the larval disc. Fucosylation is also necessary for the formation of many different glycan structures that modulate the activity of variety of proteins, including signaling and cell adhesion molecules, one or many of which may participate in disc patterning and morphogenesis.

Reducing *RnrL* function did not reduce compensatory growth as mutant cells were able to generate a normally sized posterior compartment; rather mutant cells engaged in compensatory growth appeared to be predisposed to apoptosis. In Drosophila, no mutant phenotype has been characterized at the cellular level for either *RnrL* or *RnrS*. However, *RnrL* transcription is induced at the G1 to S transition by E2F and is presumably required

for DNA synthesis (DURONIO and O'FARRELL 1994). Thus compromising *RnrL* function may render cells incapable of increasing their rate of cell-cycle progression to keep pace with the increased rate of tissue growth required following tissue ablation. Consistent with this possibility is our observation that $RnrL^{A4B5}$ restricts the growth of clones that overexpress an activated form of Yki and that the growth of these cells appears to have outpaced their rate of division. Interestingly increased RR activity is associated with many malignant cancers indicating that an increase in RR activity may be required to sustain increased levels of cell proliferation. Accordingly, RRs are the targets of several common chemotherapeutic agents used in cancer treatment (SHAO *et al.* 2006). Together, these observations suggest that some similarities may exist between compensatory growth and hyperplastic overgrowth.

Our findings also indicate that some of the differences between compensatory growth and normal growth are likely to be quantitative rather than qualitative. The *RnrL* allele that we identified may be hypomorphic and more severe alleles may perturb normal growth. When we identified the causative mutations in 3 of the complementation groups found in our screen, each disrupted a gene that likely functions during cell growth or proliferation under normal conditions, yet the requirement for these genes appears to be enhanced when additional growth is required. Interestingly, we identified mutations in*Top3α* as strongly disrupting both $sec5^{ts}$- and IR-induced compensatory growth. Topoisomerases are chemotherapeutic targets and Topoisomerase IIα was recently shown to be haploinsufficient for liver regeneration in zebrafish, suggesting that abnormally proliferating cells may be particularly sensitive to the loss of topoisomerase activity (DAMELIN and BESTOR 2007; DOVEY *et al.* 2009). Our screen may therefore have enriched for a set of mutations that reduce gene function to a level that is near the threshold required for developmental growth and is insufficient for compensatory growth, which requires either additional or more rapid cell divisions. These findings reinforce the idea that compensatory growth is intimately connected to developmental growth, but might place an increased demand on certain pathways that sustain normal cellular requirements for cell cycle progression and growth.

Our results also validate the approach of identifying EMS-induced mutations by whole-genome resequencing. In the one previous case where this strategy has been applied successfully in Drosophila, it was possible to distinguish genuine mutations from those that arose during library construction or sequencing by looking for those that had a high allele frequency (BLUMENSTIEL *et al.* 2009). Unfortunately their approach is not suitable for situations where mutations are homozygous lethal. We therefore developed a method of library construction and computational analysis that is generally applicable to mutations that are homozygous lethal and have used it successfully to identify three of the mutations generated in our screen. Moreover, our programs have also been used more recently to identify chemically-induced mutations in *C. elegans* (D. Richter, unpublished).

Finally, we have shown that the system that we have developed for studying compensatory growth is indeed capable of generating and characterizing mutations that, at least to some extent, impair compensatory growth more than normal growth. The issue of whether there are genes that are required exclusively for compensatory growth is still unresolved. However, using this system and others like it, it will be possible to conduct more extensive genetic screens for mutations that influence compensatory growth or

regeneration. The system that we have used can be extended in two ways. First, by engineering fly lines in which transposon insertions on each of the chromosome arms carry a wild-type copy of the *sec5* gene in a *sec5*^{ts} background, it should be possible to screen most of the genome. Second, by targeting FLP to a variety of tissues, it should be possible to investigate the capacity of each of those tissues for compensatory growth.

Materials and Methods

Drosophila stocks and transgenes

The *sec5^{ts}* wing disc ablation system was generated by recombination of the following: *sec5^{ts1}* (MURTHY *et al.* 2010)*, FRT40A*, *en-GAL4* (BL30564) and *UAS-FLP* (BL4539). The experimental fly stocks used were *w; sec5^{ts1}, FRT40A, en-GAL4, UAS-FLP/SM6-TM6B* and *w; FRT40A, en-GAL4, UAS-FLP*. The eye disc ablation system used *y, w, ey-FLP; sec5^{ts1}, FRT40A/SM6-TM6B*, *y, w, ey-FLP; P{mw+, ubi-GFP.nls}, sec5^{ts1}, FRT40A/SM6-TM6B* and *y, w, ey-FLP; P{mw+, ubi-lacZ}, sec5^{ts1}, FRT40A/SM6-TM6B .* The wing disc ablation system used for candidate pathway analysis employed *y, w, Ubx-FLP*; *P{mw+, ubi-GFP.nls}, sec5^{ts1}, FRT40A/SM6-TM6B* and *y, w, Ubx-FLP*; *P{mw+, ubi-lacZ}, sec5^{ts1}, FRT40A/SM6-TM6B.* The EMS screen was carried out using an isogenized stock of *w; P{mw+, ubi-GFP.nls}, FRT40A*. For clonal growth assays in the eye in the absence of ablation and for testing mutations for defects in X-ray irradiation-induced compensatory growth the stock *y, w, ey-FLP; FRT40A* was used.

The MARCM experiment used the following stocks: *w, UAS-mCD8::GFP, hs-FLP122; tub-GAL80, FRT40A; tub-GAL4/TM6B* (WU and LUO 2006) ('MARCM tester'), *w; P{mw+, ubi-GFP.nls}, FRT40A; UAS-yorkie^{S168A}, w; RnrL^{A4B5}, P{mw+, ubi-GFP.nls}, FRT40A/CyO; UAS-yorkie^{S168A}, w; P{mw+, ubi-GFP.nls}, FRT40A* and *w; RnrL^{A4B5}, P{mw+, ubi-GFP.nls}, FRT40A/CyO; TM6B/TM2. UAS-yorkie^{S168A}* expresses a mutant hyperactivated form of the Yorkie protein (OH and IRVINE 2008).

The following stocks were also used: *w; P{mw+, ubi-GFP.nls}, sec5^{ts}, FRT40A, en-GAL4, UAS-FLP/CyO, w; P{ubi-RFP.nls, mw^{+}}, FRT40A/CyO*, *w; P{mw+, ubi-GFP.nls}, FRT40A, w; FRT40A*, *y, w, ey-FLP, Ubx-FLP; FRT40A, w; P{mw+, ubi-GFP.nls}, sec5^{ts}, FRT40A/SM6-TM6B, w; FRT40A; puc^{E69}/TM6B*, *w; FRT40A; STAT-GFP*, *y, w, ey-FLP; P{mw+, ubi-GFP.nls}, bsk^{1}, sec5^{ts1}, FRT40A/SM6-TM6B, w; rn-GAL4, UAS-eiger, tub-GAL80^{ts}/TM6B* (SMITH-BOLTON *et al.* 2009), *y, w, ey-FLP/w; P{lacW}RnrL^{k06709}, FRT40A/CyO* (from BL10644), *w*; P{lacW}Gmd^{SH1606} FRT40A/CyO* (BL28286), *w; bun^{Q666X}, FRT40A/CyO* (11C4), *y, w, hs-FLP122; FRT40A.*

sec5^{ts} ablation

Unless otherwise noted, experimental animals were generated by the crosses *w; sec5^{ts1}, FRT40A, en-GAL4, UAS-FLP/SM6-TM6B* X *w; P{mw+, ubi-GFP.nls}, FRT40A* for "ablated" discs/wings and *w; FRT40A en-GAL4, UAS-FLP* X *w; P{mw+, ubi-GFP.nls}, FRT40A* for "control" discs/wings. All experiments were carried out according to the following protocol. Eggs were collected on agar grape juice plates at room temperature for 4-6 hours. Plates were moved to 18°C for 48 hours after which L1 larvae were transferred, 55 per a vial, to standard fly food supplemented with fresh yeast paste. Vials were shifted to 30°C 7.5 days after egg laying (AEL) for 48 hours. Discs were dissected at certain time points during the ablation period or animals were returned to 18°C and adult wings were collected after eclosion. Control and ablated animals were subjected to the same treatment. For experiments in which *ey-FLP* or *Ubx-FLP* were used to generate *sec5^{ts}* clones, the same

protocol was used with the following exceptions: vials were shifted to 30°C 7 days AEL for 40 hours.

Immunohistochemistry and image processing

Discs were dissected in PBS and fixed for 20 minutes at room temperature in 4% paraformaldehyde. Antibody stains were performed according to standard methods. We used mouse anti-GFP (1:500, Roche), rabbit anti-phospho-Histone H3 (1:200, Upstate), rabbit anti-cleaved Caspase3 (1:100, Cell Signaling), rabbit anti-pSmad (1:100, Cell Signaling), mouse anti-Wg (1:100, DSHB), mouse anti-βGal (1:500, Promega) and rat anti-ELAV (1:100, DSHB). All secondary antibodies were Alexa Fluor antibodies (1:500, Invitrogen). Cell Death was assessed using a TUNEL kit (Roche) and the labeling reaction was conducted for 1 hour at 37°C. Click-iT EdU labeling kit (Invitrogen) was used to mark cells in S-phase. Incorporation and detection was performed according to manufacturer's instructions. A 10 minute incubation in 10μM EdU was used. Phalloidin was used to stain the actin cytoskeleton and outline cells (1:200, Sigma). Nuclei were visualized using DAPI. Images were captured on a Leica TCS SL or a Zeiss LSM 700 confocal, except for discs in Figure 2.1, C, which were acquired on a Zeiss Axio Imager M1. All images were processed using ImageJ and Adobe Photoshop.

Images of adult eyes were reconstructed from a series of images captured in the z-dimension, using a Leica Z16 APO microscope and the montage application in the Synoptics Ltd. software. Adult wings were mounted in Gary's Magic Mountant and images were collected as a single focal plane using a Leica Z16 APO microscope.

Image analysis and quantification

For adult wing size (Figure 2.1, G), wings from 20-25 ablated and control males were removed and mounted in Gary's Magic Mountant. Wings were imaged on a Leica Z16 APO microscope. Quantification was done in Adobe Photoshop. The entire wing area was selected using the 'Quick Selection Tool' and the number of pixels was assessed using the 'Record Measurements' function. For posterior compartment size and area of GFP+ and GFP- tissue (Figures 2.3, B and C and 2.16, O), discs were imaged on a Zeiss LSM 700 confocal microscope. Quantification was done in Volocity. The posterior compartment was selected manually based on GFP expression and the area of the entire compartment or the GFP+ area was measured using the Volocity object recognition software. The GFP- area was calculated based on these two values. We estimated the rate of growth of the GFP+ tissue from the slopes ($\mu m^2 \times 10^3$/hours) of the ablated and control lines between the 12 and 36 hours AUS data points. At least 9 ablated and control discs were analyzed for each time point. A second independent experiment yielded similar results (data not shown). For the density of mitotic cells (Figure 2.4, G), discs were imaged on either a Leica TCS SL or a Zeiss LSM 700. A z-series of confocal slices was obtained through the entire disc proper epithelium. Phospho-histone H3+ cells were counted either from a z-max projection of all focal planes, manually using the ImageJ 'cell counter' plug-in or from a 3D reconstructed image in Volocity using the object recognition software. For each disc the entire posterior compartment was analyzed. The density of mitotic cells was then calculated by dividing the

total number of mitotic cells by the area of the posterior compartment. Data were combined from two independent experiments each with at least 9 ablated and control discs for each time point. Unless otherwise noted, all data were reported as box and whiskers plots in which boxes mark 25th and 75th quartiles, whiskers show high and low values and open circles show the mean. Statistical analysis was performed using a Student's two-tailed t-test.

EMS mutagenesis and screen of chromosome 2L

3-4 day old *w; P{mw+, ubi-GFP.nls}, FRT40A* males were starved for 8 hours and then fed a 25mM ethyl methanesulfonate solution in 1% sucrose for approximately 16 hours. Mutagenized males were crossed in bulk to *y, w, ey-FLP; sec5^{ts1}, FRT40A/SM6-TM6B* virgin females. Eggs were collected on agar grape juice plates for two 6-8 hour collections a day at room temperature and one overnight ~12 hour collection at 18°C. Mutagenized males were removed from the cross after 5 days. Plates were placed at 18°C and after 48 hours, freshly hatched L1 larvae were transferred, 55 per a vial, to fly food supplemented with fresh yeast paste. 7 days AEL, vials were shifted to 30°C for 40-44 hours, after which they were returned to 18°C. Single F_1 males of the genotype *y, w, ey-FLP; * P{mw+, ubi-GFP.nls}, FRT40A/ sec5^{ts1}, FRT40A* showing a reduced eye phenotype were selected. For the first round of screening (Screen A, Figure 2.8), single males were crossed to 5 *y, w, ey-FLP; FRT40A* virgin females. 5-10 males from lines in which the ratio of red (mutant) to white tissue was normal were then crossed back to 20-30 *y, w, ey-FLP; sec5^{ts1}, FRT40A/SM6-TM6B* virgin females. Eggs were collected in vials for 4-6 hours at room temperature. Vials were then transferred to 18°C. One set of F_2 progeny was maintained at 18°C until adult eclosion and was re-screened for a normal amount of red (mutant) tissue present in the adult eye. A second set was shifted to 30°C for 40-44 hours approximately 7 days AEL and re-screened for the reduced eye phenotype. For lines that re-tested positively, virgins and males from the same cross with the genotype *y, w, ey-FLP; * P{mw+, ubi-GFP.nls}, FRT40A/SM6-TM6B* were used to establish a stable stock. Mutations with allele name starting in 'A' were isolated in this round of screening. For the second round of screening (Screen B, Figure 2.8), single F_1 males were crossed directly back to 10-15 *y, w, ey-FLP; sec5^{ts1}, FRT40A/SM6-TM6B* virgin females. Eggs were collected in vials for 8-10 hour periods at room temperature and then treated and screened as described above. If the desired phenotype was observed, F_2 males were crossed to *w; Sp/CyO* virgin females to establish stable stocks. Mutations with allele name starting with 'B' were isolated Screen B.

Clonal growth analysis in the adult eye

Experimental animals were generated by crossing virgin female *y, w, ey-FLP; FRT40A* to individual mutants *(* P{mw+, ubi-GFP.nls}, FRT40A*) or the non-mutagenized isogenic parent (*P{mw+, ubi-GFP.nls}, FRT40A*). Eggs were collected directly in vials for ~10-12 hours at 25°C. One set of vials was maintained at 25°C. Another set of vials was shifted to 30°C 3 days AEL until adult eclosion. A third set of vials was treated with X-ray irradiation 3 days AEL by placing the vials in a cabinet X-ray (Faxitron TRX5200) and irradiating for 20 minutes at 125V and 3 mA for an approximate dose of 33 Gy. Animals

from 2-3 egg collections from different days were analyzed for each treatment.

Developmental timing

Eggs were collected on agar grape juice plates at room temperature for 4-6 hours. After 48 hours at 18°C, 55 L1 larvae per a vial were transferred to standard fly food supplemented with fresh yeast paste. Vials were either maintained at 18°C or shifted to 30°C 7.5 days AEL for 48 hours, after which they were returned to 18°C. Pupae were counted every 10-14 hours until all animals had pupariated. Data are presented as the fraction of larvae pupariated or the time to 50% pupariated. Data points represent the average of at least 4 vials. Error bars are one STDEV.

Twin spot analysis

Experimental animals were generated by crossing virgin females of either *y, w, ey-FLP; bun^{A5G3}, P{mw+, ubi-GFP.nls}, FRT40A/SM6-TM6B* or *w; P{mw+, ubi-GFP.nls}, FRT40A* to males of *y, w, hs-FLP122; FRT40A/SM6-TM6B*. Eggs were collected on agar grape juice plates for 4 hours at room temperature, then maintained at 25°C for 24 hours, after which 55 L1 larvae were transferred to vials containing standard fly food supplemented with yeast paste. 96 hours AEL, vials were heat shocked at 37°C for 7 minutes. At 120 hours AEL, wing discs were dissected and stained with anti-GFP and DAPI. A z-series of confocal slices through the entire disc proper epithelium was converted into a z-maximal projection. Mutant *bun^{A5G3}* or wild-type control clones were identified by 2x GFP expression and twin spots by the absence of GFP expression. This method necessarily underestimates the twin spot area, but should do so to the same degree for all images analyzed. Clones were out-lined manually in Adobe Photoshop using the 'Lasso' tool and the area was measured using the 'Record Measurements' function. Data were reported as box and whiskers plots with boxes marking 25th and 75th quartiles, whiskers showing high and low values and open circles showing the mean.

Illumina whole genome re-sequencing (WGS)

Genomic DNA was isolated from 10 gut-evacuated wandering third instar larvae per genotype, as described in (BLUMENSTIEL *et al.* 2009). Illumina libraries (ab, bc and ac) were prepared according to the Illumina paired end sample preparation guide with the following modifications. All reagents were purchased from NEB, except dATP which was from Fisher. PCR primers were from IDT and adapters from Illumina. 10-20μg of DNA was sheared by sonication in a Bioruptor (Diagenode) at 4°C, in 200μL TE for 30 minutes with 30 second on/off pulses. For the ab and bc libraries, sonicated DNA was run out on a 1.5% agarose gel and fragments 200-300bp in length were selected. For the ac library no size selection step was added. For all libraries a final size selection step was added after the PCR to remove presumed primer dimer products. Libraries were sequenced on an Illumina GAII sequencer for 36bp reads. ab and bc were sequenced on one lane using single-end reads and on one lane using paired-end reads. ac was sequenced on two lanes using paired-end reads.

WGS data analysis and SNP discovery

All Illumina reads were mapped to the 5.25 release of the *D. melanogaster* genome with MAQ version 0.7.1 ((LI *et al.* 2008), maq.sourceforge.net) using default parameter values. The .pileup and .snp MAQ output files were analyzed further using a series of custom Perl scripts. The .pileup file was used to determine coverage along 2L. We combined information from the .pileup and .snp files into one comprehensive mutation list. We disallowed any mutation with a sequencing quality score lower than 20 and any that occurred within the first 5 bp of a read. To find mutations unique to each genotype we generated data sets by intersecting mutations from two libraries and excluding mutations from the third. We did not consider mutations with an allele frequency less than 0.1, a mutant allele count less than 2 and those at positions where the average number of mapping hits for reads mapped to the position (average hits) was greater than 1. For our analysis of all combined reads (ABC) we generated a mutation list by setting the following cutoffs: an allele frequency between 0.2 and 0.8, a minimum read depth of 4, average hits less than or equal to 1 and a MAQ consensus quality score of 40. Mutation lists resulting from all analyses were refined to include only non-synonymous protein coding mutations. We then used SIFT ((KUMAR *et al.* 2009), sift.jcvi.org) to predict whether a non-synonymous mutation was likely to be deleterious or tolerated. Candidate mutations were confirmed by Sanger sequencing following PCR amplification of the desired region.

MARCM clone generation

Eggs were collected directly in vials for 4-6 hours at 25°C. Vials were heat-shocked at 37°C for 15 minutes approximately 48 hours AEL. Wandering larvae were selected for dissection 120 hours AEL. After dissected discs were mounted on slides, samples were given an arbitrary label and all subsequent imaging and data analysis was carried out blind. A series of 3-5 discs, with at least 5 clones each, were imaged for each sample and qualitative assessment of clone size and features were made prior to genotype assignment.

Figure 2.1: *A mosaic system to study compensatory growth in Drosophila imaginal discs*. (A) The genetic crosses used to generate the ablated and control animals. (B) Schematic showing the *sec5^{ts}* system. (C) The posterior compartment of a mosaic wing disc generated with *en>FLP* and an eye-antennal mosaic disc generated with *ey-FLP*. *sec5^{ts}* clones are GFP-positive (green). Sister clones are RFP-positive (red). Heterozygous cells are yellow and were largely absent. Larvae were maintained at 18° to prevent ablation of homozygous *sec5^{ts}* tissue and were dissected at the wandering stage. (D) Discs at 12 hours after upshift (AUS) show high levels of apoptosis. TUNEL (magenta) was used to label apoptotic cells. *sec5^{ts}/sec5^{ts}* cells were marked by the absence of GFP (green). Posterior is to the right. (E) Dying *sec5^{ts}* cells were cleared by a combination of basal extrusion and engulfment. Discs were dissected 12 hours AUS. Anti-cleaved Caspase3 (aC3, blue) marks dying cells, *sec5^{ts}* cells are GFP-negative (green), Phalloidin (Actin, red) outlines cells. Arrows show engulfed GFP-negative, cleaved Caspase3-positive apoptotic bodies within GFP-positive neighboring cells. Asterisk shows basally extruded GFP-negative apoptotic bodies. A single z-slice is shown. Apical is up; basal is down. (F-G) Ablated wing (*en>FLP*) or eye (*ey-FLP*) imaginal discs generated normally sized adult structures. (F) Representative adult wings and eyes from control and ablated adults. (G) Quantification of adult wing size. All graphical data is presented in a "box and whiskers" format (see Materials and Methods) unless otherwise stated.

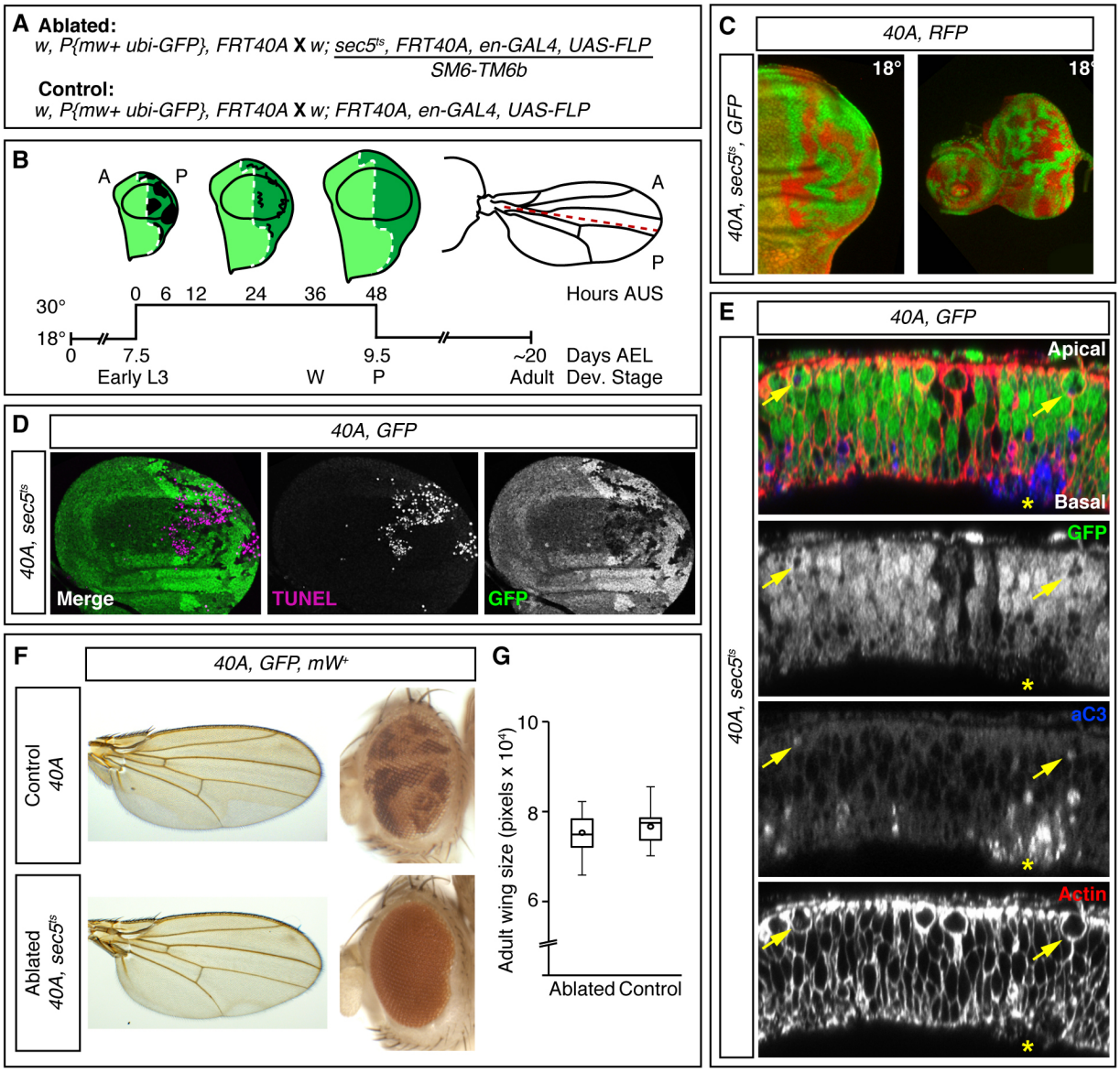
A
Ablated:
w, P{mw+ ubi-GFP}, FRT40A X w; sec5ts, FRT40A, en-GAL4, UAS-FLP / SM6-TM6b
Control:
w, P{mw+ ubi-GFP}, FRT40A X w; FRT40A, en-GAL4, UAS-FLP
B
A
P
A
P
0 6 12 24 36 48
Hours AUS
30°
18°
0
7.5
Early L3
W
9.5
P
~20
Adult
Days AEL
Dev. Stage
C
40A, RFP
40A, sec5ts, GFP
18°
18°
D
40A, GFP
40A, sec5ts
Merge
TUNEL
GFP
E
40A, GFP
40A, sec5ts
Apical
Basal
GFP
aC3
Actin
F
40A, GFP, mW+
Control 40A
Ablated 40A, sec5ts
G
Adult wing size (pixels x 10^4)
10
8
6
Ablated
Control

Figure 2.2: *Full recovery from sec5^{ts} ablation required a certain amount of time before the larval to pupal transition*.
(A-A') *sec5^{ts}* ablation did not delay the larval to pupal transition. (A) Developmental timing of pupariation for *sec5^{ts}* and control animals. Shifted 30°C ablated experiments shown as solid lines; 18°C non-ablated experiments shown as dashed lines (A') Calculated average time (days AEL) to 50% pupariation from data in (A). *sec5^{ts}* 30°C 9.8 +/- 0.2, control 30°C 9.6 +/- 0.04, *sec5^{ts}* 18°C 10.5 +/- 0.02, control 18°C 10.2 +/- 0.1. (B) Ablation induced in larvae 8 days or more AEL lead to defects in the resulting adult structures. Experimental animals were of the genotype *y, w, ey-FLP, Ubx-FLP/w; FRT40A/P{mw+, ubi-GFP.nls}, sec5^{ts}, FRT40A*. Adult eyes were entirely pigmented as the *Ubx-FLP* construct also carries a *mw+*. 8 days AEL corresponds to mid third instar at 18°C.

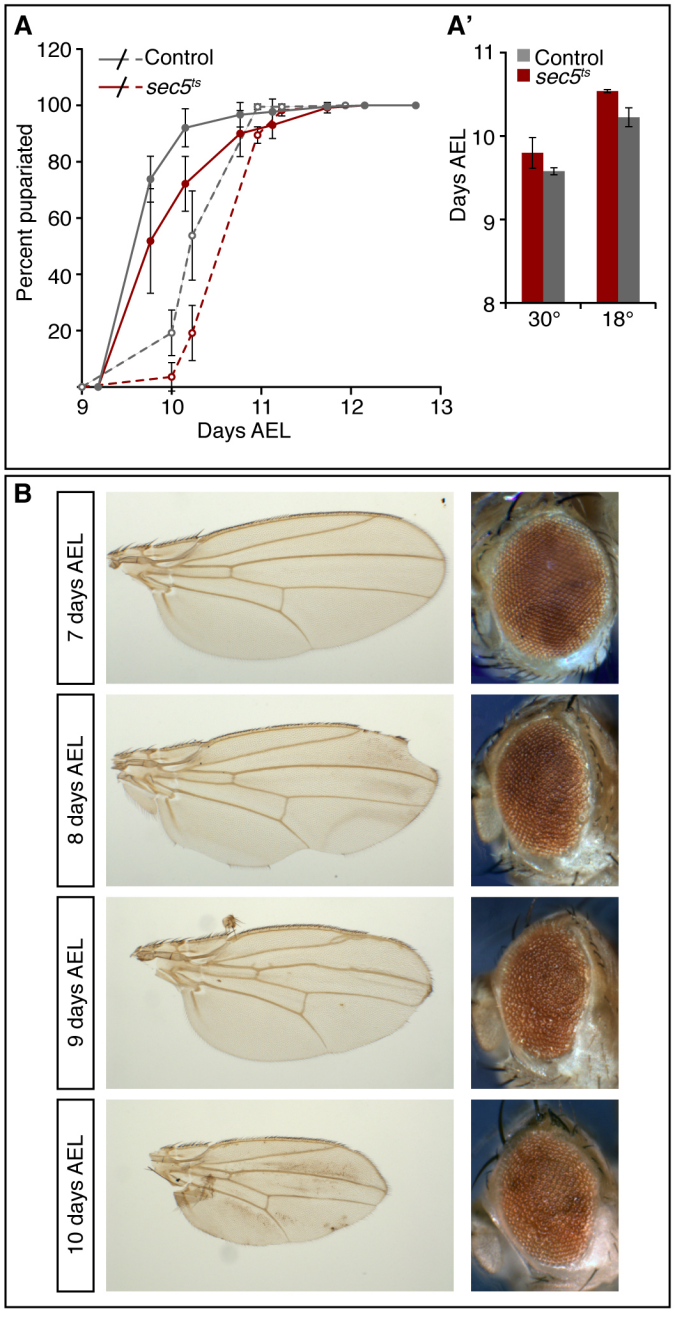
A
A'
Control
sec5ts
Percent pupariated
Days AEL
Days AEL
30°
18°
B
7 days AEL
8 days AEL
9 days AEL
10 days AEL

Figure 2.3: *sec5^{ts} ablation induces an accelerated rate of growth in the surviving tissue.* All experiments were conducted using *en>FLP*. (A-B) Ablated discs were smaller than control discs 12 hours AUS, but regained normal size by 36 hours AUS. (A-A') Discs dissected from ablated (A) or control (A') animals. Posterior is to the right. (B) Quantification of ablated anterior (A, white) and posterior (P, grey) compartment size expressed as a fraction of the average control size (red dashed line at 1). (C) Between 12 and 36 hours AUS, the GFP+ tissue in *sec5^{ts}* discs increased in size more than the corresponding tissue in control discs. The area ($\mu m^2 \times 10^4$) of GFP+ tissue in the posterior compartment is shown. Data points represent the average area. Error bars denote one STDEV. The predicted rate of growth between 12 and 36 hr AUS is 1.65×10^3 μm^2/hr for ablated discs and 1.03×10^3 μm^2/hr for control discs.

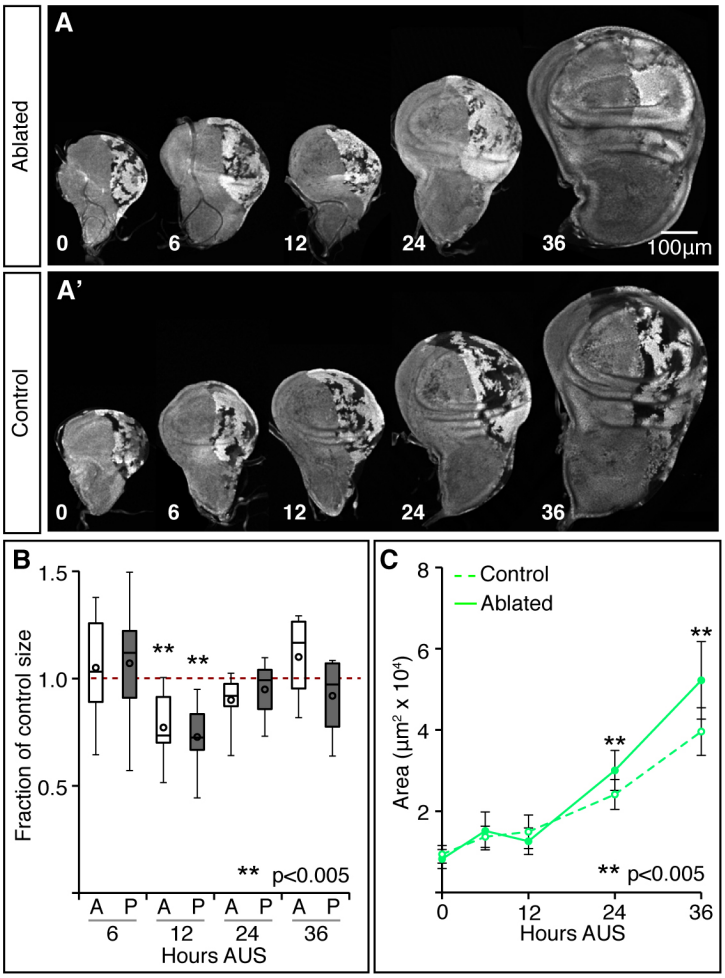
A
Ablated
0
6
12
24
36
100µm
A'
Control
0
6
12
24
36
B
Fraction of control size
1.5
1.0
0.5
**
**
** p<0.005
A P A P A P A P
6
12
24
36
Hours AUS
C
Control
Ablated
Area (µm² x 10⁴)
8
6
4
2
**
**
** p<0.005
0
12
24
36
Hours AUS

Figure 2.4: *sec5^{ts} ablation produces non-localized compensatory proliferation.*
All experiments were conducted using *en>FLP*. (A-D) Discs were stained with anti-phospho-histone H3 (PHH3, white) to mark mitotic cells and TUNEL (magenta) to mark apoptotic cells. (E-F) Discs were stained with EdU (white) to label S-phase cells and anti-cleaved Caspase3 (aC3, magenta) to mark dying cells. Ablated discs are at left (A-F) and control discs at right (A'-F'). White lines mark the approximate A-P boundary as assessed by GFP. Posterior is to the right. Images are z-max projections of confocal slices through the entire disc epithelium. Hours AUS are given in the lower right corner of each image. (A and E) Apoptotic cells were observed as early as 6 hours AUS. (B and F) High levels of apoptosis were seen at 12 hours AUS; however, no consistent co-localization between proliferating and apoptotic cells was observed. At least 20 discs from 2 independent experiments were examined. (C) Levels of apoptosis declined by 24 hours AUS. (D) By 36 hr AUS most TUNEL staining was found in residual cellular debris (small puncta present only in very basal confocal sections). More mitotic cells are visible in ablated discs than in controls. (E) Quantification of the density of mitotic cells, as marked by PHH3, in the posterior compartment of ablated and control discs. Ablated discs are shown in red. Control discs are shown in grey. Discs were analyzed at 6, 12 and 24 hours AUS and from wandering (W) larvae 36-40 hours AUS.

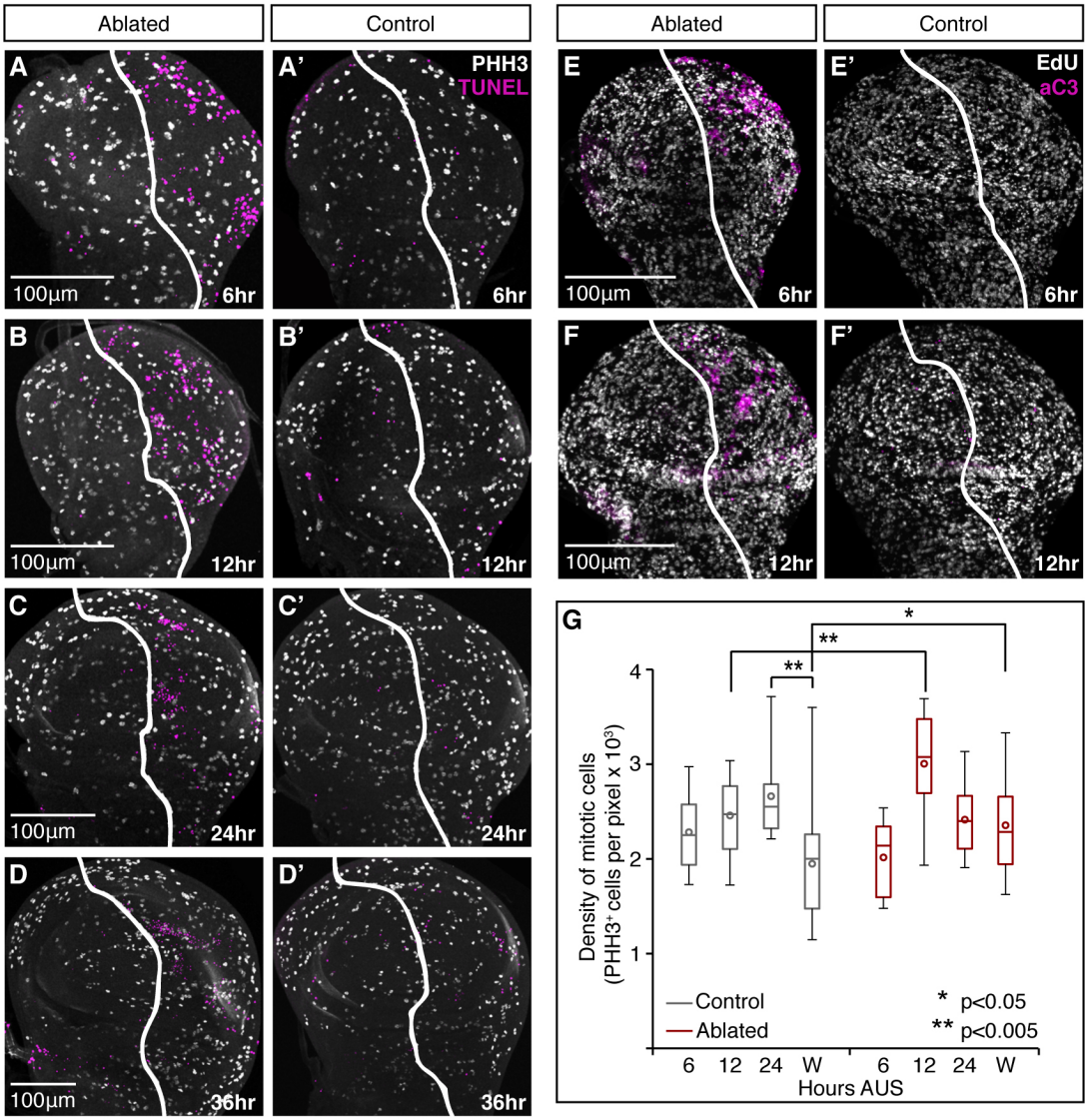
Ablated
Control
Ablated
Control
A
A'
PHH3
TUNEL
E
E'
EdU
aC3
100µm
6hr
B
B'
F
F'
12hr
C
C'
24hr
D
D'
36hr
G
Density of mitotic cells
(PHH3+ cells per pixel x 10^3)
Control
Ablated
* p<0.05
** p<0.005
6 12 24 W 6 12 24 W
Hours AUS

Figure 2.5: *The JNK pathway is required for ablation of sec5^{ts} clones.*
(A) Dying *sec5^{ts}* cells expressed elevated levels of *puc-lacZ*. Ablating wings discs were dissected 4 hours AUS. GFP marks *sec5^{ts}* cells (green), anti-cleaved caspase3 (aC3, magenta) marks dying cells and *puc-lacZ* expression was detected with anti-βGal (cyan). (B-C) Normal regeneration did not follow ablation of double mutant *sec5^{ts}*, *bsk^{1}* clones. Mosaic discs were generated using *ey-FLP*. *sec5^{ts}* and *sec5^{ts}*, *bsk^{1}* tissue carries two copies of a *P{mw+}*. Reciprocal clones are unpigmented. Residual, pigmented heterozygous tissue can be seen in the posterior of the eye. (B) Representative adult eye following ablation of *sec5^{ts}* tissue. (C) Adult eye recovered following ablation of *sec5^{ts}*, *bsk^{1}* tissue. (D-E) *bsk* was required for apoptosis of *sec5^{ts}* clones. Mosaic discs were generated using *ey-FLP*. *sec5^{ts}* and *sec5^{ts}*, *bsk^{1}* tissue is GFP-positive (green). Discs were dissected 12 hours AUS and stained for TUNEL (magenta) to mark dying cells. (D) *sec5^{ts}* cells stained positive for TUNEL. (E) Double mutant *sec5^{ts}*, *bsk^{1}* cells were not labeled by TUNEL. (F-G) Persistent *sec5^{ts}*, *bsk^{1}* clones failed to properly differentiate. Mosaic discs were generated using *ey-FLP*. *sec5^{ts}* and *sec5^{ts}*, *bsk^{1}* tissue is GFP-positive (green). Discs were dissected 24 hours AUS and stained for anti-ELAV (magenta) to mark differentiating photoreceptors. (F) By 24 hours AUS, very little *sec5^{ts}* tissue remained. Normal clusters of ommatidia were visible posterior to the morphogenetic furrow. (G) *sec5^{ts}*, *bsk^{1}* clones were not eliminated and showed reduced expression of ELAV.

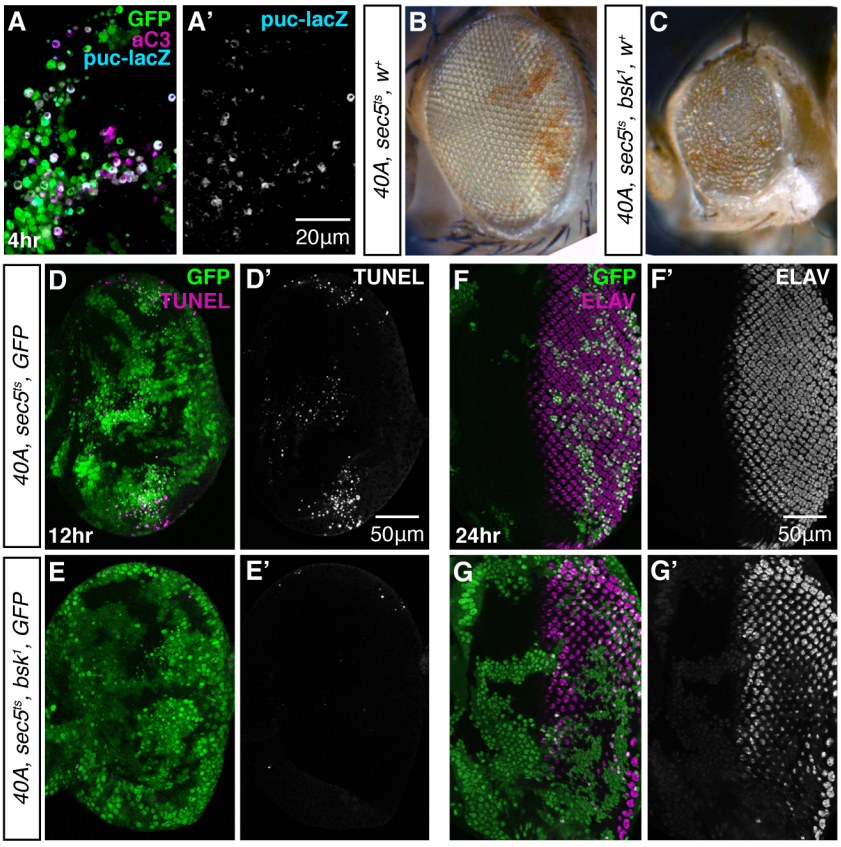
A
GFP
aC3
puc-lacZ
4hr
A'
puc-lacZ
20µm
40A, sec5ts, w+
B
40A, sec5ts, bsk1, w+
C
40A, sec5ts, GFP
D
GFP
TUNEL
12hr
D'
TUNEL
50µm
F
GFP
ELAV
24hr
F'
ELAV
50µm
40A, sec5ts, bsk1, GFP
E
E'
G
G'

Figure 2.6: *Analysis of candidate signaling pathways during sec5^{ts}-induced compensatory proliferation.*
All discs were dissected 12 hours AUS. Mosaic wing discs were generated using *Ubx-FLP*. Mosaic eye discs were produced with *ey-FLP*. Ablated discs carried *sec5^{ts}* clones. Control discs were treated identically to ablated discs and carried non-ablating clones, which were omitted here for simplicity. *sec5^{ts}* tissue was marked by GFP in all panels except C, D, I, J and M, in which *sec5^{ts}* tissue was marked by *lacZ* expression and detected with anti-βGal. All *sec5^{ts}* tissue is shown in green for consistency. (A-B) Phosphorylated Mad (pMad, red) staining was the same in control (A) and ablated (B-B') wing discs. (C-D) *STAT-GFP* (red) in control (C) and ablated (D-D') wing discs showed the same expression pattern but was more speckled in appearance in ablated discs. Note the absence of any ectopic *STAT-GFP* expression in the wing pouch despite the presence of *sec5^{ts}* clones. (E-F) Wingless (Wg, red) expression in control (E) and ablated wing discs (F-F'). Elevated Wg protein was occasionally observed coincident with *sec5^{ts}* clones that overlapped the normal Wg expression domain (white arrow head). Ectopic Wg was not observed. Frequently, s*ec5^{ts}* clones disrupted the normal expression of Wg (yellow arrow head). Boxed region is enlarged in N. (G-H) pMad (red) in control (G) and ablated (H-H') eye discs. (I-J) *STAT-GFP* expression in control (I) and ablated (J-J') eye discs. Arrow head indicates region of *STAT-GFP* puncta that overlaps with a *sec5^{ts}* clone. (K-L) Wg in control (K) and ablated (L-L') eye discs. No ectopic Wg was observed. (M) Close-up of a region of speckled *STAT-GFP* expression in an ablated wing disc showing elevated *STAT-GFP* in a dying *sec5^{ts}* cell (white arrow head) and in a wild-type cell neighboring a patch of apoptotic *sec5^{ts}* tissue (yellow arrow head). (N) Enlargement of boxed region in F' showing disruption of Wg by *sec5^{ts}* clone and non-overlap between elevated Wg and *sec5^{ts}* cells (white arrow head).

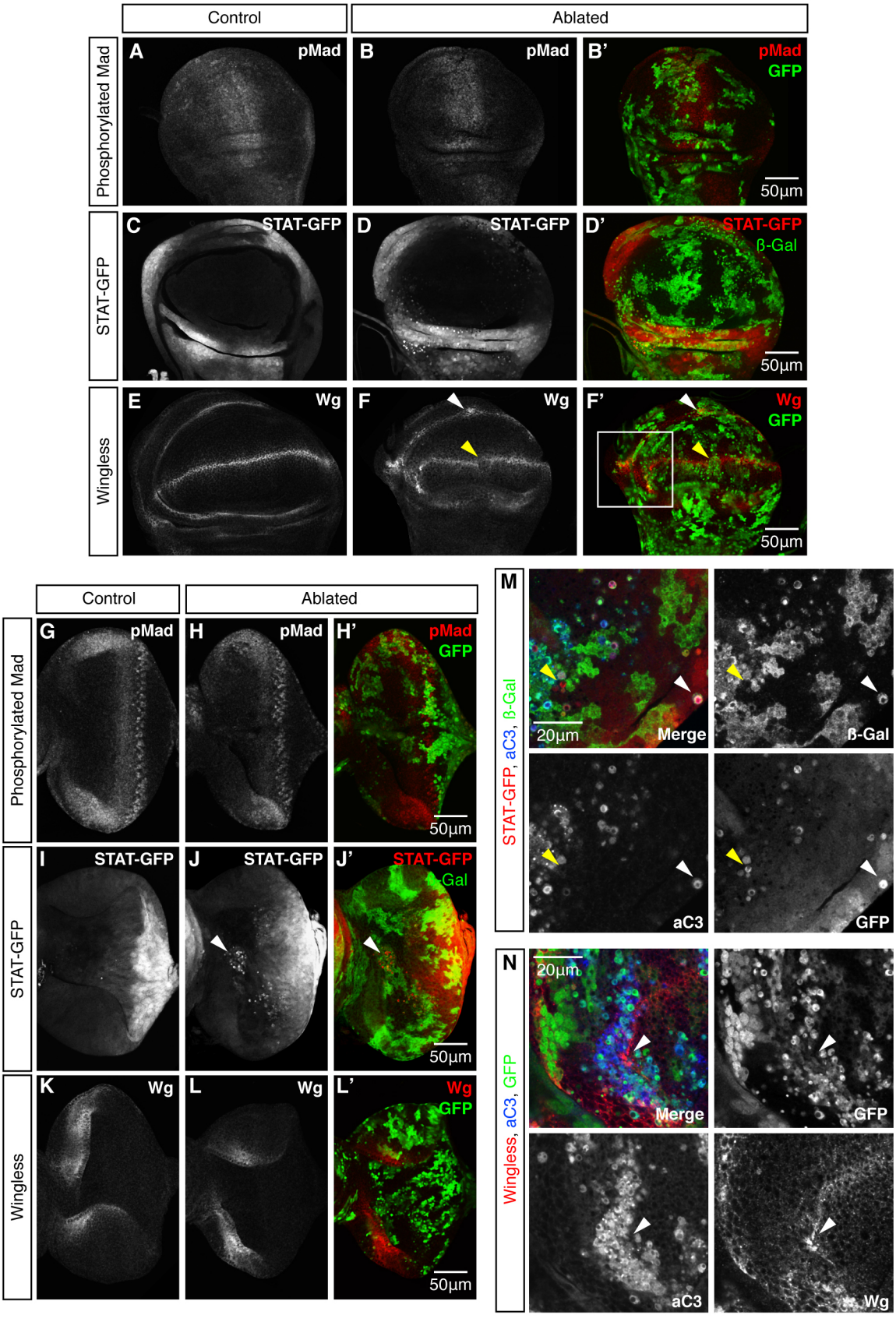
Control
Ablated
Phosphorylated Mad
STAT-GFP
Wingless
A
pMad
B
pMad
B'
pMad
GFP
50µm
C
STAT-GFP
D
STAT-GFP
D'
STAT-GFP
β-Gal
50µm
E
Wg
F
Wg
F'
Wg
GFP
50µm
Control
Ablated
Phosphorylated Mad
STAT-GFP
Wingless
G
pMad
H
pMad
H'
pMad
GFP
50µm
I
STAT-GFP
J
STAT-GFP
J'
STAT-GFP
-Gal
50µm
K
Wg
L
Wg
L'
Wg
GFP
50µm
M
STAT-GFP, aC3, β-Gal
20µm
Merge
ß-Gal
aC3
GFP
N
Wingless, aC3, GFP
20µm
Merge
GFP
aC3
Wg

Figure 2.7: *A screen to identify recessive mutations that impair compensatory proliferation.* (A-A') Schematic showing the *sec5^{ts}* system used in the eye. (A) Primary screen: in wild-type animals *sec5^{ts}* ablation resulted in adults with normally sized eyes that were entirely pigmented (red). Mutations that impair developmental or compensatory growth result in a reduced eye. (A') Secondary screen: in wild-type, non-ablated animals, the resulting adults had mosaic eyes composed of wild-type tissue (red) and *sec5^{ts}* tissue (white). Mutations that impair developmental growth result in an underrepresentation of red tissue. (B-D) Examples of phenotypes. Top panel shows the adult eye following ablation (30°C). Bottom panel shows the adult eye from a non-ablated animal (18°C). (B) The non-mutagenized parental control phenotype. (C) A mutation that failed the secondary screen and is likely to disrupt normal growth. (D) A mutation that passed the secondary screen and minimally disrupts developmental growth. (E) A panel of representative mutant phenotypes. Top panel shows the adult eye following ablation (30°C). Bottom panel shows the adult eye from a non-ablated animal (18°C). Mutants are ordered according to the severity of the phenotype at 30°C with the strongest alleles to the left. The parental control phenotype is shown at the far left for comparison.

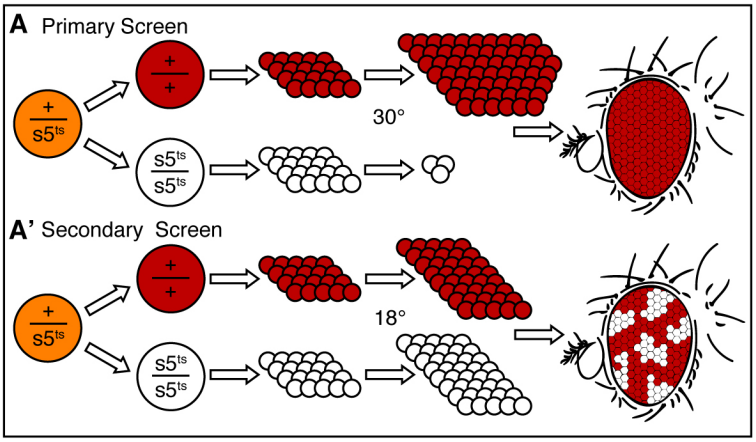
A Primary Screen
+/+
+/s5ts
s5ts/s5ts
30°
A' Secondary Screen
18°

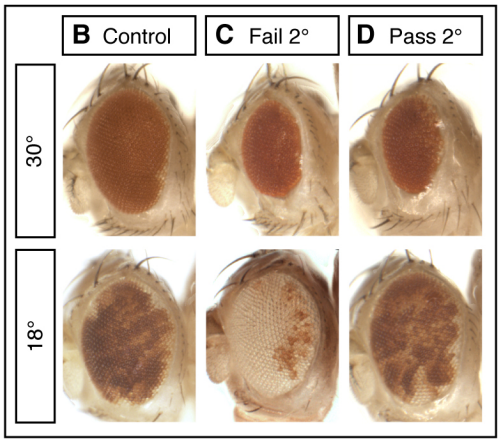
B Control
C Fail 2°
D Pass 2°
30°
18°

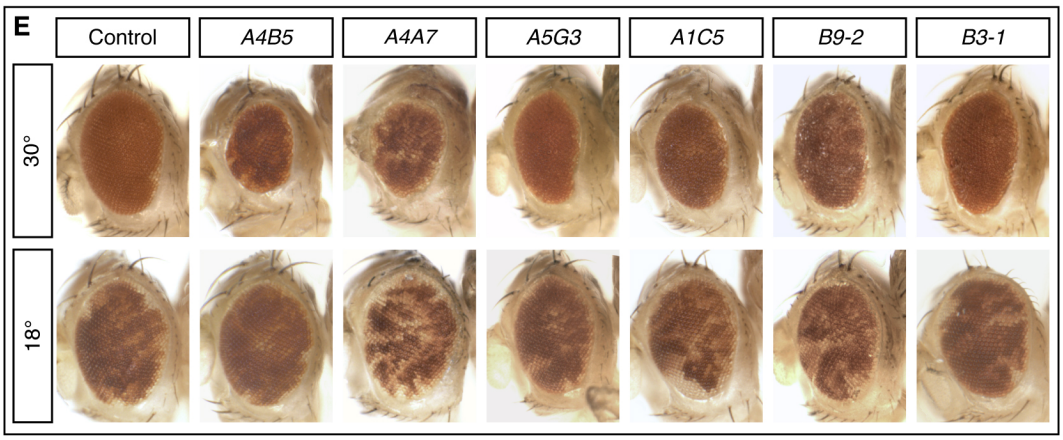
E
Control
A4B5
A4A7
A5G3
A1C5
B9-2
B3-1
30°
18°

Figure 2.8: *Flow diagram of the genetic crosses followed in the screen for mutations that selectively disrupt compensatory growth.*
See Materials and Methods for a complete description of the screen. Briefly, the screen was conducted in two stages, Screen A and Screen B, which diverged after the initial selection of F1 males. Screen A had an additional step in which the ratio of white (wild-type) to red (mutant) tissue (W:R) was assessed in the adult eye when ablation was not induced and animals were reared at 25°C. The mutagenized chromosome is shown in red throughout.

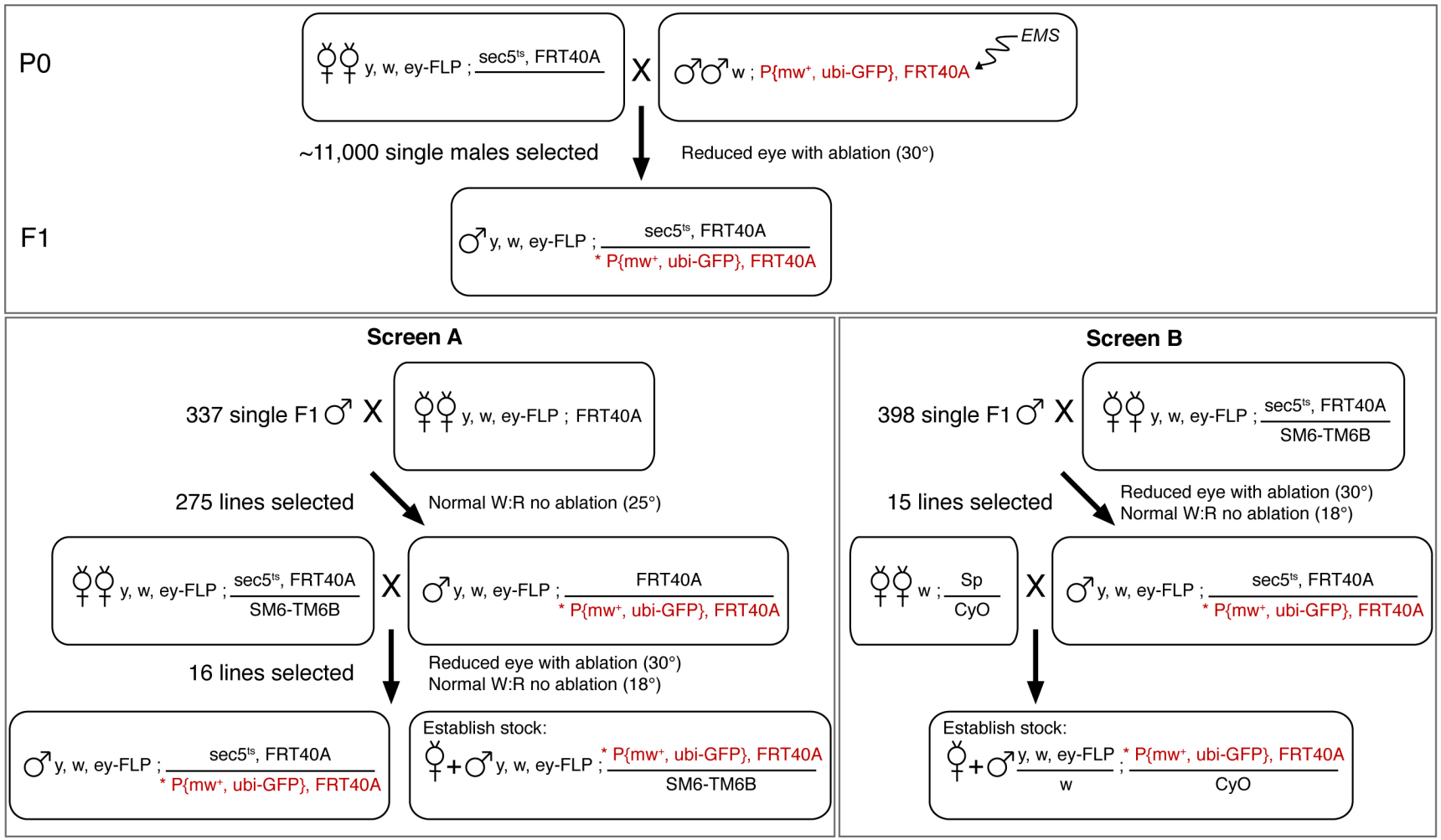
P0
y, w, ey-FLP ; sec5ts, FRT40A
X
w ; P{mw+, ubi-GFP}, FRT40A
EMS
~11,000 single males selected
Reduced eye with ablation (30°)
F1
y, w, ey-FLP ; sec5ts, FRT40A / * P{mw+, ubi-GFP}, FRT40A
Screen A
337 single F1
X
y, w, ey-FLP ; FRT40A
275 lines selected
Normal W:R no ablation (25°)
y, w, ey-FLP ; sec5ts, FRT40A / SM6-TM6B
X
y, w, ey-FLP ; FRT40A / * P{mw+, ubi-GFP}, FRT40A
16 lines selected
Reduced eye with ablation (30°)
Normal W:R no ablation (18°)
y, w, ey-FLP ; sec5ts, FRT40A / * P{mw+, ubi-GFP}, FRT40A
Establish stock:
+
y, w, ey-FLP ; * P{mw+, ubi-GFP}, FRT40A / SM6-TM6B
Screen B
398 single F1
X
y, w, ey-FLP ; sec5ts, FRT40A / SM6-TM6B
15 lines selected
Reduced eye with ablation (30°)
Normal W:R no ablation (18°)
w ; Sp / CyO
X
y, w, ey-FLP ; sec5ts, FRT40A / * P{mw+, ubi-GFP}, FRT40A
Establish stock:
+
y, w, ey-FLP / w ; * P{mw+, ubi-GFP}, FRT40A / CyO

Figure 2.9: *Clonal growth assays identify mutations with a temperature or irradiation-sensitive phenotype.*
(A, A') Range of phenotypes following *sec5*^{ts} ablation. Control used for comparison was the parental non-mutagenized phenotype. Animals with a wild-type phenotype were not selected in the screen. (B, B') Amount of red mutant tissue in adult eye at 25°C with no ablation. Control used for comparison was the parental non-mutagenized phenotype. (C, C') Amount of red mutant tissue in adult eye at 30°C. Control used for comparison was the amount of red tissue present for the same genotype at 25°C. (D, D') Amount of red mutant tissue in adult eye following IR-induced ablation. Control used for comparison was the amount of red tissue present for the same genotype in unirradiated samples. Intermediate phenotypes are indicated by W/M and NC/M for between W or NC and M, respectively and by M/S for between M and S. Members of the same lethal complementation group are indicated by colored highlights of the allele name. Alleles with an asterisks were molecularly characterized. Genotypes are listed in Materials and Methods.

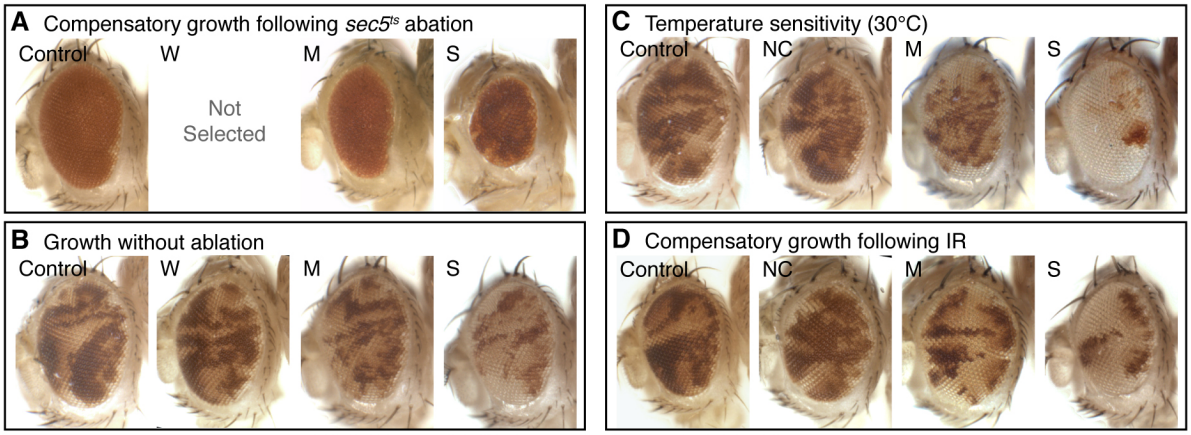

W=Wild-type; M=Moderate; S=Strong; NC=No Change
* indicates molecularly characterized alleles

	A'	B'	C'	D'
**A4B5*	S	W	NC	NC
**A5G3*	M	W	NC	M/S
**B12-3*	W/M	W	NC	NC
** B3-1*	W/M	W	NC	NC/M
A5D4	M/S	W	NC/M	NC/M
A2G1	W/M	W	NC/M	NC
B12-1	W/M	W	NC/M	NC/M
A2E9	S	W	S	NC/M
** A2I3*	M	W/M	NC	NC/M
A2B3	W/M	W/M	NC	NC
A2J5	M	W/M	NC/M	M
A2D1	M/S	W/M	NC/M	M/S
**A1C5*	M/S	W/M	M	NC/M
A4F2	M	W/M	M	NC
**A3G1*	W/M	W/M	M	NC/M
A5D9	W/M	W/M	M/S	NC/M
A1D3	M	W/M	S	NC
B6-1	S	M	NC	NC
B25-2	M/S	M	NC	M
B18-1	M	M	NC	NC
B7-1	M	M	NC	NC
** B9-2*	M	M	NC	M
B18-2	W/M	M	NC	NC
B25-1	M	M	M/S	NC
B6-2	S	M	S	M
B9-1	M/S	M/S	NC	NC/M
**A4A7*	M	M/S	NC	NC
A2A3	M/S	M/S	M/S	M
B19-1	S	M/S	S	NC
B-1	S	S	S	—
B12-2	S	S	S	—

Figure 2.10: *Mutations from the sec5^{ts} screen may also compromise blastemal regeneration.* Select mutations were assessed for their ability to dominantly modify wing disc regeneration following genetic ablation. The non-mutagenized parental chromosome was used as a control. Experimental animals were generated and regeneration scored as previously described (SMITH-BOLTON *et al.* 2009). Alleles shown in red dominantly reduced the amount of regeneration and showed both more poorly regenerated wings (>25%) and fewer well regenerated wings (75-100%). Alleles shown in grey had no effect. Alleles shown in blue apparently enhanced regeneration. Both these alleles came from Screen B and were balanced in a different genetic background than all other alleles tested, which may account for the observed phenotype. For all genotypes, data represents the average of 3 independent experiments. The total number of adult wings scored were as follows: *A4B5* 64, *A4A7* 108, Control 282, *A2G1* 204, *A1C5* 162, *A5G3* 83, *B3-1* 193, *B9-2* 209.

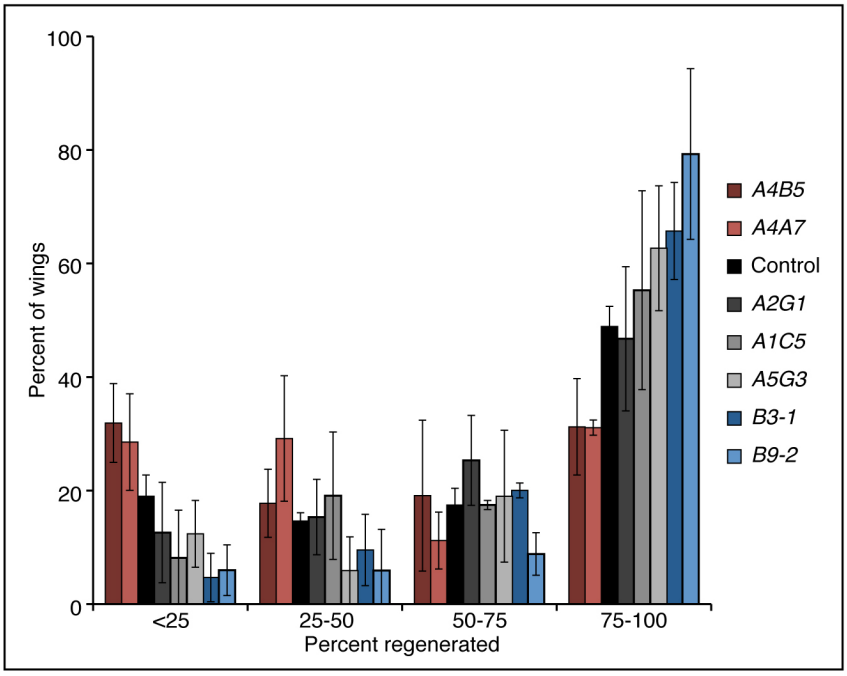
100
80
60
40
20
0
Percent of wings
<25
25-50
50-75
75-100
Percent regenerated
A4B5
A4A7
Control
A2G1
A1C5
A5G3
B3-1
B9-2

Figure 2.11: *The affected genes in 3 complementation groups identified by deficiency mapping followed by candidate gene sequencing.*
(A) Table showing the 3 lethal complementation groups with allele names, sequenced mutations, affected genes and gene function. Affected genes were identified by deficiency mapping of the lethal mutation in both members of the complementation group, followed by Sanger sequencing of candidate genes within the lethal interval. (B) Schematic showing the affected genes with the positions of the mutations found marked with respect to predicted functional domains.

A

Alleles	Mutation	Gene	Function
B9-2 *A2I3*	115bp deletion K39*	*Top3α*	DNA topoisomerase type 1A
B12-3 *A4A7*	G935E Q807*	*mtRNApol*	mitochondrial RNA polymerase
A1C5 *A3G1*	Q1244* 11bp insertion	*cmet*	kinetochore kinesin

B

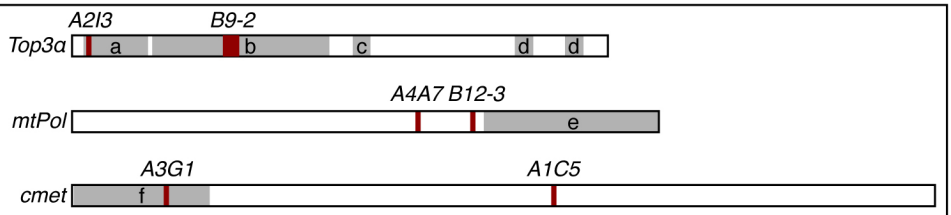

a: Toprim domain
b: Topoisomerase I active site
c: Topoisomerase DNA binding C4 zinc domain
d: GRF zinc finger
e: DNA-dependent RNA polymerase domain
f: Kinesin motor domain

Figure 2.12: *Phenotypic and preliminary mapping data for characterized putative single-hit mutants.*
(A) Adult eye phenotype for 4 mutations, *A2D1*, *A5D4*, *B12-1* and *A2G1* as compared to the non-mutagenized parental phenotype (control) following *sec5^{ts}* ablation, without any ablation and following X-ray irradiation (IR) ablation. The 'No Ablation' mosaic eyes shown were generated using *y, w, ey-FLP; FRT40A* and rearing animals at 25°C (Control, *A2D1*, *A5D4*) or *y, w, ey-FLP; sec5^{ts}, FRT40A* and keeping animals at 18°C (*A2G1*, *B12-1*). (B) Mapping data for *A2D1*, *A5D4*, *B12-1* and *A2G1*.

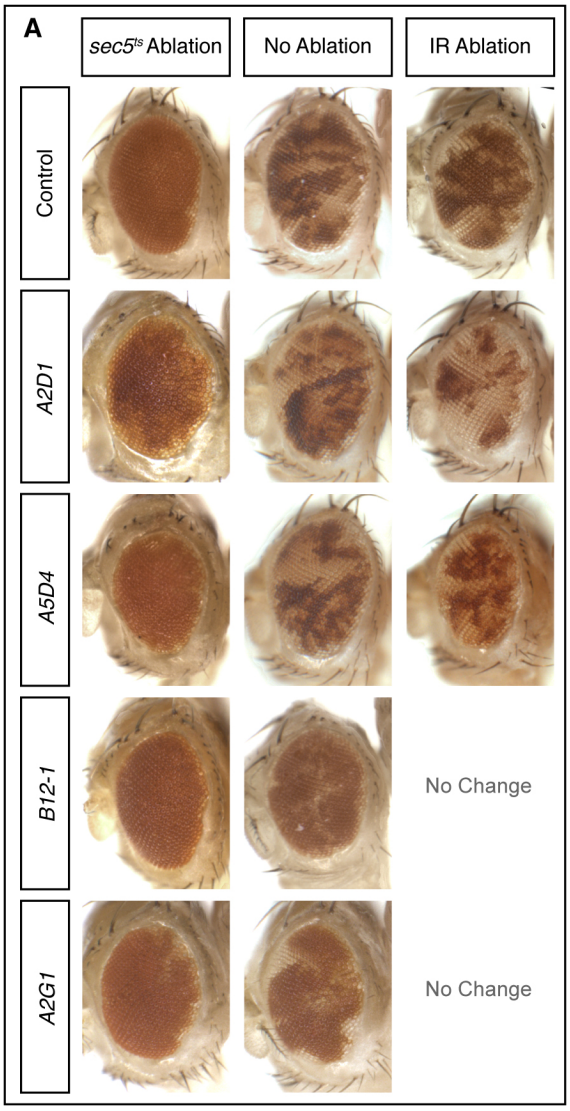

B Allele	Mapping Data
A2D1	Mapped to 16,767,504-16,824,908. Failed to complement Dfs BL24114, 24907* and 7834* Region contains 10 genes
A5D4	Complemented all Dfs in the 2009 release of the BL 2L Df kit
B12-1	Mapped to 16,824,908-16,889,200. Failed to complement Dfs BL24350, 24907, 24114 and 7835. Complements Dfs BL7834 and 23679, and P-element insertions BL20167 (disrupts *CG13280* and *midway* (*mdy*)) and BL10536 (disrupts *mdy* and *CAS/CSE1 segregation protein* (*Cas*)). Region contains 10 genes and 2 non-protein coding genes.
A2G1	Escaper phenotype (see Table 2.1) prompted test of allelism with dachsous (ds). Failed to complement spanning Dfs (BL3084 and BL8908) and ds^{38K}

* Dfs should be re-tested to confirm failure to complement

Figure 2.13: *Representative phenotypes of the 3 mutants characterized by whole genome re-sequencing.*
The phenotypes following *sec5*^{ts} ablation, in non-ablated animals raised at 25°C and following X-ray irradiation-induced (IR) damage are shown.

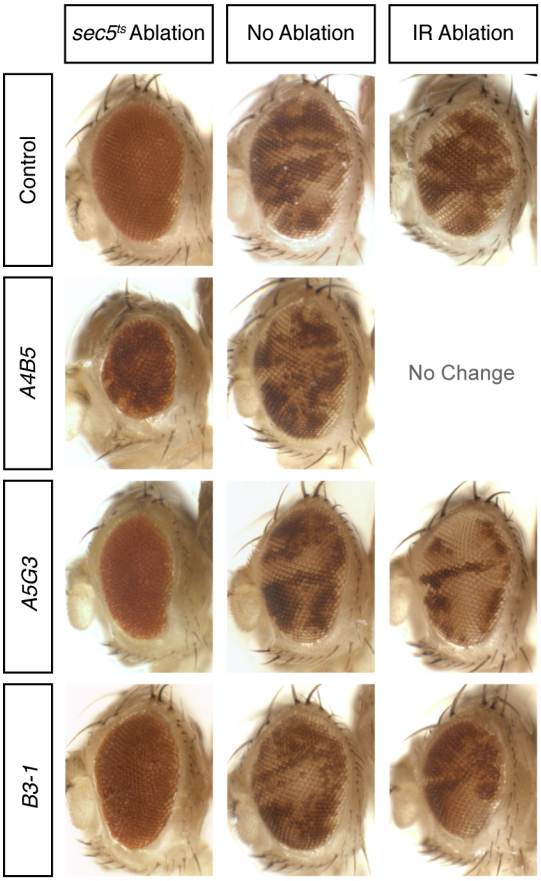
sec5ts Ablation
No Ablation
IR Ablation
Control
A4B5
No Change
A5G3
B3-1

Figure 2.14: *Identification of 3 affected genes by whole genome re-sequencing (WGS).* (A) Scheme showing the genotypes used to generate libraries for WGS and the comparison strategy used to link mutations to a single genotype. (B) Combined data from all genomic libraries (ABC). The distribution of allele frequencies of all mutations and the range selected for analysis is shown. (C) The coverage across 2L was plotted as the percent of positions on 2L with a given read depth for all 4 analyses. Inset shows the median coverage for each individual library and the approximate level of coverage for each genotype. The lines for ab and bc are essentially coincident. (D) A disproportionate percentage of mutations were found within the first 5 bases of a read, which was not explained by a bias in sequencing quality scores or base composition. The percent of total predicted mutations with a sequencing quality ≥30 was plotted as a function of their read position. The average sequencing quality as a function of read position is shown. Data represents the average of the mean quality scores from all sequencing runs. The base composition at each read position was calculated by averaging the mean % A, T, C and G at each position from each sequencing run. (E) Mutation lists were generated as described in Materials and Methods. The number of mutations remaining following each refining step is shown. (F) Schematic showing the affected genes with the positions of the mutations found marked with respect to predicted functional domains.

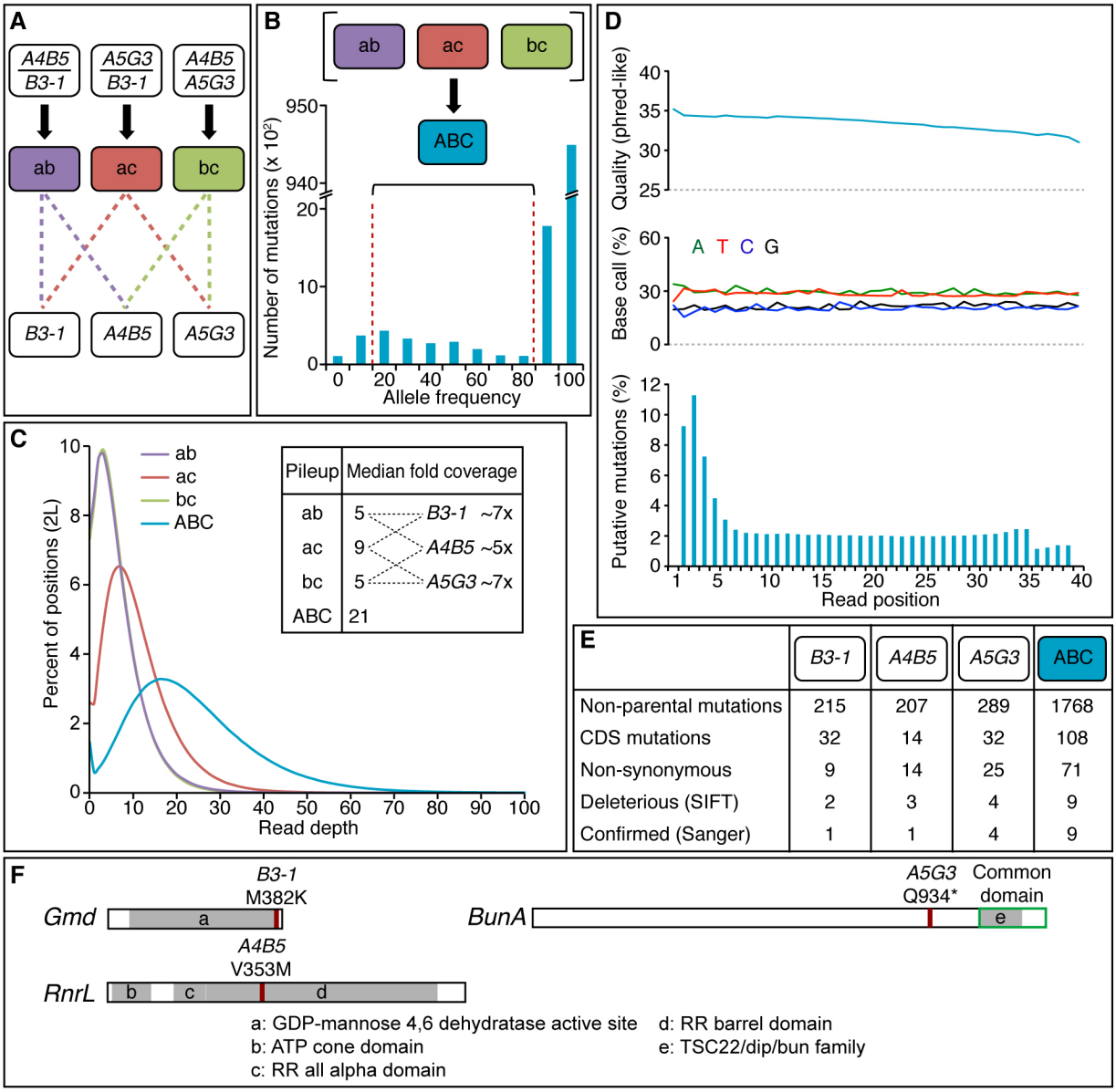
A
A4B5 / B3-1
A5G3 / B3-1
A4B5 / A5G3
ab
ac
bc
B3-1
A4B5
A5G3
B
ab
ac
bc
ABC
Number of mutations (x 10²)
950
940
20
10
0
0 20 40 60 80 100
Allele frequency
C
ab
ac
bc
ABC
Percent of positions (2L)
10
8
6
4
2
0
0 10 20 30 40 50 60 70 80 90 100
Read depth
Pileup
Median fold coverage
ab 5 B3-1 ~7x
ac 9 A4B5 ~5x
bc 5 A5G3 ~7x
ABC 21
D
Quality (phred-like)
40
35
30
25
Base call (%)
A T C G
60
30
0
Putative mutations (%)
12
10
8
6
4
2
0
1 5 10 15 20 25 30 35 40
Read position
E
B3-1 A4B5 A5G3 ABC
Non-parental mutations 215 207 289 1768
CDS mutations 32 14 32 108
Non-synonymous 9 14 25 71
Deleterious (SIFT) 2 3 4 9
Confirmed (Sanger) 1 1 4 9
F
Gmd
a
B3-1
M382K
A4B5
V353M
RnrL
b
c
d
BunA
A5G3
Q934*
Common domain
e
a: GDP-mannose 4,6 dehydratase active site
b: ATP cone domain
c: RR all alpha domain
d: RR barrel domain
e: TSC22/dip/bun family

Figure 2.15: *Representative phenotypes of second, independent alleles for the 3 mutations identified by WGS.*
All 3 alleles are shown in comparison to the non-mutagenized parental phenotype that was used as a control for screen mutants. Isogenic controls for each genotype were not available. Genotypes for *sec5^{ts}* ablation were as follows. Control: *y, w, ey-FLP; P{mw+, ubi-GFP.nls}, FRT40A/sec5^{ts}, FRT40A*; *RnrL^{k06709}*: *y, w, ey-FLP, P{lacW}RnrL^{k06709}, FRT40A/sec5^{ts}, FRT40A*; *bun^{Q666X}*: y, w, ey-FLP; *bun^{Q666X}, FRT40A/sec5^{ts}, FRT40A, en-GAL4, UAS-FLP*; *Gmd^{SH1606}*: *y, w, ey-FLP; P{lacW}Gmd^{SH1606} FRT40A/sec5^{ts}, FRT40A*;. For 'No Ablation' genotypes were as follows: *y, w, ey-FLP; P{mw+, ubi-GFP.nls}, FRT40A/ FRT40A* at 25°C; *RnrL^{k06709}*: *y, w, ey-FLP, P{lacW}RnrL^{k06709}, FRT40A/sec5^{ts}, FRT40A* at 18°C; *bun^{Q666X}*: y, w, ey-FLP; *bun^{Q666X}, FRT40A/P{mw+, ubi-GFP.nls}, FRT40A* at 25°C; *Gmd^{SH1606}*: *y, w, ey-FLP; P{lacW}Gmd^{SH1606} FRT40A/ FRT40A* at 25°C.


sec5ts Ablation
No Ablation
Control
RnrLK06709
BunG666X
GmdSH1606

Figure 2.16: *Identified mutants fell into three putative phenotypic classes*.
(A-D) The resulting adult wings after *sec5*^{ts} ablation for *bun*^{A5G3} (B) *RnrL*^{A4B5} (C) and *Gmd*$^{B3\text{-}1}$ (D) all show size defects as compared to control (A). (E-I) Wing imaginal discs dissected at 48 hr AUS and stained with PHH3 (cyan) to mark mitotic cells and TUNEL (magenta) to mark apoptotic cells. For PHH3 and TUNEL, images are z-max projections of confocal slices through the entire disc epithelium. For GFP, images are a single confocal slice. Posterior is to the left. (E-E") Parental control disc. Minimal TUNEL+ cells remain and PHH3+ cells are evident particularly in the posterior compartment. (F-F") *bun*^{A5G3} discs are noticeably smaller, but TUNEL staining is comparable to the control and proliferation is evident. (G-G") *Gmd*$^{B3\text{-}1}$ discs are indistinguishable from parental controls. (H-H") *RnrL*^{A4B5} discs are comparable in size to parental controls, but have high levels of apoptosis in the posterior compartment. Mitotic cells are still evident in the posterior compartment (I-I") *Top3α*$^{B9\text{-}2}$ discs show a similar phenotype to *RnrL*^{A4B5} discs. (J-N) High magnification images showing both TUNEL (magenta) and GFP (green). Single confocal sections through the basal portion of the disc epithelium are shown. Residual apoptotic cells in control (J), *bun*^{A5G3} (K) and *Gmd*$^{B3\text{-}1}$ (L) discs are largely GFP-. Additional apoptotic cells in *RnrL*^{A4B5} (M) and *Top3α*$^{B9\text{-}2}$ (N) discs are mostly GFP+ (i.e. mutant for *RnrL*^{A4B5} or *Top3α*$^{B9\text{-}2}$). (O) Only *bun*^{A5G3} mutant discs were smaller than controls at the end of the ablation period. Quantification of wing disc area, anterior and posterior compartments, 48 hr AUS, comparing the size of mutant discs to the control. (P) Developmental timing of pupariation of ablated (30°C) or non-ablated (18°C) *Bun*^{A5G3}, *RnrL*^{A4B5} and *Gmd*$^{B3\text{-}1}$ animals as compared to control. The calculated average time (days AEL) to 50% pupariation is shown. Error bars show one STDEV. Dashed lines mark the average time to 50% pupariation for the parental control. Ablated *RnrL*^{A4B5} animals showed a slight delay in pupariation, suggesting that the inability of these animals to compensate might result in a developmental delay. Animals carrying *bun*^{A5G3} developed more slowly than control animals with or without ablation.

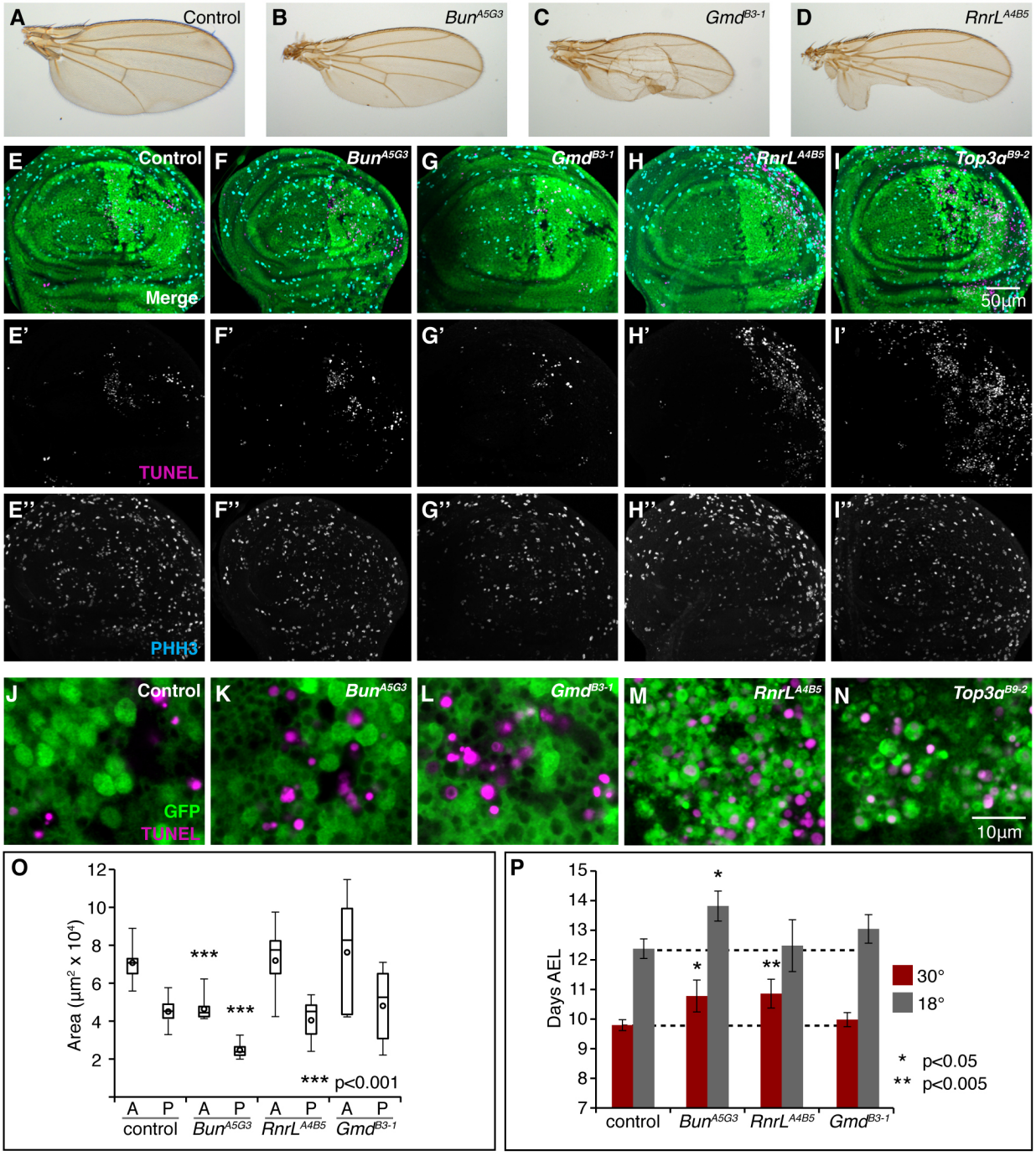
A Control
B Bun^A5G3
C Gmd^B3-1
D RnrL^A4B5
E Control
F Bun^A5G3
G Gmd^B3-1
H RnrL^A4B5
I Top3a^B9-2
Merge
50µm
E'
F'
G'
H'
I'
TUNEL
E''
F''
G''
H''
I''
PHH3
J Control
K Bun^A5G3
L Gmd^B3-1
M RnrL^A4B5
N Top3a^B9-2
GFP
TUNEL
10µm
O
Area (µm² x 10⁴)
*** p<0.001
A P
control
Bun^A5G3
RnrL^A4B5
Gmd^B3-1
P
Days AEL
30°
18°
* p<0.05
** p<0.005
control
Bun^A5G3
RnrL^A4B5
Gmd^B3-1

Figure 2.17: *$RnrL^{A4B5}$ partially suppressed overgrowth induced by overexpression of activated Yorkie.* (A-D) Wing imaginal discs with MARCM clones shown in green (GFP) and nuclei (DAPI) in blue. Scale bar is 50μm. (A-B) *$RnrL^{A4B5}$* mutant clones were comparable in size to control clones. Wing imaginal discs with MARCM clones in which GFP+ cells (green) were homozygous for either the parental control chromosome (A) or *$RnrL^{A4B5}$* (B). (C-D) *$RnrL^{A4B5}$* mutant clones over-expressing activated *yorkie* (*yki*) were noticeably smaller than control clones and stained weakly for DAPI. MARCM clones in which GFP+ cells (green) were over-expressing activated *yki* and were homozygous for either the parental control chromosome (C) or *$RnrL^{A4B5}$* (D). DAPI is shown in white for control (C') and *$RnrL^{A4B5}$* (D') discs. Single confocal sections are shown. (E-F) Clones over-expressing activated *yki* and mutant for *$RnrL^{A4B5}$* appear to have fewer and larger cells than controls. High magnification images of single clones homozygous for the parental control (E) or *$RnrL^{A4B5}$* (F) and over-expressing activated *yki*. mCD8-GFP marks the cell membrane (E and F) and DAPI marks nuclei (E' and F').

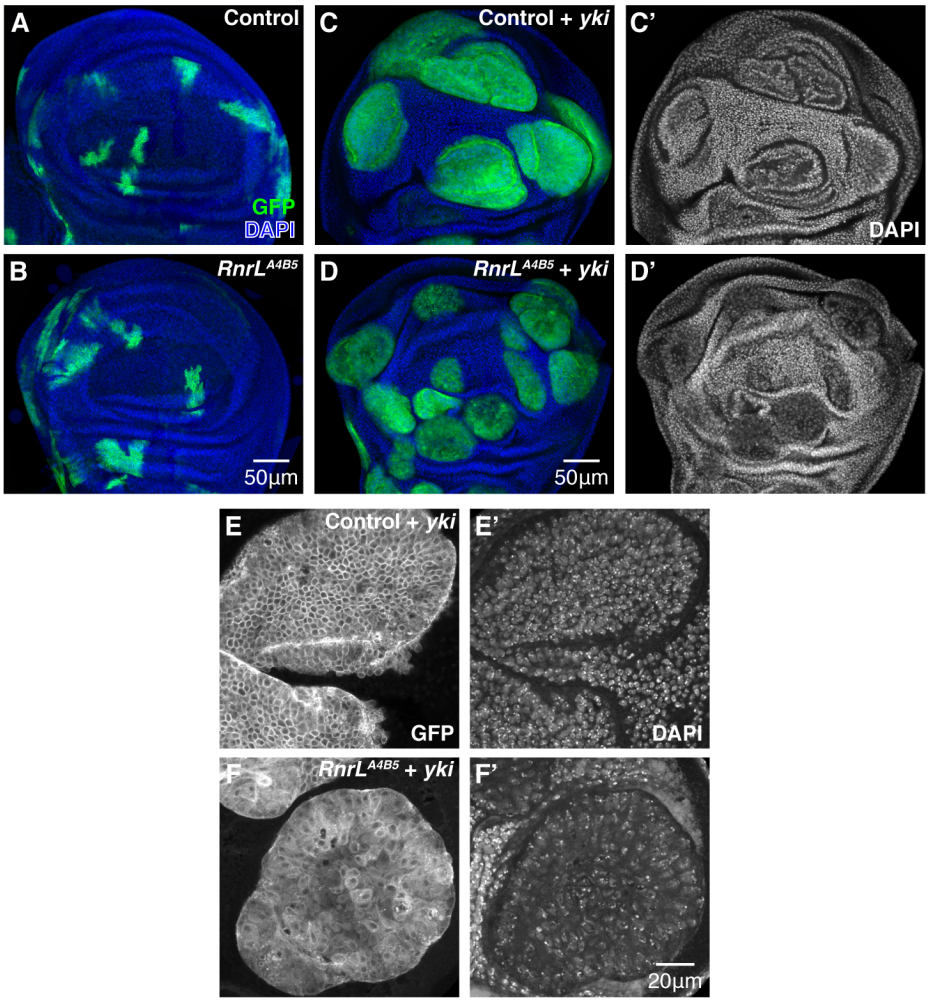
A
Control
GFP
DAPI
C
Control + yki
C'
DAPI
B
RnrL A4B5
50µm
D
RnrL A4B5 + yki
50µm
D'
E
Control + yki
GFP
E'
DAPI
F
RnrL A4B5 + yki
F'
20µm

Figure 2.18: *bun^{A5G3} mutant clones were indistinguishable in size from controls.*
Twin spot analysis of *bun^{A5G3}* clones and control clones. The 'clone' was homozygous for either *bun^{A5G3}* or the parental non-mutagenized chromosome. Clone area is expressed as a fraction of the area of the matching twin spot clone. 71 control and 93 *bun^{A5G3}* clone-twin spot pairs were analyzed. Data are shown as box and whiskers plots. See Materials and Methods for details.

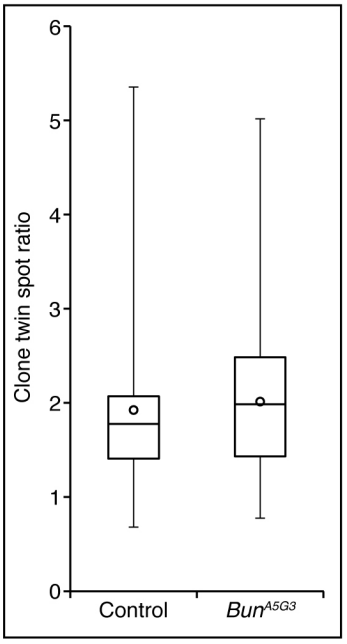
Clone twin spot ratio
6
5
4
3
2
1
0
Control
Bun^A5G3

Table 2.1: *Full description of all mutant phenotypes from sec5^{ts} screen – stock lethality, sec5^{ts} ablation and no ablation of sec5^{ts} tissue (18°C).*

Allele	Lethality	x sec5ts @ 18	x sec5ts shifted 18 to 30 6-7dAEL
A1C5	Y	some ~wt, some mild W>R to W=R	consistent, rough, mild/moderate reduced
A1D3	N - mild roughness in P of eye?	~wt	mild rough/reduced, w- left
A2A3	Y	variable: maj. W>R, some males ~wt	variable: strong rough/reduced - few slightly overgrown; eyes rough or mishapen with uneven surface
A2B3	N	variable: some ~wt, some W=R, maybe rough (few)	variable: some ~wt, some mild rough
A2D1	Y	variable: male W=R or wt, female mild W>R	rough/reduced, some bulgy or with uneven surface
A2E9	N	~wt	some PL, variable reduced, mishapen
A2G1	~Y - escapers have mild to strong wing defects, shirt, thick hairy legs, extra bristles	variable: mild W>R, W=R eyes ~normal	variable: some overgrown, some rough, some slight reduced with more bristles around eye
A2I3	Y	mean W=R, but generally less R than control	rough, mild reduced
A2J5	Y	variable: male ~wt, female W>R	variable: mild/moderate rough/reduced, w- left
A3G1	Y	~wt, few are more W=R	mild reduced, rough across
A4A7	Y	male W=R, females W>R	some PL, mild rough/reduced, w- left
A4B5	Y	~wt	rough/reduced, some PL
A4F2	~Y - homozygotes have small wings	variable: male W=R, female W>R	variable: rough/reduced to almost normal, occassional overgrown eye (1 eye, other reduced), females worse
A5D4	Y	W=R, R>W	rough/reduced
A5D9	~Y - escapers have mild to strong wing defects	Variable: some W>R, most W=R	very weak, some ~wt, some mild rough/reduced
A5G3	Y	W:R wt, but eye maybe slightly rough	rough, very mild reduced

Allele	Lethality	x sec5ts @ 18	x sec5ts shifted 18 to 30 6-7dAEL
B-1	semi-viable	~wt, slight shift in favor of W, some W=R	v. strong rough/reduced
B12-1	Y	~wt, few more W=R	very mild reduced, eye slightly narrower, rough across
B12-2	Y	wt, slightly rough?	strong rough/reduced, w- left
B12-3	Y	male ~wt; female W>R	~wt size (females reduced), rough/uneven surface
B18-1	Y	males W=R to W>R, females W>R, some rough eyes	variable, mild rough/reduced, some msshpn
B18-2	Y	variable: W=R to W>R	very mild rough/reduced, some misshapen, rough
B19-1	Y	wt, even more R	PL, strong rough/reduced
B25-1	Y	W=R to W>R esp. females	mild rough/reduced, variable, some misshapen, females worse
B25-2	Y	W=R to W>R, some rough, ~reduced?	variable - severe to mild rough/reduced
B3-1	Y	wt	mild Bar-like/misshapen, mild rough, females have extra bristles below eye
B6-1	N - homozygotes have rough eyes	wt, slightly rough	strong/moderate rough/reduced, rough across eye
B6-2	Y	~W=R, less R than wt	strong rough/reduced
B7-1	Y - few escapers no obvious phenotype	male W=R to W>R, females W>R	mild reduced, some misshapen, rough
B9-1	Y	W=R to W>R esp. females	moderate rough/reduced, w- left, some bulgy (only females kept?)
B9-2	Y	~wt to W=R	mild to moderate rough/reduced

Table 2.2: *Full description of all mutant phenotypes from sec5^{ts} screen – temperature sensitivity and IR ablation.*

Allele	**x 40A @ 18**	**x 40A @ 25** (if scored twice, observations separated by ;)	**x 40A shifted 25 to 30 3-4dAEL**	**x 40A X-ray'd 20min 3-4dAEL** (if scored twice, observations separated by ;)
A1C5	~parental/sm. clone?	mild W>R; ~wt, slight shift to W esp. in females	mild W>R ro W>R (esp. in females)	maybe slight W>R shift; same
A1D3	~parental	W=R, slight W>R shift; slight shift in favor of W	W>>>R	~same as 0kR; same as 0kR
A2A3	mild W>R to W>R	mild W>R; wt(fewer) to W>>R	W>R to W>>R	slightly stronger W>R than 0kR
A2B3	~parental/sm. clone?	W=R; ~wt, some females W>R	~wt	variable: some same as 0kR, some W>R shift; variable: some eyes more W>R than 0kR
A2D1	sm. clone to mild W>R	mild W>R; ~wt	mild W>R	W>R shift; W>R shift
A2E9	~parental/sm. clone?	~W=R, clones smaller; wt	W>>R	some same, some W>R; some same ~1/3 more W>R
A2G1	~W=R, smooth clones	W=R, normal; ~wt, clones look more contiguous	~wt to W>R, clones contiguous, 2 females with rough eyes with black spots	unclear: most same as 0kR, some more W>R; same
A2I3	male sm. clone, female mild W>R	mild W>R; mild W>R	mild W>R	only 1 adult, stronger W>R than 0kR
A2J5	mild W>R to W>R	W=R, W>R; mild W>R, esp in A	mild W>R	some same, some with all W in A; slight shift to W>R more visible in males
A3G1	~parental/sm. clone?	slight W>R shift; ~wt	~wt (few) to W>R	no obvious difference; same
A4A7	mild W>R, variable	variable W>R; W>R to W>>R (esp. females)	W>R to W>>R	few adults, same; same
A4B5	~parental	W=R; wt	~wt	same as 0kR; same as 0kR
A4F2	mild W>R	W>R; mild W>R	W>R	same as 0kR
A5D4	sm. clone to mild W>R, occassionally eyes look v. mildly rough?	W=R; ~wt, slight W>R	mild W>R	few adults, probably W>R shift; same
A5D9	sm. clone/mild W>R to W>R	mild W>R; mild W>R, some wt	mild W>R to W>>R (esp. females)	~same as 0kR, some rough/reduced eyes; most ~same, few W>>R eyes
A5G3	~parental	W=R; wt	~wt	more W>R, some strongly rough or reduced eyes; variable, more W, more rough reduced eyes

Allele	x 40A @ 18	x 40A @ 25 (if scored twice, observations separated by ;)	x 40A shifted 25 to 30 3-4dAEL	x 40A X-ray'd 20min 3-4dAEL (if scored twice, observations separated by ;)
B-1	~parental	W>>R	W>>>R	didn't score since 0kR so strong W>>R
B12-1	~parental	~wt	~wt to mild W>R	~same, few W>>R, few strongly reduced eyes; some W>R, rest same, maybe slightly more W
B12-2	~parental/sm. clone?	2 populations? W>R to W>>R; same	W>>>R	0kR are W>>R, 4kR may be worse but hard to say
B12-3	variable - ~parental to mild W>R	~wt, slight shift to W	~wt, slight shift to W	same as 0kR; same as 0kR
B18-1	mild W>R	variable W>R	mild W>R, W>R	~same, more rough/reduced eyes; same as 0kR
B18-2	mild W>R	variable W>R	W>R	same as 0kR; same as 0kR
B19-1	~parental/sm. clone?	~W=R, rough eye, mild reduced, few FLP'd	NFP	~same as 0kR
B25-1	mild W>R to W>R	mild W>R, W>R	W>R to W>>R	~same as 0kR
B25-2	mild W>R to W>R	mild W>R, W>R	mild W>R, W>R	stronger W>R than 0kR, 2 with outgrowth from eye near antenna in A
B3-1	~parental	wt	wt	maybe more W, more eyes rough/reduced, see wing defects; ~same as 0kR, maybe more wing defects (flies with stronger eye defects may have died?)
B6-1	variable - ~parental to W>>R	mild W>R, wild rough; wt to W>R slight rough	W=R to W>R rough eye, mild reduced	~same as 0kR, maybe more rough
B6-2	mild W>R, eyes with more R are ~rough with extra bristles	mild W>R, W>R	W>>R, slight rough	less R in A than 0kR (already W>R)
B7-1	sm. clone to mild W>R	mild W>R	mild W>R	same as 0kR; same as 0kR
B9-1	mild W>R	W>R	W>R	~same as 0kR but greater # of W>>R
B9-2	sm. clone to mild W>R	mild W>R	mild W>R	W>R shift, more R eyes are more reduced; W>R shift

Chapter 3

An innate cellular immune response to tissue damage in Drosophila

Abstract

Innate immune cells, in particular macrophages, play an important role in wound healing and regeneration. The molecular mechanisms underlying macrophage recruitment to and function at sites of injury are largely unexplored. The innate cellular immune system of Drosophila provides a genetically tractable model within which to investigate how blood cells respond to tissue damage. We have characterized the cellular immune response to tissue injury in larvae and found that it involves macrophage activation and lamellocyte differentiation. Macrophages clear cell corpses and lamellocytes may function to encapsulate excess cellular debris. Interestingly, mutations that block phagocytosis also reduce lamellocyte differentiation. We propose a model in which macrophages, by engulfing dying cells, become competent to trigger a broader immune response, including lamellocyte production.

Introduction

The innate cellular immune system responds to tissue injury in a wide range of organisms. Monocyte macrophages, in particular, are required to clear cellular debris and to modulate the inflammatory response. They may also impact the regenerative capacity of the damaged tissue. Despite the documented importance of macrophages in tissue recovery and repair, relatively little is known about the molecular mechanisms underlying macrophage recruitment and function in this context. Drosophila have innate cellular immune system analogous to the vetrebrate monocyte/myeloid lineage (reviewed in (EVANS *et al.* 2003; LANOT *et al.* 2001), which has served as a productive model for the study of hematopoiesis (reviewed in (EVANS *et al.* 2003)), pathogen defense (e.g. Toll signaling) (reviewed in (DIONNE and SCHNEIDER 2008)), macrophage migration (MOREIRA *et al.* 2010) and macrophage-mediated phagocytosis (reviewed in (FRANC 2002)). However, we have only a limited understanding of the cellular immune response to tissue injury.

In larvae, the cellular immune system consists of three classes of blood cells, known broadly as hemocytes ((LANOT *et al.* 2001), reviewed in (MEISTER 2004)). Plasmatocytes make up ~95% of hemocytes in healthy larvae and differentiate into macrophages to engulf pathogens and apoptotic cells. Crystal cells produce the enzymes involved in melanization reactions and lamellocytes, which are rarely present in healthy larvae, participate in encapsulation of parasitic wasp eggs and other objects too large to be phagocytosed. Hemocytes are found in the larval hematopoietic organ, the lymph gland, circulating freely in the hemolymph and in sessile bands below the cuticle (LANOT *et al.* 2001). All three hemocyte types may derive from a common pro-hemocyte precursor; however, the hematopoietic lineage is not well established. Pro-hemocytes reside in the lymph gland and a population of precursors also exists outside of the lymph gland, either in circulation or in the sessile population (LANOT *et al.* 2001; MÁRKUS *et al.* 2009).

Hemocytes are recruited to sites of larval or embryonic epidermal wounds, by adhesive capture or activate migration, respectively, where they participate in the clearance of cellular debris (BABCOCK *et al.* 2008; STRAMER *et al.* 2005). Localized ultraviolet radiation-induced damage to both the larval epidermis and pupal retina evokes wide-spread activation of the hemocyte population, which may aid in recovery (KARPAC *et al.* 2011; KELSEY *et al.* 2012). It has also been shown that hemocytes accumulate at neoplastic imaginal discs where they may promote overgrowth by the production of tumor necrosis factor (TNF) (CORDERO *et al.* 2010) or restrain it (PASTOR-PAREJA *et al.* 2008). Several recent reports have shown that plasmatocytes can act to convey local perturbations, including infection and tissue damage, to distant sites thereby promoting an appropriate systemic response (AGAISSE *et al.* 2003; DIJKERS and O'FARRELL 2007; KARPAC *et al.* 2011; PASTOR-PAREJA *et al.* 2008). These observations suggest that tissue damage elicits an inflammatory-like reaction in Drosophila. However, very little is known about how or why this response occurs.

We have assessed the cellular immune response to imaginal disc damage as induced by genetic ablation and X-ray irradiation (IR). Surprisingly, we have found that imaginal disc apoptosis generates an immune response reminiscent of that which occurs following wasp parasitization, including wide-spread differentiation of lamellocytes. Using IR, we investigated the ontogeny of lamellocytes. We provide preliminary evidence in favor of a model in which phagocytically active plasmatocytes drive the production of lamellocytes,

which may function to sequester excess cellular debris. Our results establish that ectopic apoptosis in larvae can trigger an innate cellular immune response and provide an avenue for future research into the mechanistic basis of this reaction.

Results

Activated hemocytes engulf apoptotic imaginal disc cells.

To test whether apoptosis of imaginal disc cells was sufficient to stimulate hemocyte activation we looked at discs in which cell death had been induced in a variety of ways. Several mutations that generate neoplastic overgrowth also produce substantial amounts of cell death (Figure 3.1, A and B and data not shown). We found significant numbers of hemocytes associated with these tissues, many of which were actively engulfing apoptotic cells (Figure 3.1, A). Surprisingly, we occasionally observed mature lamellocytes adhering to these discs (Figure 3.1, B). We also found hemocytes phagocytosing apoptotic cells at wing discs damaged by genetic ablation (SMITH-BOLTON *et al.* 2009) (Figure 3.1, C) and at eye and wing discs damaged by IR (Figure 3.1, D and data not shown). The genetic wing disc ablation system positively marks apoptotic cells by expression of GFP. This allowed us to also find mature macrophages in the circulating hemocyte population (Figure 3.1, E). Thus activated hemocytes are present at sites of imaginal disc damage where they phagocytose apoptotic imaginal disc cells. Some of these mature macrophages are then released back into the circulating population.

IR-induced damage leads to broad changes in the circulating hemocyte population.

We observed several additional changes in the composition of the circulating hemocyte population in animals subjected to IR. In untreated animals, the putative phagocytosis receptor Nimrod C1 (NimC1) was expressed by the vast majority of circulating hemocytes (KURUCZ *et al.* 2007) (Figure 3.2, A). Following IR, we observed an increase in the number of NimC1-negative cells (Figure 3.2, B and C). In addition, 48 hours post-IR, NimC1 frequently appeared concentrated in or outlining intracellular vacuoles (Figure 3.2, C'). Although NimC1 has not yet been implicated in the phagocytosis of apoptotic cells, its localization may generally identify phagocytic vacuoles in mature macrophages.

In addition to differences in the expression and localization of Nim1C, we also observed changes in the actin cytoskeleton of circulating hemocytes from IR-treated larvae. In control animals, circulating hemocytes appeared generally small and rounded (Figure 3.2, D). Following IR, circulating hemocytes assumed a more macrophage-like morphology, appearing larger and more spread out with extensive lamellopodia (Figure 3.2, E and F). We also found large actin-rich cells in IR-treated animals (Figure 3.2, E and F, arrow heads).

Lamellocyte differentiation is induced by imaginal disc damage.

Following IR we observed a dramatic increase in the number of lamellocytes present in the circulating hemocyte population (Figure 3.3, A). At 10 hours post-IR, we did not find evidence of mature lamellocytes (data not shown); however by 24 hours post-IR, irradiated larvae showed noticeably more lamellocytes than untreated controls (Figure 3.3, A). The number of lamellocytes continued to increase between 24 and 48 hours post-IR, with significantly more mature lamellocytes present at this later time point (Figure 3.3, A). We noted that at 48 hours post-IR, irradiated animals did not show an increase in total

hemocyte numbers (Figure 3.3, A'); rather lamellocytes composed on average 25% of a normally-sized hemocyte population.

At 24 hours post-IR, irradiated larvae also had fewer circulating hemocytes than age-matched controls. In agreement with previous reports (LANOT *et al.* 2001), we observed an increase in the number of circulating hemocytes in control animals between 0 (early/mid third instar(L3)) and 24 (wandering) hours post-mock IR (Figure 3.3, A'). Conversely, the number of circulating hemocytes did not increase in irradiated animals between 0 and 24 hours post-IR. IR-treated animals had only achieved a normal number of circulating hemocytes by 48 hours post-IR. We did not observe an increase in hemocyte cell death at 24 hours post-IR (Figure 3.4, A-C), suggesting that IR-induced apoptosis is unlikely to account for the delayed expansion of the circulating hemocyte population. Instead, mitotic arrest of proliferative hemocytes, as occurs in the dividing cells of imaginal discs in irradiated animals (JAKLEVIC and SU 2004), could account for the delay. However, without also looking at earlier time points following IR, we cannot rule out a role for hemocyte cell death.

To determine whether lamellocyte differentiation was a specific response to IR, we looked at the circulating hemocyte population of larvae undergoing wing disc-specific ablation. We observed a progressive increase in the number of lamellocytes following wing disc ablation, with maximum lamellocyte numbers reached at 72 hours post-ablation (Figure 3.3, B). Over the same time period, the total number of circulating hemocytes remained constant, at a value comparable to control animals (data not shown). In both irradiated and wing disc-ablated animals we also observed melanotic masses in the larval body cavity (Figure 3.3, C and D), which were encapsulated by lamellocytes (Figure 3.3 C' and D').

Wing disc-ablated animals had fewer lamellocytes than those subjected to IR. This difference may be due to the extent of damage present in each circumstance. Indeed, we found that both lamellocyte differentiation and the decreased total hemocyte number at 24 hours post-IR were dependent on the dose of IR administered (Figure 3.3, E and E').

In both IR-treated and wing disc-ablated animals, maximum lamellocyte differentiation and melanotic mass formation were observed well after damage was induced (Figure 3.3 A and B, 48 and 72 hours, respectively). However, in both cases, apoptotic debris was still evident at these late time points (data not shown).

Hemocyte apoptosis is sufficient but not necessary to drive lamellocyte production.

IR-induced apoptosis in early L3 larvae is largely confined to the imaginal discs (HALME *et al.* 2010). Indeed, circulating hemocytes from irradiated larvae showed no more apoptotic cells than untreated controls (Figure 3.4, A-C). However, to rule out that lamellocyte differentiation was a response to hemocyte apoptosis, we blocked cell death specifically in hemocytes and assayed lamellocyte production. We found no fewer lamellocytes in larvae in which apoptosis had been inhibited than in controls (Figure 3.4, D). Conversely, we found that ablating hemocytes lead to lamellocyte differentiation (Figure 3.4, E-G). We simultaneously expressed a pro-apoptotic factor (hid^{ala5}) and GFP using a hemocyte-specific driver. The resulting larvae showed a strong reduction in the number of GFP-positive hemocytes (Figure 3.4, E and F) and, surprisingly, a large number of lamellocytes (Figure 3.4, G). The majority of these cells were GFP-negative, suggesting

that they were not themselves expressing the pro-apoptotic factor. Thus, while hemocyte apoptosis is not necessary for robust lamellocyte differentiation, lamellocytes are produced by ectopic hemocyte apoptosis.

The majority of lamellocytes derive from Domeless or Dorothy-expressing progenitors.

Where lamellocytes come from and from which cells they derive following wasp parasitization is largely unresolved. Initial reports suggested that lamellocytes differentiate directly from circulating plasmatocytes (RIZKI 1962). The observation that lamellocytes accumulate in the lymph gland following parasitization lead to the idea that prohemocytes within the lymph gland produce lamellocytes which are then released into circulation (LANOT *et al.* 2001; SORRENTINO *et al.* 2002). Indeed mutations that affect prohemocyte function in the lymph gland largely block lamellocyte differentiation (CROZATIER *et al.* 2004; MAKKI *et al.* 2010). However, several recent reports have suggested that lamellocytes may also differentiate from progenitors outside the lymph gland (MÁRKUS *et al.* 2009) and can differentiate directly from plasmatocytes (AVET-ROCHEX *et al.* 2010; HONTI *et al.* 2010; KROEGER *et al.* 2011; STOFANKO *et al.* 2010).

To assess the origin of IR-induced lamellocytes, we used the lineage-tracing tool G-TRACE (EVANS *et al.* 2009). Our results are summarized in Table 3.1. *HmlΔ-GAL4* is expressed in a subset of larval plasmatocytes and crystal cells in the circulating and sessile population and in the posterior lobes of the lymph gland, but not in lamellocytes (GOTO *et al.* 2003). *HmlΔ-GAL4* is not expressed in prohemocytes, but analysis of its temporal expression suggested that it is an early maturation marker (JUNG *et al.* 2005). We found that almost 40% of lamellocytes derived from cells that had expressed *HmlΔ-GAL4*; of these roughly 8% continued to express *HmlΔ-GAL4* (Figure 3.5, A and C). In agreement with earlier reports, we found that *HmlΔ-GAL4* was only expressed by a subset (~60%) of circulating hemocytes and that this proportion did not change appreciably following IR (Figure 3.5, B). Our results suggest that either lamellocytes can differentiate from *HmlΔ-GAL4*-expresssing mature plasmatocytes or crystal cells or that *HmlΔ-GAL4* is expressed by a common intermediate progenitor that can give rise to all three cell types.

Eater-GAL4 is expressed by the majority of circulating hemocytes and is thought to be primarily plasmatocyte-specific, although occasional *eater-GAL4*-expressing crystal cells have been observed (KROEGER *et al.* 2011; TOKUSUMI *et al.* 2009a). We found that a small number (<10%) of IR-induced lamellocytes derive from *eater-GAL4*-expressing cells (Figure 3.5, A). We also observed occasional lamellocytes that were actively expressing *eater-GAL4* (Figure 3.5, D). At 24 hours post-IR, when mature lamellocytes first start to appear in circulation, we found evidence for *eater-GAL4*-positive cells that also expressed the lamellocyte-specific marker L1 (Figure 3.5, F). L1 detects both mature lamellocytes and small discoidal lamellocytes, which have been proposed to be predecessors of fully differentiated lamellocytes (HONTI *et al.* 2010). *Eater-GAL4*, L1-positive cells may therefore represent plasmatocytes that are shifting to a lamellocyte fate.

We also found that the proportion of *eater-GAL4*-expresssing non-lamellocyte hemocytes decreased following IR (Figure 3.5, B), suggesting a decline in the number of mature plasmatocytes. This result supports our earlier observation that the number of Nim1C-positive cells also appeared to decline following IR.

As a final marker for mature plasmatocytes we used *crq-GAL4*. *Crq-GAL4* is expressed by embryonic macrophages and a small proportion of larval hemocytes (Figure 3.5, B, (HONTI *et al.* 2010). Following IR, we found rare lamellocytes (1-2%) that had differentiated from *crq-GAL4*-expressing cells (Figure 3.5, A and E).

Msn-GAL4 is expressed specifically in lamellocytes (TOKUSUMI *et al.* 2009b). In both IR-treated and control animals no *msn-GAL4*-positive non-lamellocyte hemocytes were detected, confirming the specificity of this driver (Figure 3.5, B). Following IR, the majority of lamellocytes expressed *msn-GAL4*; however a significant proportion (~30%) were *msn-GAL4*-negative (Figure 3.5, A). We also observed incomplete overlap between *msn-GAL4* and L1 expression (Figure 3.5, G). These results suggest that there may be a certain amount of heterogeneity in the lamellocyte population.

Finally, we used two GAL4 drivers reportedly expressed in the lymph gland. *dome-GAL4* is expressed in the prohemocytes of the medullary zone (MZ) of the lymph gland and differentiating cells of the cortical zone (CZ) are derived from *dome-GAL4*-expressing prohemocytes (JUNG *et al.* 2005). We observed a similar expression pattern (Figure 3.5, H). *Dot-GAL4* is expressed in the embryonic lymph gland and shows variable expression later in the larval lymph gland (Figure 3.5, J, (KIMBRELL *et al.* 2002)). *Dot-GAL4* is also expressed in the posterior signaling center (PSC) of the larval lymph gland (Figure 3.5, J, (JUNG *et al.* 2005). Lineage tracing suggested that most cells in the lymph gland are derived from *Dot-GAL4*-expressing cells, although we did observe some variability between individuals (Figure 3.5, J).

We found that the majority of IR-induced lamellocytes were derived from cells that had expressed *Dot-GAL4* and/or *dome-GAL4* (61% and 84% respectively), suggesting that the vast majority of lamellocytes were originating in the lymph gland. However, in both irradiated and control animals we observed GFP-positive non-lamellocyte hemocytes in the circulating population (20-30%), suggesting that some proportion of circulating hemocytes are also derived from cells that have expressed these GAL4-drivers (Figure 3.5, B, I and K). Consequently we cannot rule out the possibility that IR-induced lamellocytes are differentiating from *Dot-* or *dome-GAL4*-expressing hemocytes in circulation rather than being released by the lymph gland.

In summary, our G-TRACE experiments support recent findings that lamellocytes can differentiate from cells expressing markers of mature plasmatocytes. However, the majority of IR-induced lamellocytes appear to differentiate from *Dot-* or *dome-GAL4*-expressing cells. Whether these cells reside in the lymph gland or perhaps represent a population of progenitors in circulation remains to be seen.

JNK pathway activity is increased in hemocytes following IR.

The Jun N-terminal kinase (JNK) pathway is activated by a variety of environmental stresses (reviewed in (LEPPÄ and BOHMANN 1999)) and has been implicated in hemocyte specification and function (KELSEY *et al.* 2012; OWUSU-ANSAH and BANERJEE 2009; WILLIAMS *et al.* 2006; ZETTERVALL *et al.* 2004). To assess whether the JNK pathway played a role in the hemocyte response to IR, we looked at expression of the JNK pathway reporter *puckered-lacZ* (*puc-lacZ*) (GLISE *et al.* 1995; GLISE and NOSELLI 1997; RIESGO-ESCOVAR *et al.* 1996) in circulating hemocytes following IR. We found that the proportion of *puc-lacZ*-expressing cells was increased at both 24 and 48 hours post-IR (Figure 3.6, A-C). *puc-lacZ* expression

was observed in a subset of both plasmatocytes and lamellocytes (Figure 3.6, D-G). Interestingly, when *puc-lacZ* expression was observed within aggregates of lamellocytes, not all cells showed the same level of expression (Figure 3.6, F and G).

We did not observe an increase in JNK activity in the hemocytes of wing disc-ablated animals. Wing disc ablation occurs via the expression of the JNK ligand Eiger, which induces imaginal disc cell apoptosis (SMITH-BOLTON *et al.* 2009). Hemocytes associated with ablating discs did not express *puc-lacZ*, despite robust *puc-lacZ* expression in ablating disc cells (Figure 3.7, A). In addition, the majority of *puc-lacZ*-positive cells found in circulation appeared to be engulfed GFP-positive debris (Figure 3.7, B and C). The extent of damage produced by wing disc ablation may be insufficient to induce a broad increase in hemocyte *puc-lacZ* expression. Alternatively, JNK pathway activation may be a specific response to IR.

To investigate the significance of JNK pathway activity in hemocytes following IR we attenuated pathway activity and assessed whether lamellocyte differentiation was affected. We found that mutations in Drosophila JNK, *basket* (*bsk*), and the JNK kinase kinase kinase, *misshapen* (*msn*), dominantly reduced the number of lamellocytes present in irradiated larvae. While all three alleles tested showed the same trend towards fewer lamellocytes, only *Df(2L)flp170B*, a small deficiency that deletes the entire *bsk* gene (SLUSS *et al.* 1996), had a statistically significant phenotype (Figure 3.8, A). Together these results suggest that the JNK pathway may be involved in promoting IR-induced lamellocyte formation.

To address whether JNK activity is required in plasmatocytes, lamellocytes or both we expressed a dominant negative form of *bsk* (Bsk^{DN}) using *HmlΔ-GAL4* and *He-GAL4*. *He-GAL4* is expressed in 80% of circulating hemocytes, but not in the lymph gland (ZETTERVALL *et al.* 2004). We found that *He-GAL4* was expressed in roughly 70% of IR-induced lamellocytes, with the remaining 30% being derived from cells that had not expressed *He-GAL4* (Table 3.1). Expression of Bsk^{DN} using *HmlΔ-GAL4* resulted in a substantial reduction in the number of lamellocytes without affecting overall hemocyte numbers (Figure 3.8, B). *He-GAL4*-driven expression of Bsk^{DN} had no effect (Figure 3.8, C). In addition, *HmlΔ-GAL4*-driven expression of an RNAi against *bsk* did not recapitulate the Bsk^{DN} phenotype (Figure 3.8, B); however, we have not confirmed that this RNAi construct effectively knocks down *bsk* transcription.

JNK activity in hemocytes may be required for aspects of the larval response to IR other than lamellocyte differentiation. IR induces a robust delay of the larval to pupal transition, which requires communication between damaged imaginal discs and the neuro-endocrine system (HALME *et al.* 2010). The JNK pathway may be involved in generating this delay, as loss of several JNK pathway components dominantly decreased the duration of delay (A. Halme, unpublished). The tissue-specific requirements for JNK signaling have not been addressed. We considered the possibility that JNK activity in hemocytes might be responsible for producing developmental delay following IR. We assessed the length of developmental delay following IR using *HmlΔ-GAL4* to abrogate JNK activity specifically in hemocytes. None of the genotypes evaluated showed a reproducible reduction in developmental delay, suggesting that JNK signaling in these cells is not required for this aspect of the IR response (Figure 3.8, D).

Mutations that block engulfment reduce lamellocyte differentiation.

A previous report has shown that phagocytosis and degradation of engulfed bacteria by hemocytes is required to induce expression of anti-microbial peptides (AMPs) in the fat body, raising the possibility that macrophages in Drosophila could act in a similar fashion to antigen-presenting cells in mammals (BRENNAN *et al.* 2007; HULTMARK and BORGE-RENBERG 2007). To test whether the engulfment of apoptotic cells might be a pre-requisite for lamellocyte production, we measured the number of lamellocytes in animals mutant for two phagocytosis receptors, *nimrod C1* (*nimC1*) and *draper*. *NimC1* is involved in the engulfment of certain bacterial pathogens (KURUCZ *et al.* 2007), while *draper* is required for the phagocytosis of apoptotic cells (FREEMAN *et al.* 2003; MANAKA *et al.* 2004). We found that loss of *nimC1* strongly reduced the number of lamellocytes induced by IR (Figure 3.9, A). Preliminary results with in a *draper* mutant background showed a similar phenotype (Figure 3.9, B).

Discussion

We have found that hemocytes respond to multiple types of imaginal disc apoptosis. Phagocytically active macrophages are found at the site of damage and occasionally in the circulating hemolymph. Whether these cells were resident hemocytes activated *in situ* or recruited circulating cells remains to be seen. The adhesive capture and subsequent release of larval hemocytes has been observed at epidermal wounds and may be analogous to the behavior of blood cells in vertebrates during the initial reaction to wounding (BABCOCK *et al.* 2008). Infiltrating macrophages must then exit the wound site and be released back into circulation for proper resolution of the inflammatory response. Our results indicate that phagocytically active larval macrophages, which are associated with damaged imaginal discs, are released into the hemolymph. Future experiments utilizing genetic ablation of the wing disc (SMITH-BOLTON *et al.* 2009) will allow us to simultaneously modify candidate factors in the damaged region to assess their role in hemocyte capture, activation and possibly retention.

Our results demonstrate that high levels of ectopic apoptosis in larvae produce a cellular immune response reminiscent of the reaction to parasitic wasp infestation, including increased cell spreading, altered NimC1 localization, lamellocyte differentiation and the formation of encapsulated melanotic masses (HOWELL *et al.* 2011; WILLIAMS *et al.* 2005). Lamellocyte differentiation in particular was observed when death was induced widely using IR, specifically using wing disc ablation and in the hemocyte population itself.

The immune reaction to deposition of a parasitic wasp egg comprises four steps: the egg first becomes coated in an unidentified protein layer; plasmatocytes adhere to this layer and spread around the egg cordoning it off from the hemocoel; lamellocyte differentiation and recruitment complete the capsule and the ensuing melanization destroys the egg (HOWELL *et al.* 2011; RIZKI and RIZKI 1992; RUSSO *et al.* 1996; WILLIAMS *et al.* 2005). Lamellocytes have also been shown to encapsulate other foreign objects including human hair (LANOT *et al.* 2001) and damaged imaginal disc and fat body tissue (RIZKI and RIZKI 1980). It is assumed that the encapsulation process proceeds similarly irrespective of the targeted tissue. It is not known what allows the immune system to recognize these "non-self" objects, although fragmentary evidence suggests that extracellular matrix proteins may play a role (HOWELL *et al.* 2011; PASTOR-PAREJA *et al.* 2008; RIZKI and RIZKI 1980). In addition, how recruited plasmatocytes then communicate with the lymph gland and sessile hemocyte population to trigger the systemic production of lamellocytes is completely unknown.

It is curious that tissue damage would trigger lamellocyte production. Unfortunately we were unable to determine the contents of the melanotic masses found in affected animals. One possibility is that lamellocytes encapsulate excess or residual cellular debris. Although we did not find lamellocytes directly associated with apoptotic cells in irradiated or wing disc-ablated animals, they were found adhering to highly apoptotic neoplastic imaginal discs. We also noted that lamellocytes did not accumulate in the hemolymph until significantly after apoptosis had been induced. This delay may indicate that a residual effect of the damage rather than the initial insult is triggering lamellocyte production.

Our results also allowed us to examine certain features of lamellocyte production. In irradiated larvae, lamellocytes comprised a quarter of the total circulating hemocyte population. While the expansion of circulating hemocytes that is characteristic during

larval development was delayed in irradiated animals, final hemocyte numbers were comparable to untreated controls. Therefore, lamellocyte differentiation may occur at the expense of other cell types. Indeed, we also observed a decrease in the proportion of circulating cells expressing the plasmatocyte markers, *eater-GAL4* and NimC1. A recent report suggested that wasp parasitization may also favor the production of lamellocytes over plasmatocytes in the lymph gland (KRZEMIEN *et al.* 2010b), indicating that plasmatocytes and lamellocytes may share a common progenitor. Alternatively, other hemocytes, such as plasmatocytes and macrophages, that would normally contribute to the circulating population may instead be associated with damaged tissues, thus decreasing overall circulating hemocyte numbers.

In agreement with recent reports, our lineage tracing revealed that a small portion of lamellocytes were derived from cells expressing markers of mature plasmatocytes (AVET-ROCHEX *et al.* 2010; HONTI *et al.* 2010; KROEGER *et al.* 2011; STOFANKO *et al.* 2010). However the vast majority likely come from prohemocytes in the lymph gland, which had expressed *dome-GAL4* or *Dot-GAL4*. Interestingly, a notable proportion also differentiated from cells that had expressed *HmlΔ-GAL4*. While *HmlΔ-GAL4* is not expressed by prohemocytes, it is thought to be an early marker for hemocyte maturation, including plasmatocytes and crystal cells (GOTO *et al.* 2003; JUNG *et al.* 2005). Thus lamellocytes may derive both from undifferentiated prohemocytes and from intermediate progenitors that switch from the production of plasmatocytes and crystal cells to lamellocytes.

Dome encodes a receptor of the Janus kinase/Signal-transducer and activator of transcription (JAK/STAT) pathway (BROWN *et al.* 2001) and expression of *dome* is thought to be regulated by JAK/STAT activation through *dome* (HOMBRÍA *et al.* 2005). Thus our results suggest that the predominant progenitor of IR-induced lamellocytes experienced JAK/STAT pathway activation prior to assuming lamellocyte fate. There is wide-spread evidence to suggest that components of the JAK/STAT pathway are both necessary and sufficient for lamellocyte differentiation. Larvae carrying a dominant gain-of-function allele of the Drosophila JAK *hopscotch* ($Hop^{Tum\text{-}l}$) show lymph gland hypertrophy, melanotic mass formation and excessive lamellocyte differentiation (HARRISON *et al.* 1995; LUO *et al.* 1995). In addition, overexpression of $Hop^{Tum\text{-}l}$ in hemocytes leads to the overproduction of lamellocytes (ZETTERVALL *et al.* 2004). Loss of function alleles of either *hop* or the single Drosophila STAT, *stat92E*, reduce lamellocyte differentiation following wasp parasitization (SORRENTINO *et al.* 2004). Recent results, however, have suggested that the JAK/STAT pathway may be employed differently by prohemocytes. Following wasp parasitization, downregulation of JAK/STAT signaling is required for the differentiation of lamellocytes (MAKKI *et al.* 2010). Thus JAK/STAT signaling may promote lamellocyte fate in differentiating hemocytes while also maintaining prohemocytes in an undifferentiated state.

Whether the *dome* expression that we observed in lamellocytes occurred in prohemocytes and was down-regulated to allow for differentiation or in differentiating hemocytes to promote lamellocyte fate is unclear. In support of the former, we did not observe active *dome-GAL4* expression in differentiated lamellocytes at 48 hours post-IR nor did we see expression of the JAK/STAT pathway reporter, *STAT-GFP* (BACH *et al.* 2007), in circulating hemocytes 24 hours or 48 hours post-IR (data not shown). However, it is possible that JAK/STAT pathway activity is a transient event that occurs within the first 24

hours following IR. Investigation of JAK/STAT pathway reporters at these earlier time points is necessary to address this possibility.

We also observed hemocytes in the circulating population of both irradiated and control animals that had expressed *dome-GAL4* or *Dot-GAL4*, but were not lamellocytes. These cells complicate the interpretation of our lineage tracing experiments as we cannot differentiate between lamellocytes that originated in the lymph gland from those that differentiated from these cells in circulation. The presence of these cells at a developmental stage prior to normal lymph gland lysis, may support the existence of a population of prohemocyte-like cells in circulation. It would be interesting to determine at what point in development these cells can first be found in circulation and whether cells actively expressing *dome-GAL4*, as are found in the lymph gland, are ever observed. Interestingly, the circulating cells that had expressed *dome-GAL4* often had a small, rounded morphology, reminiscent of prohemocytes ((LANOT *et al.* 2001), Figure 3.5, I).

Circulating and sessile hemocytes in the larvae are derived from embryonic hemocytes (HOLZ *et al.* 2003). Recently, it was suggested that expansion of the larval hemocyte population was driven by the proliferation of mature embryonic plasmatocytes rather than by prohemocytes (MAKHIJANI *et al.* 2011). Our observation that small, rounded hemocytes, derived from *dome-GAL4*-expressing cells were present in the circulating hemolymph suggests that cells with prohemocyte characteristics are present outside the larval lymph gland. If, indeed, all circulating and sessile hemocytes are derived from mature embryonic plasmatocytes, then a subpopulation may revert to a more prohemocyte-like state. How this identity switch occurs is a fascinating question for further inquiry.

IR also lead to an increase in the proportion of hemocytes expressing the JNK pathway reporter *puc-lacZ*. We observed JNK activity in both plasmatocytes and lamellocytes. JNK activity could increase following IR for a variety of reasons. The JNK pathway can be activated by a broad range of stress stimuli, the outcome of which is strongly context-dependent and includes apoptosis, proliferation and differentiation (reviewed in (LEPPÄ and BOHMANN 1999)). In Drosophila, the role of JNK in promoting apoptosis is well established (reviewed in (KANDA and MIURA 2004)); however JNK has also been shown to confer resistance to oxidative stress at both the tissue and organismal level (BITEAU *et al.* 2008; KARPAC *et al.* 2009; WANG *et al.* 2003). JNK also plays a role in regulation of epithelial cell movements (reviewed in (XIA and KARIN 2004)) and has recently been shown to promote the ability of healthy epithelial cells to engulf their sick or dying neighbors (OHSAWA *et al.* 2011). Increases in JNK activity have also been observed in the circulating hemocytes of wasp parasitized larvae (WILLIAMS *et al.* 2006).

We did not detect apoptosis in the hemocyte population following IR. Thus the increased JNK activity we observed is unlikely to be driving hemocyte death. We did see broad changes in hemocyte morphology which could be JNK mediated; however we could not establish a clear correlation between *puc-lacZ*-positive cells and those with a more spread morphology (data not shown). Interestingly, increased JNK signaling has been observed in plasmatocytes both adjacent and distal to the site of UV-induced retinal injury. (KELSEY *et al.* 2012). The exact role of JNK in this context is uncertain – whether it serves to promote engulfment or participates in another capacity has not been established.

The JNK pathway has previously been implicated in both the production and function of lamellocytes. Overexpression of a constitutively active form of the JNK kinase

hemipterous (*Hep*^{CA}) in circulating and sessile hemocytes is sufficient to drive lamellocyte differentiation (ZETTERVALL *et al.* 2004), although the identity of the lamellocyte producing cells in these populations is unknown. Increasing levels of reactive oxygen species (ROS) in the prohemocytes of the lymph gland promotes prohemocyte differentiation into all 3 cell types, at least in part via JNK pathway activation (OWUSU-ANSAH and BANERJEE 2009). Thus increasing JNK pathway activity can induce lamellocyte differentiation from a range of progenitors. However, knock-down of *bsk* in hemocytes using *HmlΔ-GAL4* did not prevent lamellocyte differentiation following wasp parasitization (WILLIAMS *et al.* 2006). As we have found that only a subset of lamellocytes are derived from *HmlΔ-GAL4*-expressing cells, it is possible that other unaffected progenitors were able to compensate for the decrease in lamellocyte production. Alternatively, the JNK pathway may be sufficient but not necessary for lamellocyte differentiation. JNK activity is also involved in regulating turnover of the actin cytoskeleton and reducing JNK function blocks effective encapsulation (reviewed (WILLIAMS *et al.* 2006; XIA and KARIN 2004)). Thus the *puc-lacZ* expression that we observed in lamellocytes may also be related to their ability to engage in encapsulation.

Our results suggest that reducing JNK signaling at the organismal level decreases lamellocyte production. However, abrogating JNK activity specifically in the hemocyte population gave conflicting results. Consistent with a role for JNK in lamellocyte function rather than production, knocking down JNK signaling using *He-GAL4*, which is expressed in the majority of IR-induced lamellocytes, did not affect lamellocyte numbers. It is therefore unlikely that JNK activity is required cell autonomously for lamellocyte differentiation. Alternatively, *He-GAL4* expression may be turned on in lamellocytes after the requirement for JNK signaling has passed. Using *dome-GAL4*, which is likely to be expressed in lamellocyte progenitors, to modify JNK signaling could address this possibility.

Using *HmlΔ-GAL4* to block JNK signaling, gave an inconsistent phenotype. We observed a strong reduction in lamellocyte numbers when a dominant negative allele of *bsk* was expressed, but no effect when RNAi was used to knock down *bsk* expression. This latter result is in agreement with the aforementioned report, which, using *HmlΔ-GAL4*-driven *bsk* RNAi, failed to detect decreased lamellocyte production following wasp parasitization (WILLIAMS *et al.* 2006). It is possible that expression of *Bsk*^{DN} modifies JNK signaling more strongly than knockdown of *bsk* using RNAi, which may only partially reduce *bsk* expression. It is unlikely that the observed phenotype is due to an unknown factor in the genetic background of the *Bsk*^{DN} line, as *He-GAL4*-driven expression showed no effect. Rather the reduced lamellocyte differentiation we observed using *HmlΔ-GAL4*-driven *Bsk*^{DN} may suggest that JNK activity is required in a subset of hemocytes that do not express *He-GAL4*. One candidate population are the cells of the lymph gland as *HmlΔ-GAL4* is expressed in cells within the cortical zone while *He-GAL4* expression is absent (GOTO *et al.* 2003; ZETTERVALL *et al.* 2004).

We note that the *HmlΔ-GAL4*-driven reduction in lamellocytes (~70% of control) is disproportionate to the number of lamellocyte progenitors which expressed *HmlΔ-GAL4* (~40%), which could indicate that JNK activity is required non-autonomously for lamellocyte differentiation, possibly within the plasmatocyte population. A more strictly plasmatocyte driver, such as *eater-GAL4*, could be used to assess this possibility. Interestingly, expression of the pro-apoptotic factor *hid* using *HmlΔ-GAL4* lead to non-autonomous lamellocyte production. Hid induces apoptosis by inhibiting the activity of

Drosophila inhibitor-of-apoptosis protein 1 (DIAP1) (VUCIC *et al.* 1998). DIAP1 blocks apoptosis by negatively regulating both Caspase activation and Drosophila tumor-necrosis factor receptor-associated factor 1 (DTRAF1), which activates JNK (KURANAGA *et al.* 2002). Thus our observations provide preliminary evidence for a model in which stress-induced JNK signaling in plasmatocytes non-autonomously triggers lamellocyte differentiation. Future experiments will directly test this hypothesis.

If plasmatocytes are responsible for cuing the differentiation of lamellocytes, they may do so by producing systemic factors. Alternatively, plasmatocytes could act as antigen-presenting cells, using their capacity as phagocytes to internalize immunogenic factors and then represent this encounter on their cell surface. Such a role has been hinted at by the observation that plasmatocyte engulfment and degradation of bacteria is necessary for the robust production of AMPs by the fat body (BRENNAN *et al.* 2007; HULTMARK and BORGE-RENBERG 2007). We found that loss of the putative phagocytosis receptors, NimC1 and Draper, strongly reduced lamellocyte production. Thus the phagocytic activity of plasmatocytes may be required to trigger lamellocyte differentiation. Whether the phagocytosis of cellular debris prompts plasmatocytes to secrete humoral signals or enables them to present immunogenic signals is not known. In addition, it will be interesting to assess whether phagocytic activity is required for the observed increased in JNK signaling.

Materials and Methods

Drosophila stocks and husbandry

Neoplastic eye-antennal imaginal discs were generated with the following: *y, w, ey-FLP; FRT42D cl/CyO twist-GFP*, *w; FRT42D P3C/CyO twist-GFP* (CLASSEN *et al.* 2009) and *w; FRT42D vps25^{A3}/CyO twist-GFP* (VACCARI and BILDER 2005).

Wing disc specific ablation was produced with the following lines: *w; rn-GAL4, UAS-eiger, tub-GAL80^{ts}/TM6b* (SMITH-BOLTON *et al.* 2009), *w; UAS-GFP; rn-GAL4, UAS-eiger, tub-GAL80^{ts}/TM6b*, *OregonR* and *w; UAS-GFP*.

In addition, we used the following stocks: *OregonR*, *w^{1118}*, *w^{1118}; UAS-GFP.nls* (BL4775), *w; UAS-hid^{ala5}* gift from Andreas Bergmann, w; *UAS-RHG miRNA* (*UAS-mir^{RHG}* in text) (SIEGRIST *et al.* 2010), *UAS-Act5C.mRFP* (BL24778), *w; UAS-RFP, UAS-FLP, ubi>stop>GFP.nls/CyO* (G-TRACE in text) (EVANS *et al.* 2009), *w^{1118}; HmlΔ -GAL4* (BL30139), *w^{1118}; HmlΔ -GAL4, UAS-2xEGFP* (BL30140), *w*; He-GAL4* (BL8699), *y^{1}, w*; crq-GAL4* (BL25041), *w; eater-GAL4* (TOKUSUMI *et al.* 2009a), *w, eater-GAL4, UAS-2xEYFP* (TOKUSUMI *et al.* 2009a), *w; msnF9-GAL4* (*msn-GAL4* in text) (TOKUSUMI *et al.* 2009a), *w; msnF9-GAL4, UAS-2xEGFP/SM6 Cy Roi* (TOKUSUMI *et al.* 2009a), *w*; Dot-GAL4* (BL6902), *w, dome-GAL4/FM7i* (*UAS-EYFP* removed by recombination from *w, dome-GAL4, UAS-EYFP/FM7i* gift from Utpal Banerjee), *w, UAS-hepRNAi* (VDRC47507).

The following lines were out-crossed into *w^{1118}* for 3 generations before being re-balanced) *w; UAS-bskRNAi/SM6-TM6B* (from VDRC34138), *w; puc^{E69}/TM6B*, *w; bsk^{1}/CyO Act-GFP*, *w; Df(2L)FLP170b/CyO Act-GFP*, *w; P{PZ}msn^{06946}*, *ry^{506}/TM6b*, *w; UAS-Bsk^{DN}/TM6B*.

+/w; draper^{delta5rec8} #2/TM3 Serrate-GFP (gift from Mathew Freeman; out-crossed to *OregonR* for 4 generations before being re-balanced, genotype confirmed by PCR), *+; nimC1^{Δ308} #4/CyO Actin-GFP* (A ~350bp deletion leading to a frameshift and premature stop; isolated from *eiger^{1}* and *eiger^{3}* stocks (IGAKI *et al.* 2002) and out-crossed to *OregonR* for 4 generations before being re-balanced; primer and sequence information available upon request).

All animals were raised on standard fly food supplemented with fresh yeast paste. For all wing disc ablation and IR experiments, eggs were first collected on grape juice agar plates and 55 freshly hatched L1 larvae were transferred per a vial of fly food to maximize developmental synchrony. Wing disc ablation was performed as previously described (SMITH-BOLTON *et al.* 2009). For all IR experiments, animals were raised at 25°C. Four days, or approximately 92 hours, after egg laying (AEL) uncapped vials with staged larvae were placed in cabinet X-ray and irradiated as described below.

X-ray irradiation

Animals were irradiated in a Faxitron TRX5200 cabinet X-ray machine at 125V and 3 mA for an approximate dose of 1.5 Gy/minute.

Hemocyte counts

Circulating hemocytes were collected in PBS by making a small tear in the larval posterior cuticle. For counts from individual larvae, each animal was bled into 10μL of PBS and the entire volume was transferred to a Neubauer Improved hemocytometer. 10 larvae at minimum were used per genotype or experimental condition. Data is reported as box and whiskers plots in which boxes mark 25th and 75th quartiles, whiskers show high and low values and open circles show the mean. For pooled counts, 10 larvae were bled into 100μL of PBS, 10μL of which was added to a Neubauer Improved hemocytometer. Obtained values were used to calculate the average value per an individual larva. At least 3 independent experiments per genotype or experimental condition were analyzed. Data are represented as the mean of 3 or more independent experiments, shown in bar graph form with error bars showing one standard deviation. Statistical analysis was performed using a Student's two-tailed t-test. Initial experiments compared the data obtained from individual versus pooled counts and found them to be similar (data not shown). Hemocytes were counted manually on a Zeiss Axio Imager M1. Lamellocytes were identified by morphology.

Immunohistochemistry and image processing

Imaginal discs were dissected in PBS and fixed for 20 minutes in 4% paraformaldehyde (PFA) at room temperature. Lymph glands were isolated from larval fillets treated similarly. Antibody stains were carried out following standard procedures. Hemocytes were collected from 10-20 experimental larvae, by bleeding from a small tear in the posterior cuticle into a 10-fold volume of PBS. Cells were then transferred to a coverslip and allowed to settle for 30 minutes at room temperature in a humidity chamber. All subsequent steps were performed directly on the coverslip. Cells were fixed in 4% PFA in PBS for 7 minutes at room temperature, washed 3 times in PBS, permeablized for 5 minutes in 1% triton in PBS (PBT), blocked for 5 minutes in 10% normal goat serum (NGS) in PBT and then incubated with primary antibody in 10% NGS in PBT either overnight at 4°C or for 30 minutes at room temperature. Washes were carried out in PBT and secondary incubation was performed for 30 minutes at room temperature in 10% NGS in PBT. Cells were then washed 2 times in PBT, followed by 2 washes in PBS. A final 5 minute incubation with DAPI or TO-PRO-3 (Invitrogen) in PBS or a 20 minute incubation with Phalloidin (1:200, Sigma) was performed where desired. Coverslips were mounted in Slowfade Gold Antifade (Molecular Probes). Primary antibodies used were mouse anti-GFP (1:500, Roche), mouse anti-βGal (1:500, Promega), anti-cleaved Caspase3 (1:100, Cell Signaling), plasmatocyte-specific anti-P1 (1:100) (KURUCZ *et al.* 2007), lamellocyte-specific anti-L1 (1:100) (HONTI *et al.* 2010) and pan-hemocyte anti-H2 (1:100) (KURUCZ *et al.* 2003) were kindly provided by Istvan Ando. Apoptotic cells were labeled using a TUNEL kit (Roche) according to manufacturer's specifications. All secondary antibodies were Alexa Fluor antibodies (1:500, Invitrogen). Images were collected on a Leica TCS SL or a Zeiss LSM 700 confocal or a Zeiss Axio Imager M1 and were processed using ImageJ and Adobe Photoshop.

G-TRACE experiments

Larvae were loosely staged by 4-6 hour egg collections directly in vials on standard fly food supplemented with yeast paste. Fours days AEL, animals were irradiated as described above. 48 hours post-IR, 10 wandering larvae were picked for analysis. For unirradiated samples, wandering larvae were collected 24 hours post-mock IR. Hemocytes were collected and labeled with anti-GFP and DAPI, as described above. For lamellocytes, at least 100 individual cells were scored per genotype. Reported results are from one of two independent experiments that yielded similar results. For non-lamellocyte hemocytes between 150-350 cells were analyzed per a genotype. Cells were scored as GFP- RFP- (black), GFP+ RFP- (green), GFP- RFP+ (red) and GFP+ RFP+ (yellow).

Figure 3.1: *Hemocytes participate in the clearance of apoptotic imaginal disc cells.*
(A) Confocal section through a neoplastic vps25 mutant eye-antennal disc. Dying cells are marked by cleaved caspase3 (aC3, white). Hemocytes are stained with H2 (magenta). Arrow head shows engulfed cell corpse. (B) Confocal section through a neoplastic P3C mutant eye-antennal disc stained for aC3 (white), F-actin (green) and L1 (magenta). Arrow head identifies associated lamellocyte. (C) Z-slice through an ablating wing imaginal disc. Cells expressing pro-apoptotic *eiger* are in green (GFP). Hemocytes are stained with H2 (magenta). Arrow heads show internalized cell debris. Apical is up. (D) Basal confocal section through a wild-type (*OregonR*) eye-antennal disc 24 hours post-IR. aC3 (white) marks dying cells. H2 (magenta) marks hemocytes. (E, E') Confocal section of circulating hemocytes from wing disc-ablated larva stained for F-actin (magenta) and GFP (green). For genotype information for wing disc ablated larvae see materials and methods.

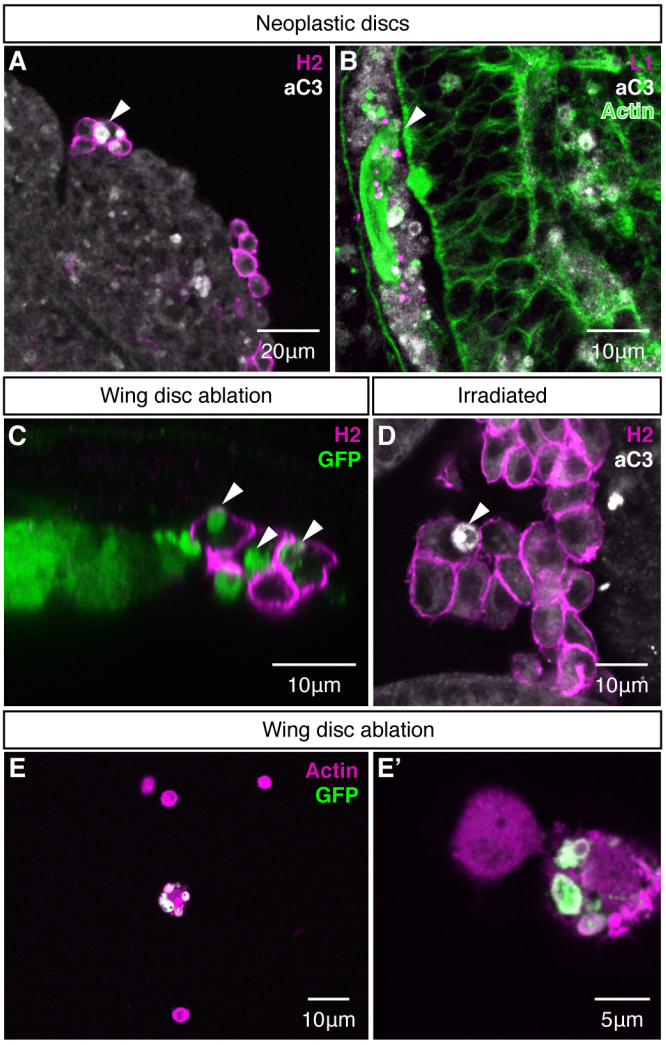
Neoplastic discs
A
H2
aC3
20µm
B
L1
aC3
Actin
10µm
Wing disc ablation
Irradiated
C
H2
GFP
10µm
D
H2
aC3
10µm
Wing disc ablation
E
Actin
GFP
10µm
E'
5µm

Figure 3.2: *IR causes broad changes in the circulating hemocyte population*.
(A-C) Circulating hemocytes from control (A, A') and irradiated larvae at 24 (B, B') and 48 (C, C') hours post-IR stained for P1 (magenta) and To-Pro (white). White box marks enlarged area. Arrow head shows altered P1 localization. (D-F) F-actin (white) stain of circulating hemocytes from control (D) and irradiated larvae at 24 (E) and 48 (F) hours post-IR. Arrow heads show markedly actin-rich cells. Genotype for all panels is *OregonR*.

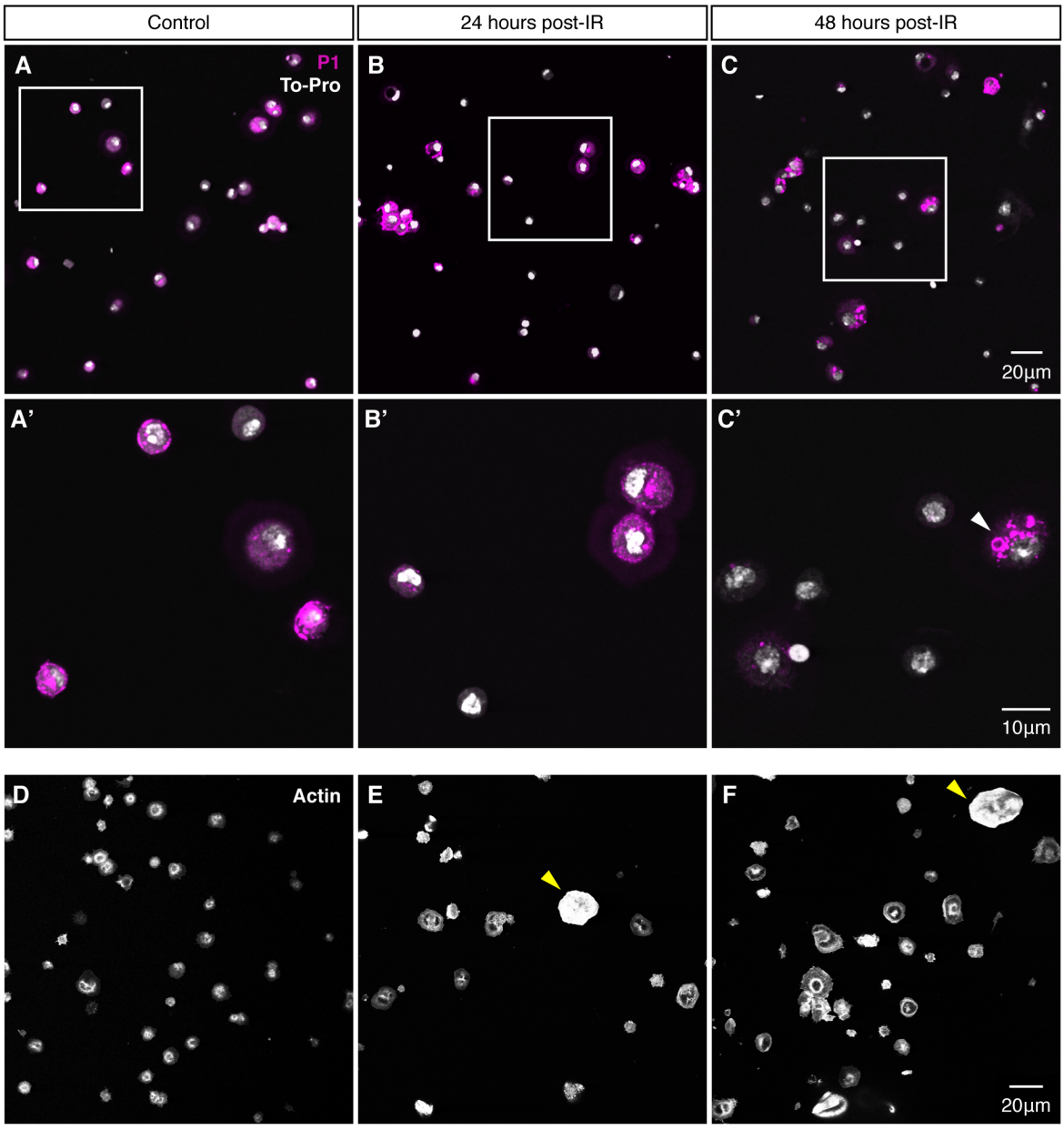
Control
24 hours post-IR
48 hours post-IR
A
P1
To-Pro
B
C
20µm
A'
B'
C'
10µm
D
Actin
E
F
20µm

Figure 3.3: *IR and wing disc ablation induce lamellocyte differentiation and melanotic mass formation.*
(A, A') Quantification of circulating lamellocyte (A) and total hemocyte (A') numbers in control versus irradiated *OregonR* larvae. At 48 hours post-IR control animals have pupariated and are not available for analysis. (B) Quantification of circulating lamellocytes in larvae undergoing wing disc ablation. Experimental animals were obtained by crossing *w; rn-GAL4, UAS-eiger, tub-GAL80^{ts}/TM6b* to *OregonR*. *+/TM6B* larvae were used as the control. Control animals had all pupariated by the 24 hour time point. Ablating animals delay pupariation by ~48 hours. (C, C') DIC (C) and confocal (C') images of a melanotic mass from an irradiated *OregonR* larva 48 hours post-IR. L1 marks lamellocytes (magenta) and To-Pro marks nuclei (white). (D, D') DIC (D) and epifluorescence (D') images of a melanotic mass from wing disc ablated larvae 72 hours post-ablation stained for L1 (magenta) and DAPI (white). (E, E') Lamellocyte (E) and total hemocyte (E') counts for larvae subjected to increasing IR doses. N/A indicates no larvae available for analysis due to pupariation.

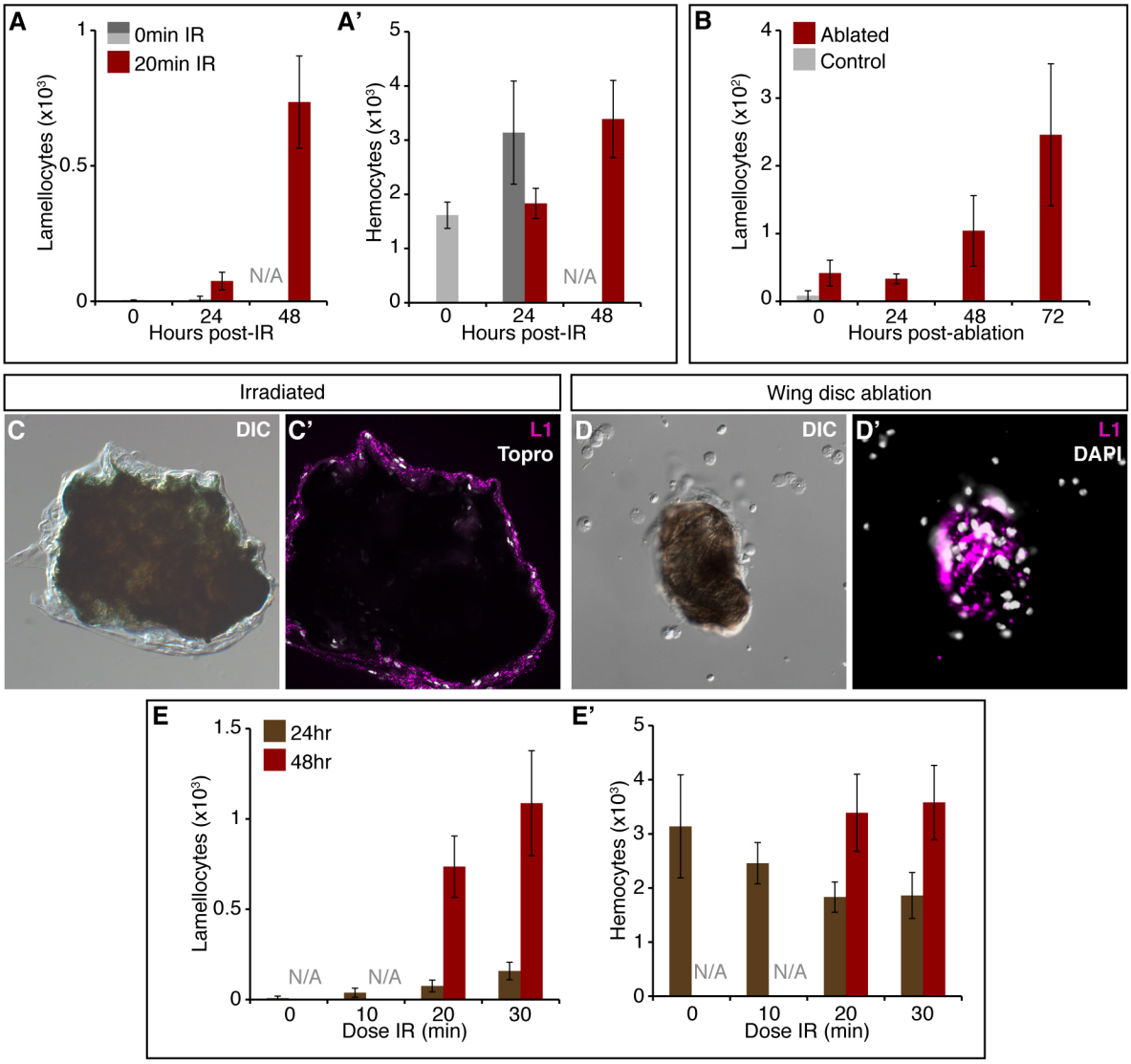
A
0min IR
20min IR
Lamellocytes (x10³)
Hours post-IR
N/A
A'
Hemocytes (x10³)
Hours post-IR
N/A
B
Ablated
Control
Lamellocytes (x10²)
Hours post-ablation
Irradiated
Wing disc ablation
C
DIC
C'
L1
Topro
D
DIC
D'
L1
DAPI
E
24hr
48hr
Lamellocytes (x10³)
Dose IR (min)
N/A
N/A
E'
Hemocytes (x10³)
Dose IR (min)
N/A
N/A

Figure 3.4: *Hemocyte apoptosis is sufficient but not necessary for lamellocyte induction.* (A-C) Circulating hemocytes from control (A) and irradiated larvae at 24 (B) and 48 (C) hours post-IR stained for TUNEL (red) and DAPI (blue). Progeny from the genetic cross *HmlΔ-GAL4, UAS-2xEGFP* X *w; UAS-GFP.nls* were analyzed. GFP is omitted for clarity. Values shown in lower right corner are the % TUNEL-positive cells (n>350 cells). (D) Total circulating hemocyte and lamellocyte counts at 48 hours post-IR for control (GFP) versus larvae in which cell death was inhibited using mir^{RHG}. (E-G) Etherized whole larvae from the crosses *HmlΔ-GAL4, UAS-2xEGFP* X *UAS-Act5C.mRFP* (E) or *HmlΔ-GAL4, UAS-2xEGFP* X *UAS-*hid^{ala5} (F) showing the relative reduction in the hemocyte population in *UAS-*hid^{ala5}-expressing animals. Images were captured with the same gain. (G) Circulating hemocytes from *UAS-*hid^{ala5}-expressing larvae. Lamellocytes are marked by L1 (red), *HmlΔ-GAL4*-expressing cells are marked by GFP (green) and nuclei are marked by DAPI (blue). Arrow heads identify GFP-negative lamellocytes. (G') DIC image of cells in (G).

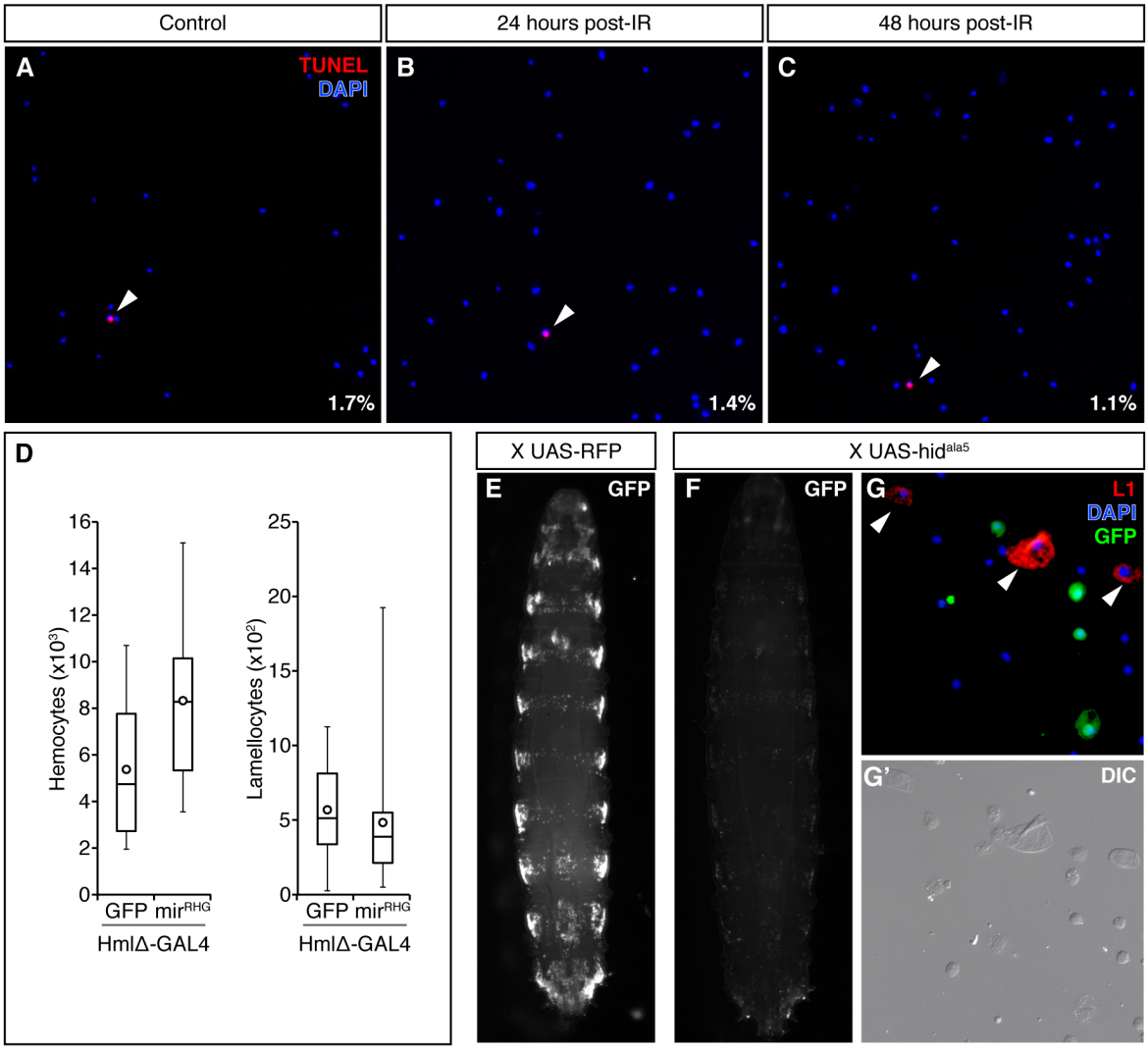
Control
24 hours post-IR
48 hours post-IR
A
TUNEL
DAPI
1.7%
B
1.4%
C
1.1%
D
Hemocytes (x10³)
Lamellocytes (x10²)
GFP mirRHG
HmlΔ-GAL4
X UAS-RFP
X UAS-hidala5
E
GFP
F
GFP
G
L1
DAPI
GFP
G'
DIC

Figure 3.5: *Lineage tracing reveals complex origins for IR-induced lamellocytes*.
Lineage tracing using G-TRACE. Cells that have never expressed the GAL4 driver (GFP-, RFP-) are in black, cells actively expressing the GAL4 driver (GFP+, RFP+) are in yellow, cells that have just turned the GAL4 driver on (GFP-, RFP+) are in red, and cells that expressed the GAL4 driver but have since turned it off (GFP+, RFP-) are in green. (A) Quantification of G-TRACE data for lamellocytes at 48 hours post-IR with the given GAL4 drivers. (B) Quantification of G-TRACE data for all other circulating hemocytes in unirradiated animals and at 48 hours post-IR for the given GAL4 drivers. (C-E) Arrow heads indicate lamellocytes expressing *HmlΔ-GAL4* (C), *eater-GAL4* (D) or derived from a *crq-GAL4*-expressing cell (E). (F) Examples of L1-postive (red), *eater-GAL4*-expressing (green) lamellocytes 24 hours post-IR. (G) Example of the incomplete overlap between L1 (red) and *msn-GAL4* (green) in the lamellocyte population. (H-I) G-TRACE expression pattern for *dome-GAL4* in the lymph gland (H) and in the circulating hemocyte population (I) for unirradiated animals. (J-K) G-TRACE expression pattern for *Dot-GAL4* in the lymph gland (H), arrow head identifies the PSC, and in the circulating hemocyte population (I) for unirradiated animals.

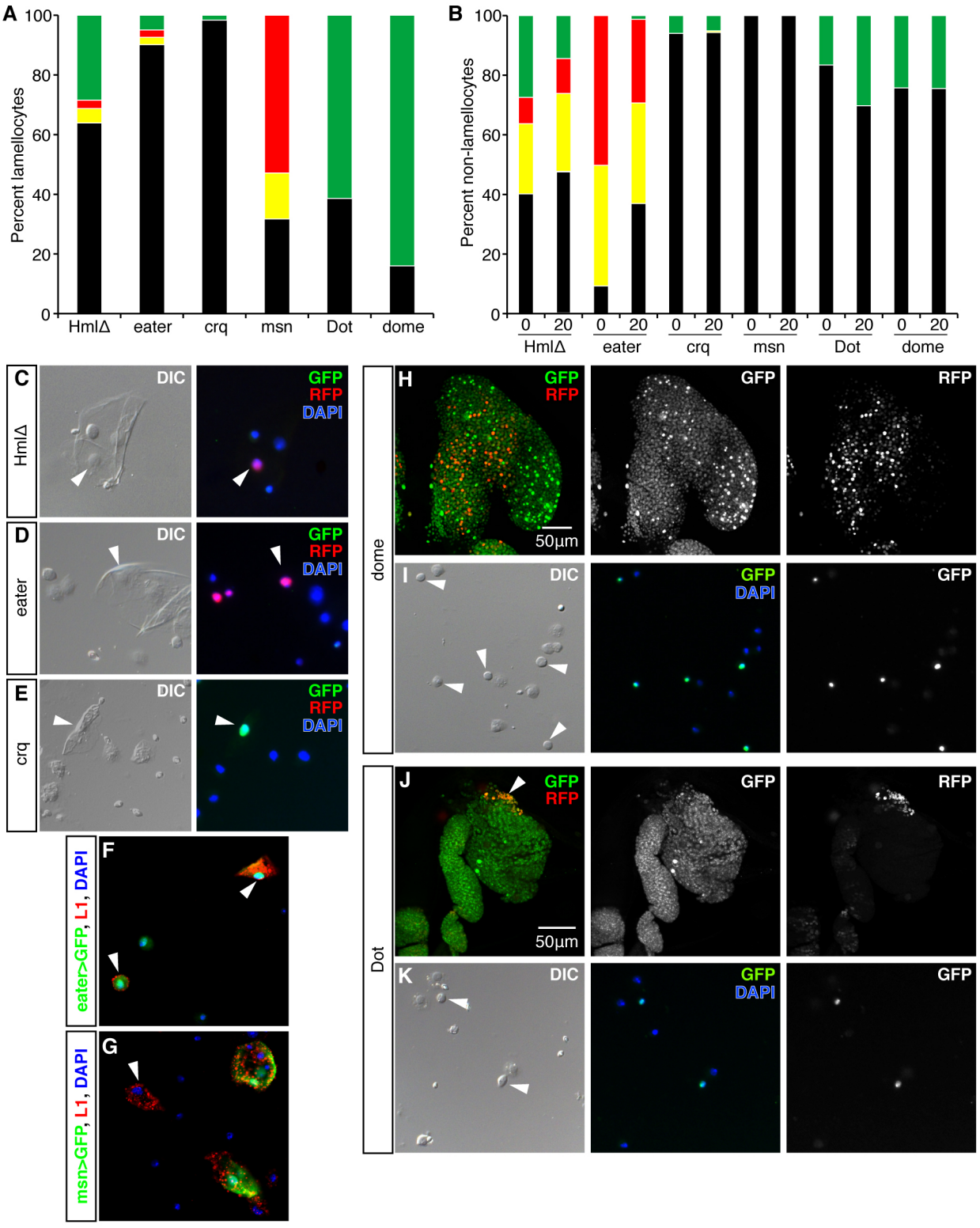
A
Percent lamellocytes
100
80
60
40
20
0
HmlΔ
eater
crq
msn
Dot
dome
B
Percent non-lamellocytes
0 20 0 20 0 20 0 20 0 20 0 20
HmlΔ
eater
crq
msn
Dot
dome
C
HmlΔ
D
eater
E
crq
DIC
GFP
RFP
DAPI
F
eater>GFP, L1, DAPI
G
msn>GFP, L1, DAPI
H
dome
I
J
Dot
K
50µm
GFP

Figure 3.6: *IR leads to an increase in puc-lacZ expression in circulating hemocytes.* (A-C) Confocal images of circulating hemocytes showing *puc-lacZ* expression (red) and nuclei (DAPI) from unirradiated (A) and irradiated larvae 24 hours post-IR (B) and 48 hours post-IR (C). Values shown in lower right corner are the % *puc-lacZ*-positive cells (n>500 cells). (D-E) *puc-lacZ* (red) expression in circulating plasmatocytes marked by *eater-GAL4, UAS-2xEYFP* (D) and P1 (E). (F-G) *puc-lacZ* (red) expression in circulating lamellocytes marked by *msn-GAL4, UAS-2xEYFP* (D) and L1 (E).

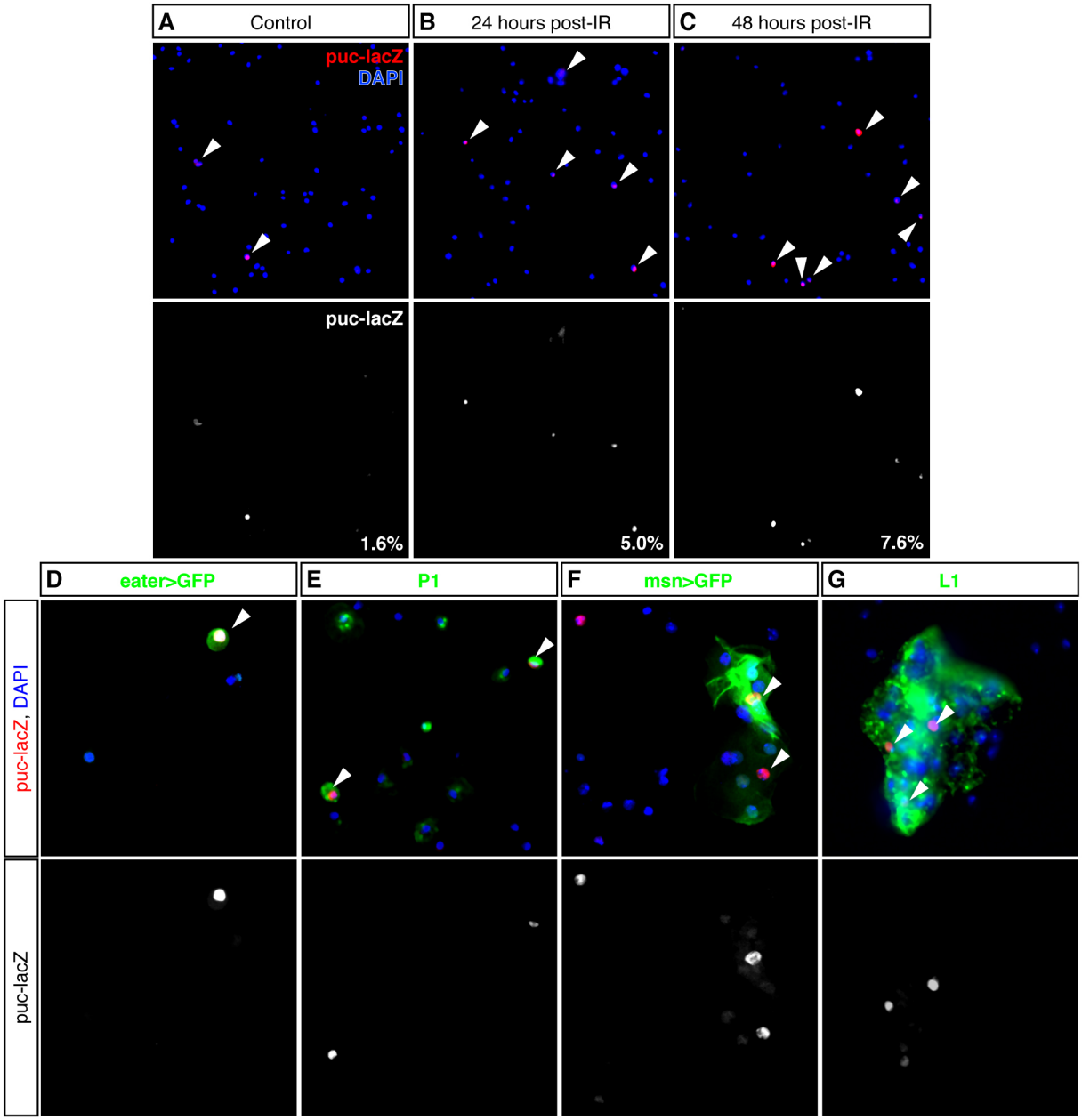
A Control
B 24 hours post-IR
C 48 hours post-IR
puc-lacZ
DAPI
puc-lacZ
1.6%
5.0%
7.6%
D eater>GFP
E P1
F msn>GFP
G L1
puc-lacZ, DAPI
puc-lacZ

Figure 3.7: *puc-lacZ expression is unchanged in hemocytes from larvae undergoing wing disc ablation.*
(A-A’’’) Confocal section through an ablating wing disc showing *eiger*-expressing cells (A’, green), *puc-lacZ* expression (A”, magenta) and associated hemocytes marked by H2 (A’’’, cyan). Merged image in (A). (B-C’’’) Epifluorescence image of circulating hemocytes from larvae undergoing wing disc ablation showing an engulfed *puc-lacZ*-, GFP-positive cell. (B) DIC image of cells in (C). (C) Merged fluorescent image showing puc-lacZ (magenta), GFP (green) and nuclei (cyan). Individual channels are shown in (C’-C’’’).

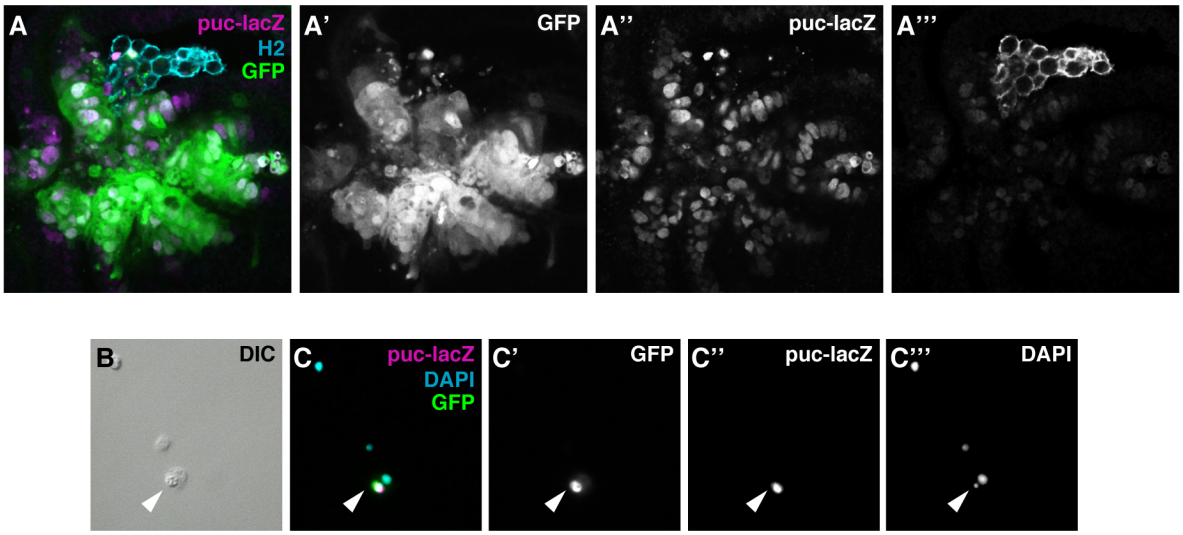
A
puc-lacZ
H2
GFP
A'
GFP
A''
puc-lacZ
A'''
B
DIC
C
puc-lacZ
DAPI
GFP
C'
GFP
C''
puc-lacZ
C'''
DAPI

Figure 3.8: *JNK pathway may be required in a subset of hemocytes for lamellocyte induction following IR.*
(A) Dominant modification of lamellocyte production by mutations in JNK pathway components. Lamellocyte counts 48 hours post-IR for control versus larvae carrying mutations in *bsk* and *msn*. Mutant alleles were crossed to *OregonR* to generate experimental animals. The progeny of the genetic cross *OregonR* X w^{1118} were used as the control (OR) (B) Quantification of circulating hemocytes and lamellocytes 48 hours post-IR in larvae using *HmlΔ-GAL4* to express a dominant-negative allele of *bsk* (Bsk^{DN}) or an RNAi to *bsk* (Bsk^{IR}) as compared to control (GFP). (C) Quantification of circulating lamellocytes 48 hours post-IR using *He-GAL4* to express Bsk^{DN} as compared to control (GFP). (D) Quantification of the delay of pupariation following IR when *HmlΔ-GAL4* was used to express a Bsk^{DN}, Bsk^{IR} or an RNAi to *hemipterous* (Hep^{IR}) as compared to control (GFP).

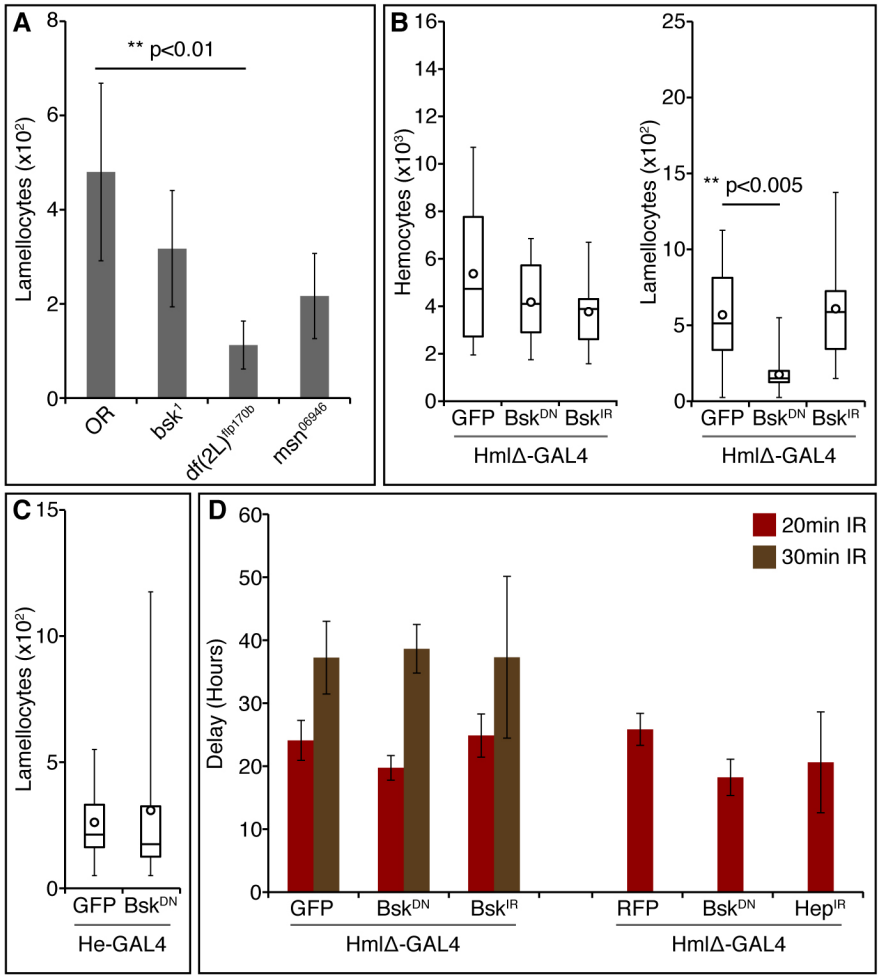
A
** p<0.01
Lamellocytes (x10²)
OR
bsk¹
df(2L)Hp170b
msn06946
B
Hemocytes (x10³)
GFP BskDN BskIR
HmlΔ-GAL4
** p<0.005
Lamellocytes (x10²)
GFP BskDN BskIR
HmlΔ-GAL4
C
Lamellocytes (x10²)
GFP BskDN
He-GAL4
D
20min IR
30min IR
Delay (Hours)
GFP BskDN BskIR
HmlΔ-GAL4
RFP BskDN HepIR
HmlΔ-GAL4

Figure 3.9: *The phagocytosis receptors NimC1 and draper are required for IR-induced lamellocyte differentiation.*
(A) Quantification of circulating lamellocytes 48 hours post-IR in larvae mutant for *NimC1* compared to control. (B) Quantification of circulating lamellocytes 48 hours post-IR in larvae mutant for *draper* compared to control. Alleles of *NimC1* and *draper* were out-crossed to *OregonR* for 4 generations before being re-isolated. Wild-type siblings from the final out-cross were used to generate the control genotypes.

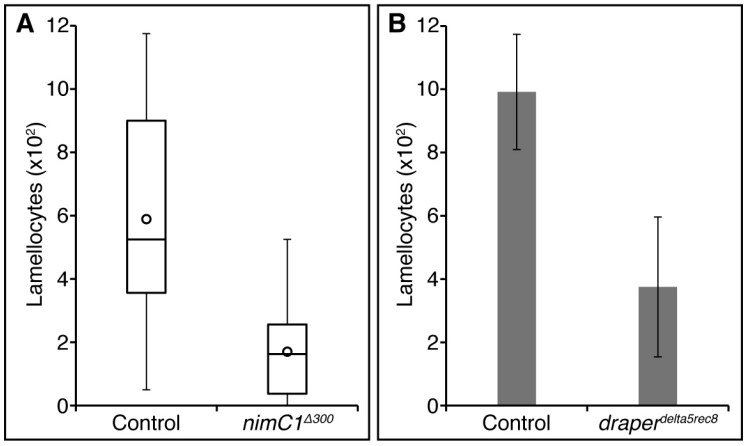
A
B
Lamellocytes (x10²)
0
2
4
6
8
10
12
Control
nimC1Δ300
draperdelta5rec8

Table 3.1: *Summary of IR-induced lamellocyte lineage tracing*

GAL4 driver	Reported expression	% of IR-induced lamellocytes		
		Active (GFP+/-, RFP+)	Previous (GFP+, RFP-)	None (GFP-, RFP-)
HmlΔ	Plasmatocytes, crystal cells and intermediate progentirors	8	28	64
He	80% of all non-lymph gland hemocytes	70	1	29
eater	Mature plasmatocytes	5	5	90
crq	Embryonic macrophages	0	2	98
Dot	Embryonic lymph gland; PSC	0	61	39
dome	Prohemocytes in larval lymph gland	0	84	16
msn	Lamellocytes	68	0	32

References:

ABBOTT, L. C., G. H. KARPEN and G. SCHUBIGER, 1981 Compartmental restrictions and blastema formation during pattern regulation in Drosophila imaginal leg discs. Developmental Biology **87:** 64-75.

ADDISON, W. R., W. J. BROOK, L. D. QUERENGESSER, S. Y. TIONG and M. A. RUSSELL, 1995 Analysis of an enhancer trap expressed in regenerating Drosophila imaginal discs. Genome **38:** 724-736.

ADLER, P. N., and M. MACQUEEN, 1984 Cell proliferation and DNA replication in the imaginal wing disc of Drosophila melanogaster. Developmental Biology **103:** 28-37.

AGAISSE, H., U. M. PETERSEN, M. BOUTROS, B. MATHEY-PREVOT and N. PERRIMON, 2003 Signaling role of hemocytes in Drosophila JAK/STAT-dependent response to septic injury. Developmental Cell **5:** 441-450.

ALFONSO, T. B., and B. W. JONES, 2002 gcm2 promotes glial cell differentiation and is required with glial cells missing for macrophage development in Drosophila. Developmental Biology **248:** 369-383.

ARBOUZOVA, N. I., and M. P. ZEIDLER, 2006 JAK/STAT signalling in Drosophila: insights into conserved regulatory and cellular functions. Development **133:** 2605-2616.

ASHA, H., I. NAGY, G. KOVACS, D. STETSON, I. ANDO *et al.*, 2003 Analysis of Ras-induced overproliferation in Drosophila hemocytes. Genetics **163:** 203-215.

AVET-ROCHEX, A., K. BOYER, C. POLESELLO, V. GOBERT, D. OSMAN *et al.*, 2010 An in vivo RNA interference screen identifies gene networks controlling Drosophila melanogaster blood cell homeostasis. BMC Developmental Biology **10:** 65.

BABCOCK, D. T., A. R. BROCK, G. S. FISH, Y. WANG, L. PERRIN *et al.*, 2008 Circulating blood cells function as a surveillance system for damaged tissue in Drosophila larvae. Proceedings of the National Academy of Sciences of the United States of America **105:** 10017-10022.

BACH, E. A., L. A. EKAS, A. AYALA-CAMARGO, M. S. FLAHERTY, H. LEE *et al.*, 2007 GFP reporters detect the activation of the Drosophila JAK/STAT pathway in vivo. Gene Expression Patterns **7:** 323-331.

BADENHORST, P., M. VOAS, I. REBAY and C. WU, 2002 Biological functions of the ISWI chromatin remodeling complex NURF. Genes & Development **16:** 3186-3198.

BARD, F., L. CASANO, A. MALLABIABARRENA, E. WALLACE, K. SAITO *et al.*, 2006 Functional genomics reveals genes involved in protein secretion and Golgi organization. Nature **439:** 604-607.

BATAILLÉ, L., B. AUGÉ, G. FERJOUX, M. HAENLIN and L. WALTZER, 2005 Resolving embryonic blood cell fate choice in Drosophila: interplay of GCM and RUNX factors. Development **132:** 4635-4644.

BECKER, D. J., and J. B. LOWE, 2003 Fucose: biosynthesis and biological function in mammals. Glycobiology **13:** 41R-53R.

BELY, A. E., and K. G. NYBERG, 2010 Evolution of animal regeneration: re-emergence of a field. Trends in Ecology & Evolution **25:** 161-170.

BERGANTIÑOS, C., M. COROMINAS and F. SERRAS, 2010 Cell death-induced regeneration in wing imaginal discs requires JNK signalling. Development **137:** 1169-1179.

BERGMANN, A., and H. STELLER, 2010 Apoptosis, stem cells, and tissue regeneration. Science Signaling **3:** re8.

BERNARDONI, R., V. VIVANCOS and A. GIANGRANDE, 1997 glide/gcm is expressed and required in the scavenger cell lineage. Developmental Biology **191:** 118-130.
BITEAU, B., C. E. HOCHMUTH and H. JASPER, 2008 JNK activity in somatic stem cells causes loss of tissue homeostasis in the aging Drosophila gut. Cell Stem Cell **3:** 442-455.
BLAIR, S. S., 1992 Engrailed expression in the anterior lineage compartment of the developing wing blade of Drosophila. Development **115:** 21-33.
BLANCO, E., M. RUIZ-ROMERO, S. BELTRAN, M. BOSCH, A. PUNSET *et al.*, 2010 Gene expression following induction of regeneration in Drosophila wing imaginal discs. Expression profile of regenerating wing discs. BMC Developmental Biology **10:** 94.
BLUMENSTIEL, J. P., A. C. NOLL, J. A. GRIFFITHS, A. G. PERERA, K. N. WALTON *et al.*, 2009 Identification of EMS-induced mutations in Drosophila melanogaster by whole-genome sequencing. Genetics **182:** 25-32.
BOSCH, M., J. BAGUÑÀ and F. SERRAS, 2008 Origin and proliferation of blastema cells during regeneration of Drosophila wing imaginal discs. The International Journal of Developmental Biology **52:** 1043-1050.
BOSCH, M., F. SERRAS, E. MARTÍN-BLANCO and J. BAGUÑÀ, 2005 JNK signaling pathway required for wound healing in regenerating Drosophila wing imaginal discs. Developmental Biology **280:** 73-86.
BRAUN, A., B. LEMAITRE, R. LANOT, D. ZACHARY and M. MEISTER, 1997 Drosophila immunity: analysis of larval hemocytes by P-element-mediated enhancer trap. Genetics **147:** 623-634.
BRENNAN, C. A., J. R. DELANEY, D. S. SCHNEIDER and K. V. ANDERSON, 2007 Psidin is required in Drosophila blood cells for both phagocytic degradation and immune activation of the fat body. Current Biology **17:** 67-72.
BROCKES, J. P., and A. KUMAR, 2008 Comparative aspects of animal regeneration. Annual Review of Cell and Developmental Biology **24:** 525-549.
BROOK, W. J., L. M. OSTAFICHUK, J. PIORECKY, M. D. WILKINSON, D. J. HODGETTS *et al.*, 1993 Gene expression during imaginal disc regeneration detected using enhancer-sensitive P-elements. Development **117:** 1287-1297.
BROWN, S., N. HU and J. C. HOMBRÍA, 2001 Identification of the first invertebrate interleukin JAK/STAT receptor, the Drosophila gene domeless. Current Biology **11:** 1700-1705.
BRÜCKNER, K., L. KOCKEL, P. DUCHEK, C. M. LUQUE, P. RØRTH *et al.*, 2004 The PDGF/VEGF receptor controls blood cell survival in Drosophila. Developmental Cell **7:** 73-84.
BRYANT, P. J., 1971 Regeneration and duplication following operations in situ on the imaginal discs of Drosophila melanogaster. Developmental Biology **26:** 637-651.
BRYANT, P. J., 1975 Pattern formation in the imaginal wing disc of Drosophila melanogaster: fate map, regeneration and duplication. Journal of Experimental Zoology **193:** 49-77.
BRYANT, P. J., and P. SIMPSON, 1984 Intrinsic and extrinsic control of growth in developing organs. The Quarterly Review of Biology **59:** 387-415.
CHERA, S., L. GHILA, K. DOBRETZ, Y. WENGER, C. BAUER *et al.*, 2009 Apoptotic cells provide an unexpected source of Wnt3 signaling to drive hydra head regeneration. Developmental Cell **17:** 279-289.
CHO, N. K., L. KEYES, E. JOHNSON, J. HELLER, L. RYNER *et al.*, 2002 Developmental control of blood cell migration by the Drosophila VEGF pathway. Cell **108:** 865-876.

CHOW, A., B. D. BROWN and M. MERAD, 2011 Studying the mononuclear phagocyte system in the molecular age. Nature Reviews Immunology **11:** 788-798.
CICILIOT, S., and S. SCHIAFFINO, 2010 Regeneration of mammalian skeletal muscle. Basic mechanisms and clinical implications. Current Pharmaceutical Design **16:** 906-914.
CLASSEN, A.-K., B. D. BUNKER, K. F. HARVEY, T. VACCARI and D. BILDER, 2009 A tumor suppressor activity of Drosophila Polycomb genes mediated by JAK-STAT signaling. Nature Genetics **41:** 1150-1155.
CONLON, I., and M. RAFF, 1999 Size control in animal development. Cell **96:** 235-244.
CORDERO, J. B., J. P. MACAGNO, R. K. STEFANATOS, K. E. STRATHDEE, R. L. CAGAN *et al.*, 2010 Oncogenic Ras diverts a host TNF tumor suppressor activity into tumor promoter. Developmental Cell **18:** 999-1011.
CROZATIER, M., and M. MEISTER, 2007 Drosophila haematopoiesis. Cell Microbiology **9:** 1117-1126.
CROZATIER, M., J.-M. UBEDA, A. VINCENT and M. MEISTER, 2004 Cellular immune response to parasitization in Drosophila requires the EBF orthologue collier. PLoS Biology **2:** E196.
DAMELIN, M., and T. H. BESTOR, 2007 The decatenation checkpoint. British Journal of Cancer **96:** 201-205.
DIANGELO, J. R., M. L. BLAND, S. BAMBINA, S. CHERRY and M. J. BIRNBAUM, 2009 The immune response attenuates growth and nutrient storage in Drosophila by reducing insulin signaling. Proceedings of the National Academy of Sciences of the United States of America.
DIJKERS, P. F., and P. H. O'FARRELL, 2007 Drosophila calcineurin promotes induction of innate immune responses. Current Biology **17:** 2087-2093.
DIONNE, M. S., and D. S. SCHNEIDER, 2008 Models of infectious diseases in the fruit fly Drosophila melanogaster. Disease Models and Mechanisms **1:** 43-49.
DOBENS, L. L., T. HSU, V. TWOMBLY, W. M. GELBART, L. A. RAFTERY *et al.*, 1997 The Drosophila bunched gene is a homologue of the growth factor stimulated mammalian TSC-22 sequence and is required during oogenesis. Mechanisms of Development **65:** 197-208.
DOVEY, M., E. E. PATTON, T. BOWMAN, T. NORTH, W. GOESSLING *et al.*, 2009 Topoisomerase II alpha is required for embryonic development and liver regeneration in zebrafish. Molecular and Cellular Biology **29:** 3746-3753.
DURONIO, R. J., and P. H. O'FARRELL, 1994 Developmental control of a G1-S transcriptional program in Drosophila. Development **120:** 1503-1515.
DUVIC, B., J. A. HOFFMANN, M. MEISTER and J. ROYET, 2002 Notch signaling controls lineage specification during Drosophila larval hematopoiesis. Current Biology **12:** 1923-1927.
EKENGREN, S., Y. TRYSELIUS, M. S. DUSHAY, G. LIU, H. STEINER *et al.*, 2001 A humoral stress response in Drosophila. Current Biology **11:** 714-718.
ELLEDGE, S. J., Z. ZHOU and J. B. ALLEN, 1992 Ribonucleotide reductase: regulation, regulation, regulation. Trends in Biochemical Sciences **17:** 119-123.
EMING, S. A., M. HAMMERSCHMIDT, T. KRIEG and A. ROERS, 2009 Interrelation of immunity and tissue repair or regeneration. Seminars in Cell & Developmental Biology **20:** 517-527.

EVANS, C. J., V. HARTENSTEIN and U. BANERJEE, 2003 Thicker than blood: conserved mechanisms in Drosophila and vertebrate hematopoiesis. Developmental Cell **5:** 673-690.

EVANS, C. J., J. M. OLSON, K. T. NGO, E. KIM, N. E. LEE *et al.*, 2009 G-TRACE: rapid Gal4-based cell lineage analysis in Drosophila. Nature Methods **6:** 603-605.

FAIN, M. J., and B. STEVENS, 1982 Alterations in the cell cycle of Drosophila imaginal disc cells precede metamorphosis. Developmental Biology **92:** 247-258.

FAN, Y., and A. BERGMANN, 2008 Distinct mechanisms of apoptosis-induced compensatory proliferation in proliferating and differentiating tissues in the Drosophila eye. Developmental Cell **14:** 399-410.

FAUSTO, N., J. S. CAMPBELL and K. J. RIEHLE, 2006 Liver regeneration. Hepatology **43:** S45-53.

FAUVARQUE, M.-O., and M. J. WILLIAMS, 2011 Drosophila cellular immunity: a story of migration and adhesion. Journal of Cell Science **124:** 1373-1382.

FOSSETT, N., S. G. TEVOSIAN, K. GAJEWSKI, Q. ZHANG, S. H. ORKIN *et al.*, 2001 The Friend of GATA proteins U-shaped, FOG-1, and FOG-2 function as negative regulators of blood, heart, and eye development in Drosophila. Proceedings of the National Academy of Sciences of the United States of America **98:** 7342-7347.

FRANC, N. C., 2002 Phagocytosis of apoptotic cells in mammals, caenorhabditis elegans and Drosophila melanogaster: molecular mechanisms and physiological consequences. Frontiers in Bioscience **7:** d1298-1313.

FRANC, N. C., J. L. DIMARCQ, M. LAGUEUX, J. HOFFMANN and R. A. EZEKOWITZ, 1996 Croquemort, a novel Drosophila hemocyte/macrophage receptor that recognizes apoptotic cells. Immunity **4:** 431-443.

FRANGOGIANNIS, N. G., 2008 The immune system and cardiac repair. Pharmacological Research **58:** 88-111.

FREEMAN, M. R., J. DELROW, J. KIM, E. JOHNSON and C. Q. DOE, 2003 Unwrapping glial biology: Gcm target genes regulating glial development, diversification, and function. Neuron **38:** 567-580.

FRENCH, V., P. J. BRYANT and S. V. BRYANT, 1976 Pattern regulation in epimorphic fields. Science **193:** 969-981.

FUKAZAWA, T., Y. NAORA, T. KUNIEDA and T. KUBO, 2009 Suppression of the immune response potentiates tadpole tail regeneration during the refractory period. Development **136:** 2323-2327.

GAO, H., X. WU and N. FOSSETT, 2009 Upregulation of the Drosophila Friend of GATA gene U-shaped by JAK/STAT signaling maintains lymph gland prohemocyte potency. Molecular and Cellular Biology **29:** 6086-6096.

GEISSMANN, F., M. G. MANZ, S. JUNG, M. H. SIEWEKE, M. MERAD *et al.*, 2010 Development of monocytes, macrophages, and dendritic cells. Science **327:** 656-661.

GIBSON, M. C., and G. SCHUBIGER, 1999 Hedgehog is required for activation of engrailed during regeneration of fragmented Drosophila imaginal discs. Development **126:** 1591-1599.

GLISE, B., H. BOURBON and S. NOSELLI, 1995 hemipterous encodes a novel Drosophila MAP kinase kinase, required for epithelial cell sheet movement. Cell **83:** 451-461.

GLISE, B., and S. NOSELLI, 1997 Coupling of Jun amino-terminal kinase and Decapentaplegic signaling pathways in Drosophila morphogenesis. Genes & Development **11:** 1738-1747.

GLUDERER, S., E. BRUNNER, M. GERMANN, V. JOVAISAITE, C. LI *et al.*, 2010 Madm (Mlf1 adapter molecule) cooperates with Bunched A to promote growth in Drosophila. The Journal of Biology **9:** 9.

GLUDERER, S., S. OLDHAM, F. RINTELEN, A. SULZER, C. SCHÜTT *et al.*, 2008 Bunched, the Drosophila homolog of the mammalian tumor suppressor TSC-22, promotes cellular growth. BMC Developmental Biology **8:** 10.

GOTO, A., T. KADOWAKI and Y. KITAGAWA, 2003 Drosophila hemolectin gene is expressed in embryonic and larval hemocytes and its knock down causes bleeding defects. Developmental Biology **264:** 582-591.

GRIGORIAN, M., L. MANDAL and V. HARTENSTEIN, 2011 Hematopoiesis at the onset of metamorphosis: terminal differentiation and dissociation of the Drosophila lymph gland. Development Genes and Evolution **221:** 121-131.

GRUSCHE, F. A., J. L. DEGOUTIN, H. E. RICHARDSON and K. F. HARVEY, 2011 The Salvador/Warts/Hippo pathway controls regenerative tissue growth in Drosophila melanogaster. Developmental Biology **350:** 255-266.

HADORN, E., and D. BUCK, 1962 Ober Entwicklungsleistungen transplantierter Teilstucke von Flugel-Imaginalscheiben von Drosophila melanogaster. Revue Suisse de Zoologie **69:** 302–310.

HALDER, G., and R. L. JOHNSON, 2011 Hippo signaling: growth control and beyond. Development **138:** 9-22.

HALME, A., M. CHENG and I. K. HARIHARAN, 2010 Retinoids regulate a developmental checkpoint for tissue regeneration in Drosophila. Current Biology **20:** 458-463.

HARRISON, D. A., R. BINARI, T. S. NAHREINI, M. GILMAN and N. PERRIMON, 1995 Activation of a Drosophila Janus kinase (JAK) causes hematopoietic neoplasia and developmental defects. The EMBO Journal **14:** 2857-2865.

HAYNIE, J. L., and P. J. BRYANT, 1977 The Effects of X-rays on the Proliferation Dynamics of Cells in the Imaginal Wing Disc of Drosophila melanogaster. Roux's Archives of Developmental Biology **183:** 85-100.

HOLZ, A., B. BOSSINGER, T. STRASSER, W. JANNING and R. KLAPPER, 2003 The two origins of hemocytes in Drosophila. Development **130:** 4955-4962.

HOMBRÍA, J. C.-G., S. BROWN, S. HÄDER and M. P. ZEIDLER, 2005 Characterisation of Upd2, a Drosophila JAK/STAT pathway ligand. Developmental Biology **288:** 420-433.

HONTI, V., G. CSORDÁS, R. MÁRKUS, E. KURUCZ, F. JANKOVICS *et al.*, 2010 Cell lineage tracing reveals the plasticity of the hemocyte lineages and of the hematopoietic compartments in Drosophila melanogaster. Molecular Immunology **47:** 1997-2004.

HOWELL, L., C. J. SAMPSON, M. J. XAVIER, E. BOLUKBASI, M. M. S. HECK *et al.*, 2011 A directed miniscreen for genes involved in the Drosophila anti-parasitoid immune response. Immunogenetics.

HUANG, J., S. WU, J. BARRERA, K. MATTHEWS and D. PAN, 2005 The Hippo signaling pathway coordinately regulates cell proliferation and apoptosis by inactivating Yorkie, the Drosophila Homolog of YAP. Cell **122:** 421-434.

HUH, J. R., M. GUO and B. A. HAY, 2004 Compensatory proliferation induced by cell death in the Drosophila wing disc requires activity of the apical cell death caspase Dronc in a nonapoptotic role. Current Biology **14:** 1262-1266.

HULTMARK, D., and K. BORGE-RENBERG, 2007 Drosophila immunity: is antigen processing the first step? Current Biology **17:** R22-24.

IGAKI, T., H. KANDA, Y. YAMAMOTO-GOTO, H. KANUKA, E. KURANAGA *et al.*, 2002 Eiger, a TNF superfamily ligand that triggers the Drosophila JNK pathway. The EMBO Journal **21:** 3009-3018.

IRVING, P., J.-M. UBEDA, D. DOUCET, L. TROXLER, M. LAGUEUX *et al.*, 2005 New insights into Drosophila larval haemocyte functions through genome-wide analysis. Cell Microbiology **7:** 335-350.

JAKLEVIC, B. R., and T. T. SU, 2004 Relative contribution of DNA repair, cell cycle checkpoints, and cell death to survival after DNA damage in Drosophila larvae. Current Biology **14:** 23-32.

JIANG, H., P. H. PATEL, A. KOHLMAIER, M. O. GRENLEY, D. G. MCEWEN *et al.*, 2009 Cytokine/Jak/Stat signaling mediates regeneration and homeostasis in the Drosophila midgut. Cell **137:** 1343-1355.

JOHNSTON, L. A., and G. SCHUBIGER, 1996 Ectopic expression of wingless in imaginal discs interferes with decapentaplegic expression and alters cell determination. Development **122:** 3519-3529.

JUNG, S.-H., C. J. EVANS, C. UEMURA and U. BANERJEE, 2005 The Drosophila lymph gland as a developmental model of hematopoiesis. Development **132:** 2521-2533.

KANDA, H., and M. MIURA, 2004 Regulatory roles of JNK in programmed cell death. The Journal of Biochemistry **136:** 1-6.

KARPAC, J., J. HULL-THOMPSON, M. FALLEUR and H. JASPER, 2009 JNK signaling in insulin-producing cells is required for adaptive responses to stress in Drosophila. Aging Cell **8:** 288-295.

KARPAC, J., A. YOUNGER and H. JASPER, 2011 Dynamic coordination of innate immune signaling and insulin signaling regulates systemic responses to localized DNA damage. Developmental Cell **20:** 841-854.

KARPEN, G. H., and G. SCHUBIGER, 1981 Extensive regulatory capabilities of a Drosophila imaginal disk blastema. Nature **294:** 744-747.

KELSEY, E. M., X. LUO, K. BÜCKNER and H. JASPER, 2012 Schnurri regulates hemocyte function to promote tissue recovery after DNA damage. Journal of Cell Science.

KIEHLE, C. P., and G. SCHUBIGER, 1985 Cell proliferation changes during pattern regulation in imaginal leg discs of Drosophila melanogaster. Developmental Biology **109:** 336-346.

KIMBRELL, D. A., C. HICE, C. BOLDUC, K. KLEINHESSELINK and K. BECKINGHAM, 2002 The Dorothy enhancer has Tinman binding sites and drives hopscotch-induced tumor formation. Genesis **34:** 23-28.

KLEBES, A., A. SUSTAR, K. KECHRIS, H. LI, G. SCHUBIGER *et al.*, 2005 Regulation of cellular plasticity in Drosophila imaginal disc cells by the Polycomb group, trithorax group and lama genes. Development **132:** 3753-3765.

KOCKS, C., J. H. CHO, N. NEHME, J. ULVILA, A. M. PEARSON *et al.*, 2005 Eater, a transmembrane protein mediating phagocytosis of bacterial pathogens in Drosophila. Cell **123:** 335-346.

KOH, T. J., and L. A. DIPIETRO, 2011 Inflammation and wound healing: the role of the macrophage. Expert Reviews in Molecular Medicine **13:** e23.

KONDO, S., N. SENOO-MATSUDA, Y. HIROMI and M. MIURA, 2006 DRONC coordinates cell death and compensatory proliferation. Molecular and Cellular Biology **26:** 7258-7268.

KROEGER, P. T., T. TOKUSUMI and R. A. SCHULZ, 2011 Transcriptional regulation of eater gene expression in Drosophila blood cells. Genesis.

KRZEMIEN, J., M. CROZATIER and A. VINCENT, 2010a Ontogeny of the Drosophila larval hematopoietic organ, hemocyte homeostasis and the dedicated cellular immune response to parasitism. The International Journal of Developmental Biology **54:** 1117-1125.

KRZEMIEŃ, J., L. DUBOIS, R. MAKKI, M. MEISTER, A. VINCENT *et al.*, 2007 Control of blood cell homeostasis in Drosophila larvae by the posterior signalling centre. Nature **446:** 325-328.

KRZEMIEN, J., J. OYALLON, M. CROZATIER and A. VINCENT, 2010b Hematopoietic Progenitors and hemocyte lineages in the Drosophila lymph gland. Developmental Biology.

KUMAR, P., S. HENIKOFF and P. C. NG, 2009 Predicting the effects of coding non-synonymous variants on protein function using the SIFT algorithm. Nature Protocols **4:** 1073-1081.

KURANAGA, E., H. KANUKA, T. IGAKI, K. SAWAMOTO, H. ICHIJO *et al.*, 2002 Reaper-mediated inhibition of DIAP1-induced DTRAF1 degradation results in activation of JNK in Drosophila. Nature Cell Biology **4:** 705-710.

KURUCZ, E., R. MÁRKUS, J. ZSÁMBOKI, K. FOLKL-MEDZIHRADSZKY, Z. DARULA *et al.*, 2007 Nimrod, a putative phagocytosis receptor with EGF repeats in Drosophila plasmatocytes. Current Biology **17:** 649-654.

KURUCZ, E., C.-J. ZETTERVALL, R. SINKA, P. VILMOS, A. PIVARCSI *et al.*, 2003 Hemese, a hemocyte-specific transmembrane protein, affects the cellular immune response in Drosophila. Proceedings of the National Academy of Sciences of the United States of America **100:** 2622-2627.

LANGEVIN, J., M. J. MORGAN, J.-B. SIBARITA, S. ARESTA, M. MURTHY *et al.*, 2005 Drosophila exocyst components Sec5, Sec6, and Sec15 regulate DE-Cadherin trafficking from recycling endosomes to the plasma membrane. Developmental Cell **9:** 365-376.

LANOT, R., D. ZACHARY, F. HOLDER and M. MEISTER, 2001 Postembryonic hematopoiesis in Drosophila. Developmental Biology **230:** 243-257.

LEBESTKY, T., T. CHANG, V. HARTENSTEIN and U. BANERJEE, 2000 Specification of Drosophila hematopoietic lineage by conserved transcription factors. Science **288:** 146-149.

LEBESTKY, T., S.-H. JUNG and U. BANERJEE, 2003 A Serrate-expressing signaling center controls Drosophila hematopoiesis. Genes & Development **17:** 348-353.

LEE, N., C. MAURANGE, L. RINGROSE and R. PARO, 2005 Suppression of Polycomb group proteins by JNK signalling induces transdetermination in Drosophila imaginal discs. Nature **438:** 234-237.

LEMAITRE, B., and J. HOFFMANN, 2007 The host defense of Drosophila melanogaster. Annual Review of Immunology **25:** 697-743.

LEPPÄ, S., and D. BOHMANN, 1999 Diverse functions of JNK signaling and c-Jun in stress response and apoptosis. Oncogene **18:** 6158-6162.

LI, F., Q. HUANG, J. CHEN, Y. PENG, D. R. ROOP *et al.*, 2010 Apoptotic cells activate the "phoenix rising" pathway to promote wound healing and tissue regeneration. Science Signaling **3:** ra13.

LI, H., J. RUAN and R. DURBIN, 2008 Mapping short DNA sequencing reads and calling variants using mapping quality scores. Genome Research **18:** 1851-1858.

LUO, H., W. P. HANRATTY and C. R. DEAROLF, 1995 An amino acid substitution in the Drosophila hopTum-l Jak kinase causes leukemia-like hematopoietic defects. The EMBO Journal **14:** 1412-1420.

MAEDA, S., H. KAMATA, J.-L. LUO, H. LEFFERT and M. KARIN, 2005 IKKbeta couples hepatocyte death to cytokine-driven compensatory proliferation that promotes chemical hepatocarcinogenesis. Cell **121:** 977-990.

MAIA, A. F., C. S. LOPES and C. E. SUNKEL, 2007 BubR1 and CENP-E have antagonistic effects upon the stability of microtubule-kinetochore attachments in Drosophila S2 cell mitosis. Cell Cycle **6:** 1367-1378.

MAKHIJANI, K., B. ALEXANDER, T. TANAKA, E. RULIFSON and K. BRÜCKNER, 2011 The peripheral nervous system supports blood cell homing and survival in the Drosophila larva. Development **138:** 5379-5391.

MAKKI, R., M. MEISTER, D. PENNETIER, J.-M. UBEDA, A. BRAUN *et al.*, 2010 A short receptor downregulates JAK/STAT signalling to control the Drosophila cellular immune response. PLoS Biology **8:** e1000441.

MANAKA, J., T. KURAISHI, A. SHIRATSUCHI, Y. NAKAI, H. HIGASHIDA *et al.*, 2004 Draper-mediated and phosphatidylserine-independent phagocytosis of apoptotic cells by Drosophila hemocytes/macrophages. The Journal of Biological Chemistry **279:** 48466-48476.

MANDAL, L., J. A. MARTINEZ-AGOSTO, C. J. EVANS, V. HARTENSTEIN and U. BANERJEE, 2007 A Hedgehog- and Antennapedia-dependent niche maintains Drosophila haematopoietic precursors. Nature **446:** 320-324.

MÁRKUS, R., B. LAURINYECZ, E. KURUCZ, V. HONTI, I. BAJUSZ *et al.*, 2009 Sessile hemocytes as a hematopoietic compartment in Drosophila melanogaster. Proceedings of the National Academy of Sciences of the United States of America **106:** 4805-4809.

MARTÍN, F. A., S. C. HERRERA and G. MORATA, 2009 Cell competition, growth and size control in the Drosophila wing imaginal disc. Development **136:** 3747-3756.

MARTIN, P., and S. J. LEIBOVICH, 2005 Inflammatory cells during wound repair: the good, the bad and the ugly. Trends Cell Biol **15:** 599-607.

MATHEW, L. K., S. SENGUPTA, A. KAWAKAMI, E. A. ANDREASEN, C. V. LÖHR *et al.*, 2007 Unraveling tissue regeneration pathways using chemical genetics. The Journal of Biological Chemistry **282:** 35202-35210.

MATHIAS, J. R., B. J. PERRIN, T.-X. LIU, J. KANKI, A. T. LOOK *et al.*, 2006 Resolution of inflammation by retrograde chemotaxis of neutrophils in transgenic zebrafish. Journal of Leukocyte Biology **80:** 1281-1288.

MATTILA, J., L. OMELYANCHUK, S. KYTTÄLÄ, H. TURUNEN and S. NOKKALA, 2005 Role of Jun N-terminal Kinase (JNK) signaling in the wound healing and regeneration of a Drosophila melanogaster wing imaginal disc. The International Journal of Developmental Biology **49:** 391-399.

MAVES, L., and G. SCHUBIGER, 2003 Transdetermination in Drosophila imaginal discs: a model for understanding pluripotency and selector gene maintenance. Current Opinion in Genetic and Development **13:** 472-479.

MCCLURE, K. D., and G. SCHUBIGER, 2007 Transdetermination: Drosophila imaginal disc cells exhibit stem cell-like potency. The International Journal of Biochemistry & Cell Biology **39:** 1105-1118.

MCCLURE, K. D., and G. SCHUBIGER, 2008 A screen for genes that function in leg disc regeneration in Drosophila melanogaster. Mechanisms of Development **125:** 67-80.

McClure, K. D., A. Sustar and G. Schubiger, 2008 Three genes control the timing, the site and the size of blastema formation in Drosophila. Developmental Biology **319:** 68-77.
Meister, M., 2004 Blood cells of Drosophila: cell lineages and role in host defence. Current Opinion in Immunology **16:** 10-15.
Mesquita, D., A. Dekanty and M. Milán, 2010 A dp53-dependent mechanism involved in coordinating tissue growth in Drosophila. PLoS Biology **8:** e1000566.
Milán, M., S. Campuzano and A. García-Bellido, 1997 Developmental parameters of cell death in the wing disc of Drosophila. Proceedings of the National Academy of Sciences of the United States of America **94:** 5691-5696.
Minakhina, S., and R. Steward, 2006 Melanotic mutants in Drosophila: pathways and phenotypes. Genetics **174:** 253-263.
Minakhina, S., and R. Steward, 2010 Hematopoietic stem cells in Drosophila. Development **137:** 27-31.
Minakhina, S., W. Tan and R. Steward, 2011 JAK/STAT and the GATA factor Pannier control hemocyte maturation and differentiation in Drosophila. Developmental Biology **352:** 308-316.
Mondal, B. C., T. Mukherjee, L. Mandal, C. J. Evans, S. A. Sinenko *et al.*, 2011 Interaction between differentiating cell- and niche-derived signals in hematopoietic progenitor maintenance. Cell **147:** 1589-1600.
Moreira, S., B. Stramer, I. Evans, W. Wood and P. Martin, 2010 Prioritization of competing damage and developmental signals by migrating macrophages in the Drosophila embryo. Current Biology **20:** 464-470.
Murthy, M., R. O. Teodoro, T. P. Miller and T. L. Schwarz, 2010 Sec5, a member of the exocyst complex, mediates Drosophila embryo cellularization. Development **137:** 2773-2783.
Nejak-Bowen, K. N., and S. P. S. Monga, 2011 Beta-catenin signaling, liver regeneration and hepatocellular cancer: sorting the good from the bad. Seminars in Cancer Biology **21:** 44-58.
Nelson, R. E., L. I. Fessler, Y. Takagi, B. Blumberg, D. R. Keene *et al.*, 1994 Peroxidasin: a novel enzyme-matrix protein of Drosophila development. The EMBO Journal **13:** 3438-3447.
Niethammer, P., C. Grabher, A. T. Look and T. J. Mitchison, 2009 A tissue-scale gradient of hydrogen peroxide mediates rapid wound detection in zebrafish. Nature **459:** 996-999.
O'Brochta, D. A., and P. J. Bryant, 1987 Distribution of S-phase cells during the regeneration of Drosophila imaginal wing discs. Developmental Biology **119:** 137-142.
Oh, H., and K. D. Irvine, 2008 In vivo regulation of Yorkie phosphorylation and localization. Development **135:** 1081-1088.
Ohsawa, S., K. Sugimura, K. Takino, T. Xu, A. Miyawaki *et al.*, 2011 Elimination of oncogenic neighbors by JNK-mediated engulfment in Drosophila. Developmental Cell **20:** 315-328.
Okajima, T., B. Reddy, T. Matsuda and K. D. Irvine, 2008 Contributions of chaperone and glycosyltransferase activities of O-fucosyltransferase 1 to Notch signaling. BMC Biology **6:** 1.

OKAJIMA, T., A. XU, L. LEI and K. D. IRVINE, 2005 Chaperone activity of protein O-fucosyltransferase 1 promotes notch receptor folding. Science **307:** 1599-1603.
OWUSU-ANSAH, E., and U. BANERJEE, 2009 Reactive oxygen species prime Drosophila haematopoietic progenitors for differentiation. Nature **461:** 537-541.
PAN, D., 2010 The hippo signaling pathway in development and cancer. Developmental Cell **19:** 491-505.
PASTOR-PAREJA, J. C., M. WU and T. XU, 2008 An innate immune response of blood cells to tumors and tissue damage in Drosophila. Disease Models and Mechanisms **1:** 144-154; discussion 153.
PELLETTIERI, J., P. FITZGERALD, S. WATANABE, J. MANCUSO, D. R. GREEN *et al.*, 2010 Cell death and tissue remodeling in planarian regeneration. Developmental Biology **338:** 76-85.
PÉREZ-GARIJO, A., F. A. MARTÍN and G. MORATA, 2004 Caspase inhibition during apoptosis causes abnormal signalling and developmental aberrations in Drosophila. Development **131:** 5591-5598.
PÉREZ-GARIJO, A., F. A. MARTÍN, G. STRUHL and G. MORATA, 2005 Dpp signaling and the induction of neoplastic tumors by caspase-inhibited apoptotic cells in Drosophila. Proceedings of the National Academy of Sciences of the United States of America **102:** 17664-17669.
PÉREZ-GARIJO, A., E. SHLEVKOV and G. MORATA, 2009 The role of Dpp and Wg in compensatory proliferation and in the formation of hyperplastic overgrowths caused by apoptotic cells in the Drosophila wing disc. Development **136:** 1169-1177.
PERI, F., 2010 Breaking ranks: how leukocytes react to developmental cues and tissue injury. Current Opinion in Genetics & Development **20:** 416-419.
PETERSEN, C. P., and P. W. REDDIEN, 2008 Smed-betacatenin-1 is required for anteroposterior blastema polarity in planarian regeneration. Science **319:** 327-330.
PLANK, J. L., S. H. CHU, J. R. POHLHAUS, T. WILSON-SALI and T.-S. HSIEH, 2005 Drosophila melanogaster topoisomerase IIIalpha preferentially relaxes a positively or negatively supercoiled bubble substrate and is essential during development. The Journal of Biological Chemistry **280:** 3564-3573.
POODRY, C. A., and D. F. WOODS, 1999 Control of the developmental timer for Drosophila pupariation. Roux's Archives of Developmental Biology **199:** 219-227.
POSS, K. D., 2010 Advances in understanding tissue regenerative capacity and mechanisms in animals. Nature Reviews Genetics **11:** 710-722.
QIU, P., P. C. PAN and S. GOVIND, 1998 A role for the Drosophila Toll/Cactus pathway in larval hematopoiesis. Development **125:** 1909-1920.
REDD, M. J., L. COOPER, W. WOOD, B. STRAMER and P. MARTIN, 2004 Wound healing and inflammation: embryos reveal the way to perfect repair. Philosophical Transactions of the Royal Society of London. Series B, Biological Sciences **359:** 777-784.
REMILLIEUX-LESCHELLE, N., P. SANTAMARIA and N. B. RANDSHOLT, 2002 Regulation of larval hematopoiesis in Drosophila melanogaster: a role for the multi sex combs gene. Genetics **162:** 1259-1274.
RIESGO-ESCOVAR, J. R., M. JENNI, A. FRITZ and E. HAFEN, 1996 The Drosophila Jun-N-terminal kinase is required for cell morphogenesis but not for DJun-dependent cell fate specification in the eye. Genes & Development **10:** 2759-2768.
RIZKI, T. M., 1962 Experimental analysis of hemocyte morphology in insects. American Zoologist **2:** 247-256.

RIZKI, T. M., and R. M. RIZKI, 1980 Hemocyte Responses to Implanted Tissues in Drosophila melanogaster Larvae. Wilhelm Roux's Archives of Developmental Biology **189:** 207-213.

RIZKI, T. M., and R. M. RIZKI, 1992 Lamellocyte differentiation in Drosophila larvae parasitized by Leptopilina. Developmental and Comparative Immunology **16:** 103-110.

ROOS, C., M. KOLMER, P. MATTILA and R. RENKONEN, 2002 Composition of Drosophila melanogaster proteome involved in fucosylated glycan metabolism. The Journal of Biological Chemistry **277:** 3168-3175.

RUS, F., E. KURUCZ, R. MÁRKUS, S. A. SINENKO, B. LAURINYECZ *et al.*, 2006 Expression pattern of Filamin-240 in Drosophila blood cells. Gene Expression Patterns **6:** 928-934.

RUSSELL, M. A., L. OSTAFICHUK and S. SCANGA, 1998 Lethal P-lacZ insertion lines expressed during pattern respecification in the imaginal discs of Drosophila. Genome **41:** 7-13.

RUSSO, J., S. DUPAS, F. FREY, Y. CARTON and M. BREHELIN, 1996 Insect immunity: early events in the encapsulation process of parasitoid (Leptopilina boulardi) eggs in resistant and susceptible strains of Drosophila. Parasitology **112 (Pt 1):** 135-142.

RYOO, H. D., T. GORENC and H. STELLER, 2004 Apoptotic cells can induce compensatory cell proliferation through the JNK and the Wingless signaling pathways. Developmental Cell **7:** 491-501.

SAMPATH, D., V. A. RAO and W. PLUNKETT, 2003 Mechanisms of apoptosis induction by nucleoside analogs. Oncogene **22:** 9063-9074.

SÁNCHEZ ALVARADO, A., 2000 Regeneration in the metazoans: why does it happen? Bioessays **22:** 578-590.

SÁNCHEZ ALVARADO, A., 2007 Stem cells and the Planarian Schmidtea mediterranea. Comptes rendus Biology **330:** 498-503.

SÁNCHEZ ALVARADO, A., and P. A. TSONIS, 2006 Bridging the regeneration gap: genetic insights from diverse animal models. Nature Reviews Genetics **7:** 873-884.

SARIN, S., V. BERTRAND, H. BIGELOW, A. BOYANOV, M. DOITSIDOU *et al.*, 2010 Analysis of multiple ethyl methanesulfonate-mutagenized Caenorhabditis elegans strains by whole-genome sequencing. Genetics **185:** 417-430.

SCHUBIGER, G., 1971 Regeneration, duplication and transdetermination in fragments of the leg disc of Drosophila melanogaster. Developmental Biology **26:** 277-295.

SEARS, H. C., C. J. KENNEDY and P. A. GARRITY, 2003 Macrophage-mediated corpse engulfment is required for normal Drosophila CNS morphogenesis. Development **130:** 3557-3565.

SHAO, J., B. ZHOU, B. CHU and Y. YEN, 2006 Ribonucleotide reductase inhibitors and future drug design. Current Cancer Drug Targets **6:** 409-431.

SIEGRIST, S. E., N. S. HAQUE, C.-H. CHEN, B. A. HAY and I. K. HARIHARAN, 2010 Inactivation of both Foxo and reaper promotes long-term adult neurogenesis in Drosophila. Current Biology **20:** 643-648.

SIMPSON, P., P. BERREUR and J. BERREUR-BONNENFANT, 1980 The initiation of pupariation in Drosophila: dependence on growth of the imaginal discs. Journal of Embryology & Experimental Morphology **57:** 155-165.

SINENKO, S. A., E. K. KIM, R. WYNN, P. MANFRUELLI, I. ANDO *et al.*, 2004 Yantar, a conserved arginine-rich protein is involved in Drosophila hemocyte development. Developmental Biology **273:** 48-62.

SINENKO, S. A., L. MANDAL, J. A. MARTINEZ-AGOSTO and U. BANERJEE, 2009 Dual role of wingless signaling in stem-like hematopoietic precursor maintenance in Drosophila. Developmental Cell **16:** 756-763.

SLUSS, H. K., Z. HAN, T. BARRETT, D. C. GOBERDHAN, C. WILSON *et al.*, 1996 A JNK signal transduction pathway that mediates morphogenesis and an immune response in Drosophila. Genes & Development **10:** 2745-2758.

SMITH-BOLTON, R. K., M. I. WORLEY, H. KANDA and I. K. HARIHARAN, 2009 Regenerative growth in Drosophila imaginal discs is regulated by Wingless and Myc. Developmental Cell **16:** 797-809.

SORRENTINO, R. P., Y. CARTON and S. GOVIND, 2002 Cellular immune response to parasite infection in the Drosophila lymph gland is developmentally regulated. Developmental Biology **243:** 65-80.

SORRENTINO, R. P., J. P. MELK and S. GOVIND, 2004 Genetic analysis of contributions of dorsal group and JAK-Stat92E pathway genes to larval hemocyte concentration and the egg encapsulation response in Drosophila. Genetics **166:** 1343-1356.

SORRENTINO, R. P., T. TOKUSUMI and R. A. SCHULZ, 2007 The Friend of GATA protein U-shaped functions as a hematopoietic tumor suppressor in Drosophila. Developmental Biology **311:** 311-323.

SRIVATSAN, A., Y. HAN, J. PENG, A. K. TEHRANCHI, R. GIBBS *et al.*, 2008 High-precision, whole-genome sequencing of laboratory strains facilitates genetic studies. PLoS Genetics **4:** e1000139.

ST JOHNSTON, D., 2002 The art and design of genetic screens: Drosophila melanogaster. Nature Reviews Genetics **3:** 176-188.

STIEPER, B. C., M. KUPERSHTOK, M. V. DRISCOLL and A. W. SHINGLETON, 2008 Imaginal discs regulate developmental timing in Drosophila melanogaster. Developmental Biology **321:** 18-26.

STOCUM, D. L., and J. A. CAMERON, 2011 Looking proximally and distally: 100 years of limb regeneration and beyond. Developmental Dynamics **240:** 943-968.

STOFANKO, M., S. Y. KWON and P. BADENHORST, 2010 Lineage tracing of lamellocytes demonstrates Drosophila macrophage plasticity. PLoS ONE **5:** e14051.

STOICK-COOPER, C. L., R. T. MOON and G. WEIDINGER, 2007a Advances in signaling in vertebrate regeneration as a prelude to regenerative medicine. Genes & Development **21:** 1292-1315.

STOICK-COOPER, C. L., G. WEIDINGER, K. J. RIEHLE, C. HUBBERT, M. B. MAJOR *et al.*, 2007b Distinct Wnt signaling pathways have opposing roles in appendage regeneration. Development **134:** 479-489.

STOLL, G., and H. W. MÜLLER, 1999 Nerve injury, axonal degeneration and neural regeneration: basic insights. Brain Pathology **9:** 313-325.

STRAMER, B., M. WINFIELD, T. SHAW, T. H. MILLARD, S. WOOLNER *et al.*, 2008 Gene induction following wounding of wild-type versus macrophage-deficient Drosophila embryos. EMBO Reports **9:** 465-471.

STRAMER, B., W. WOOD, M. J. GALKO, M. J. REDD, A. JACINTO *et al.*, 2005 Live imaging of wound inflammation in Drosophila embryos reveals key roles for small GTPases during in vivo cell migration. The Journal of Cell Biology **168:** 567-573.

SUN, G., and K. D. IRVINE, 2011 Regulation of Hippo signaling by Jun kinase signaling during compensatory cell proliferation and regeneration, and in neoplastic tumors. Developmental Biology **350:** 139-151.

SUSTAR, A., and G. SCHUBIGER, 2005 A transient cell cycle shift in Drosophila imaginal disc cells precedes multipotency. Cell **120:** 383-393.

TANAKA, H., H. ARAKAWA, T. YAMAGUCHI, K. SHIRAISHI, S. FUKUDA *et al.*, 2000 A ribonucleotide reductase gene involved in a p53-dependent cell-cycle checkpoint for DNA damage. Nature **404:** 42-49.

TANIMOTO, H., S. ITOH, P. TEN DIJKE and T. TABATA, 2000 Hedgehog creates a gradient of DPP activity in Drosophila wing imaginal discs. Molecular Cell **5:** 59-71.

TAUB, R., 2004 Liver regeneration: from myth to mechanism. Nature Reviews Molecular Cell Biology **5:** 836-847.

TENNANT, R., 1931 A maximun point in an effect of prolonged X-ray irradiation upon Drosophila larvae. Science **73:** 567-568.

TEPASS, U., L. I. FESSLER, A. AZIZ and V. HARTENSTEIN, 1994 Embryonic origin of hemocytes and their relationship to cell death in Drosophila. Development **120:** 1829-1837.

TOKUSUMI, T., D. A. SHOUE, Y. TOKUSUMI, J. R. STOLLER and R. A. SCHULZ, 2009a New hemocyte-specific enhancer-reporter transgenes for the analysis of hematopoiesis in Drosophila. Genesis **47:** 771-774.

TOKUSUMI, T., R. P. SORRENTINO, M. RUSSELL, R. FERRARESE, S. GOVIND *et al.*, 2009b Characterization of a lamellocyte transcriptional enhancer located within the misshapen gene of Drosophila melanogaster. PLoS ONE **4:** e6429.

TSENG, A.-S., D. S. ADAMS, D. QIU, P. KOUSTUBHAN and M. LEVIN, 2007 Apoptosis is required during early stages of tail regeneration in Xenopus laevis. Developmental Biology **301:** 62-69.

VACCARI, T., and D. BILDER, 2005 The Drosophila tumor suppressor vps25 prevents nonautonomous overproliferation by regulating notch trafficking. Developmental Cell **9:** 687-698.

VUCIC, D., W. J. KAISER and L. K. MILLER, 1998 Inhibitor of apoptosis proteins physically interact with and block apoptosis induced by Drosophila proteins HID and GRIM. Molecular and Cellular Biology **18:** 3300-3309.

WALTZER, L., G. FERJOUX, L. BATAILLÉ and M. HAENLIN, 2003 Cooperation between the GATA and RUNX factors Serpent and Lozenge during Drosophila hematopoiesis. The EMBO Journal **22:** 6516-6525.

WANG, M. C., D. BOHMANN and H. JASPER, 2003 JNK signaling confers tolerance to oxidative stress and extends lifespan in Drosophila. Developmental Cell **5:** 811-816.

WANG, Y., and G. S. SHADEL, 1999 Stability of the mitochondrial genome requires an amino-terminal domain of yeast mitochondrial RNA polymerase. Proceedings of the National Academy of Sciences of the United States of America **96:** 8046-8051.

WELLS, B. S., and L. A. JOHNSTON, 2012 Maintenance of imaginal disc plasticity and regenerative potential in Drosophila by p53. Developmental Biology **361:** 263-276.

WELLS, B. S., E. YOSHIDA and L. A. JOHNSTON, 2006 Compensatory proliferation in Drosophila imaginal discs requires Dronc-dependent p53 activity. Current Biology **16:** 1606-1615.

WILLIAMS, M. J., I. ANDO and D. HULTMARK, 2005 Drosophila melanogaster Rac2 is necessary for a proper cellular immune response. Genes to Cells **10:** 813-823.

WILLIAMS, M. J., M.-L. WIKLUND, S. WIKMAN and D. HULTMARK, 2006 Rac1 signalling in the Drosophila larval cellular immune response. Journal of Cell Science **119:** 2015-2024.
WOOD, W., C. FARIA and A. JACINTO, 2006 Distinct mechanisms regulate hemocyte chemotaxis during development and wound healing in Drosophila melanogaster. The Journal of Cell Biology **173:** 405-416.
WU, J., L. FENG and T.-S. HSIEH, 2010 Drosophila topo IIIalpha is required for the maintenance of mitochondrial genome and male germ-line stem cells. Proceedings of the National Academy of Sciences of the United States of America **107:** 6228-6233.
WU, J. S., and L. LUO, 2006 A protocol for mosaic analysis with a repressible cell marker (MARCM) in Drosophila. Nature Protocols **1:** 2583-2589.
WU, X., M. YAMADA-MABUCHI, E. J. MORRIS, P. S. TANWAR, L. DOBENS *et al.*, 2008 The Drosophila homolog of human tumor suppressor TSC-22 promotes cellular growth, proliferation, and survival. Proceedings of the National Academy of Sciences of the United States of America **105:** 5414-5419.
XIA, Y., and M. KARIN, 2004 The control of cell motility and epithelial morphogenesis by Jun kinases. Trends Cell Biol **14:** 94-101.
YUCEL, J. K., J. D. MARSZALEK, J. R. MCINTOSH, L. S. GOLDSTEIN, D. W. CLEVELAND *et al.*, 2000 CENP-meta, an essential kinetochore kinesin required for the maintenance of metaphase chromosome alignment in Drosophila. The Journal of Cell Biology **150:** 1-11.
ZETTERVALL, C.-J., I. ANDERL, M. J. WILLIAMS, R. PALMER, E. KURUCZ *et al.*, 2004 A directed screen for genes involved in Drosophila blood cell activation. Proceedings of the National Academy of Sciences of the United States of America **101:** 14192-14197.